NASA TECHNICAL MEMORANDUM

NASA TM X-1226

NASA TM X-1226

EFFECT OF ELEVON DEFLECTION AND OF MODEL COMPONENTS ON AERODYNAMIC CHARACTERISTICS OF A MANNED LIFTING ENTRY VEHICLE AT MACH MUMBERS OF 0.20 TO 1.20

by Charles D. Harris

Langley Research Center
Langley Station, Hampton, Va.

NATIONAL AERONAUTICS AND SPACE ADMINISTRATION • WASHINGTON, D. C. • APRIL 1966

NASA TM X-1226

EFFECT OF ELEVON DEFLECTION AND OF MODEL COMPONENTS ON AERODYNAMIC CHARACTERISTICS OF A MANNED LIFTING ENTRY VEHICLE AT MACH NUMBERS OF 0.20 TO 1.20

By Charles D. Harris

Langley Research Center
Langley Station, Hampton, Va.

NATIONAL AERONAUTICS AND SPACE ADMINISTRATION

EFFECT OF ELEVON DEFLECTION AND OF MODEL COMPONENTS ON AERODYNAMIC CHARACTERISTICS OF A MANNED LIFTING ENTRY VEHICLE AT MACH NUMBERS OF 0.20 TO 1.20*

By Charles D. Harris
Langley Research Center

SUMMARY

An investigation was made in the Langley 8-foot transonic pressure tunnel of the static longitudinal and lateral stability and control characteristics of a manned lifting entry vehicle with canted tip fins and center-line dorsal fin, designated HL-10. The investigation was made at Mach numbers from 0.20 to 1.20 and through an angle-of-attack range from approximately -2° to 24° at fixed sideslip angles of approximately 0°, 3°, and 5°. The results include the effect on the aerodynamic characteristics of uniform and differential elevon deflection, of the addition of a center-line dorsal fin, and of two geometrically different tip fins. In general, the complete vehicle with tip fins toed in 10.8° and rolled out 8.5° was stable and controllable and had favorable yaw due to roll for most test conditions.

INTRODUCTION

Studies of the aerodynamic characteristics of manned lifting entry vehicles having maximum hypersonic lift-drag ratios of about 1 have been made by the National Aeronautics and Space Administration, Langley Research Center. Initial investigations (refs. 1 to 4) indicated a basic blunt body that possessed considerable promise in meeting the design requirements of capability for reentry into and maneuverability within the earth's atmosphere and capability of conventional horizontal landing. This vehicle, having a 74° swept delta planform, a blunt nose, and extensive boattailing, has been designated the basic HL-10 (horizontal lander 10).

An extensive wind-tunnel program was undertaken to establish a suitable configuration for all operational Mach numbers and a summary of results for several configurations tested in a range of Mach numbers from low subsonic to hypersonic speeds is given in reference 5.

---

*Title, Unclassified.

The present investigation is an extension of that of reference 4 and incorporates geometric modifications to the outboard dorsal fins, an enlarged center-line dorsal fin, and modified elevon planform. The results include the effect of elevons uniformly deflected for pitch control and differentially deflected for roll control and the incremental effect on the aerodynamic characteristics of the addition of a center-line dorsal fin and two geometrically different outboard dorsal fins. The investigation was made at Mach numbers from 0.20 to 1.20 and through an angle-of-attack range from approximately -2° to 24° at fixed sideslip angles of approximately 0°, 3°, and 5°.

SYMBOLS

The lift and drag data are referred to the stability axes, the rolling-moment and yawing-moment data are referred to the body axes, and the side-force and pitching-moment data are referred to the common lateral axis of the stability and body axes (fig. 1). The origin of the stability and body axes is the moment reference point located longitudinally 53 percent of the body length behind the vehicle nose and 1.25 percent of the body length below the reference center line. All coefficients are based on the total projected planform area (tip fins excluded), the span, and the length of the model.

The units used for the physical quantities in this paper are given both in the International System of Units (SI) and in the U.S. Customary Units. Factors relating the two systems are given in reference 6.

b reference span used for computations; maximum width of body without tip dorsal fins (model value 26.19 cm (10.31 in.))

C_A axial-force coefficient adjusted to a condition of free-stream static pressure within the sting cavity

$C_{A,b}$ base axial-force coefficient

C_D drag coefficient, $\frac{\text{Drag force}}{qS}$

C_L lift coefficient, $\frac{\text{Lift force}}{qS}$

C_l rolling-moment coefficient, $\frac{\text{Rolling moment}}{qSb}$

$C_{l_\beta} = \frac{\Delta C_l}{\Delta \beta}$ per degree

C_m pitching-moment coefficient, $\frac{\text{Pitching moment}}{qSl}$

C_n yawing-moment coefficient, $\frac{\text{Yawing moment}}{qSb}$

$C_{n_\beta} = \frac{\Delta C_n}{\Delta \beta}$ per degree

C_Y side-force coefficient, $\frac{\text{Side force}}{qS}$

L/D lift-drag ratio, C_L/C_D

l reference length used for computations; distance from body nose to body base (model value, 40.64 cm (16.00 in.))

M Mach number of undisturbed stream

q dynamic pressure of undisturbed stream, N/m^2 (psf)

R Reynolds number based on model reference length l

S reference area equal to projected planform area with elevons (model value 0.0590 m^2 (0.6344 sq ft))

X_b, Y_b, Z_b body axes

X_S, Y_S, Z_S stability axes

α angle of attack measured relative to center line of model, deg

β angle of sideslip, deg

δ_a differential roll control deflection, equal to right elevon deflection angle minus left elevon deflection angle, deg

δ_e elevon deflection angle measured in plane perpendicular to hinge line, positive with trailing edge down, deg

ϵ fin toe-in angle, angle between model vertical plane of symmetry and fin outer surface measured in horizontal reference plane of model (see fig. 2(b))

ϕ fin roll-out angle; angle between model vertical plane of symmetry and fin outer surface measured in plane normal to fin roll axis (see fig. 2(b))

APPARATUS

Tunnel

The investigation was made in the Langley 8-foot transonic pressure tunnel. The test section of this tunnel is square in cross section with the upper and lower walls axially slotted to permit changing the test-section Mach number continuously from 0 to over 1.20 with negligible effects of choking and blockage. The total pressure of the tunnel air can be varied from a minimum value of about 0.25 atmosphere at all test Mach numbers to a maximum value of about 1.5 atmospheres at transonic Mach numbers and about 2.0 atmospheres at Mach numbers of 0.40 and less. The tunnel air is dried sufficiently to avoid condensation effects.

Model

The 40.64-cm (16.00-in.) model was constructed of molded fiberglass with a steel core and included movable elevons. The center-line dorsal fin was of aluminum. Three-view drawings showing details of the HL-10 configuration and tip-fin orientation are presented in figures 2(a) and 2(b). The body cross-section ordinates with tip fins off are presented in table I. A photograph of the HL-10 configuration used in the present investigation is shown in figure 2(c). The body and various components are identified as follows:

Basic body B: Original body with no fins, as in reference 4

Fin E_2: Center-line dorsal fin

Fin I_2: Tip dorsal fins with toe-in angle ϵ of 16° and roll-out angle ϕ of 9.5°

Fin I_3: Tip dorsal fins with toe-in angle ϵ of 10.8° and roll-out angle ϕ of 8.5°

These model designations were assigned to the model as part of the overall test program numbering system.

The I_3 tip fins were unsymmetrical about the center line in that the 8.5° roll-out was the average of 9° 10' roll-out on the left tip fin and 7° 50' on the right tip fin. In subsequent tests (see refs. 7 to 10), the tip fins were revised so that both left and right fin

had a roll-out angle of 8.5°. This revised fin is designated fin I_4.

Instrumentation

Aerodynamic force and moments were measured with a six-component internal strain-gage balance. The model and balance were supported by a conventional sting which, in turn, was attached to a remotely controlled sideslip mechanism. A static-pressure orifice, located in the balance cavity, was connected to a pressure transducer. The overall forces and moments on the model, the angle of attack, and the static pressure in the balance cavity were recorded electronically on punch cards.

TESTS, CORRECTIONS, AND ACCURACY

Tests

The investigation was made at Mach numbers from 0.20 to 1.20, at stagnation pressures from 1 atmosphere at Mach numbers of 0.80 and below to approximately 1/3 atmosphere at a Mach number of 1.20, and at a stagnation temperature of 322° K (120° F). The Reynolds number and dynamic pressures of the investigation are shown in figure 3. The tests were made at angles of attack from approximately -2° to 24° at fixed angles of sideslip of approximately 0°, 3°, and 5°.

The investigation included tests to determine the effect on the aerodynamic characteristics of the elevons uniformly deflected for pitch control with both the I_2 and I_3 tip fins, the effect on the aerodynamic characteristics of the elevons differentially deflected for roll control with and without the I_3 tip fins, and the incremental effect on the aerodynamic characteristics of the outboard and center-line dorsal fins. Uniform elevon deflections from $\delta_e = -20^\circ$ to $\delta_e = 10^\circ$ and a differential elevon deflection of $\delta_a = -20^\circ$ referenced to $\delta_e = \pm 10^\circ$ were investigated.

All tests, except where noted, were conducted with a 0.254-cm (0.10-in.) strip of No. 60 carborundum grit along the 12.5-percent-chord line on both the upper and lower surface of the body.

Corrections

The axial-force coefficient C_A was adjusted to a condition of free-stream static pressure within the balance cavity. Representative values of the base-axial-force adjustment $C_{A,b}$ are shown in figure 4. The aerodynamic force and moment data presented herein are considered to be free of tunnel boundary interference and no sting interference corrections have been made to the data except to the extent of the partial correction for sting interference inherent in the base-pressure correction. The angle of attack and

sideslip angle have been corrected for the deflection of the balance and sting support under aerodynamic load.

Maximum balance error, based on 0.5 percent of the maximum design load of each component, is estimated to be within the following limits:

For all Mach numbers:

α, deg	±0.10
M	±0.005

For Mach number of 0.80:

C_N	±0.0053
C_A	±0.0013
C_m	±0.0005
C_l	±0.0001
C_n	±0.0003
C_Y	±0.0013

For Mach numbers other than 0.80, for which the dynamic pressures were substantially less than that at M = 0.80, the accuracy of the data expressed in aerodynamic-coefficient form was correspondingly poorer than that listed.

The nominal sideslip angles of approximately 0^o, 3^o, and 5^o vary under aerodynamic loading within $\pm 0.05^o$ at $\beta = 0^o$ to $\pm 0.44^o$ at $\beta = 5^o$. Nominal values are used to identify data but actual values were used to compute stability parameters.

PRESENTATION OF RESULTS

Basic longitudinal aerodynamic characteristics are presented in figures 5 to 9 and the basic lateral characteristics are presented in figures 10 to 14 and summarized in figures 15 to 17. An outline of the contents of the data figures is as follows:

	Figure
Basic longitudinal aerodynamic characteristics:	
Effect of model components	5
Effect of uniform elevon deflection (BE_2I_2)	6
Effect of uniform elevon deflection (BE_2I_3)	7
Effect of differential elevon deflection (BE_2)	8
Effect of differential elevon deflection (BE_2I_3)	9

The longitudinal performance and stability results at sideslip angles other than 0° are in close agreement with those at $\beta = 0^\circ$ and are not presented.

DISCUSSION

Longitudinal Aerodynamic Characteristics

The addition of the center-line fin (E_2) to the basic body had almost no effect on the lift or pitching-moment characteristics, but did add an increment of drag which resulted in a reduction of the maximum untrimmed lift-drag ratios through the Mach number range. (See fig. 5.) Addition of the tip fins to the basic body with center-line fin (E_2) resulted in a negative shift in the pitching-moment curves for Mach numbers below 1.00 (fig. 5(c)), with negative trim angles of attack indicated for the I_2 tip-fin configuration for Mach numbers of 0.80 and below ($\delta_e = 0^\circ$). The reduced toe-in and roll-out orientation of the I_3 tip fins as compared to the I_2 tip fins resulted in a general improvement in longitudinal stability characteristics and an increase in maximum untrimmed lift-drag ratios.

Uniform deflection of the elevons on the basic body with center-line fin (E_2) and either the I_2 tip fins (fig. 6) or the I_3 tip fins (fig. 7) provided trim capability over a large portion of the angle-of-attack range with no major deficiencies in longitudinal stability near trim. Trimmed lift-drag ratios were slightly higher for the configuration with the I_3 tip fins.

The sensitivity of the model to flow conditions at low Reynolds numbers is indicated in figure 7 by the transition-grit-off data at $M = 0.20$.

Directional and Lateral Stability Characteristics

The values of the directional and lateral stability derivatives shown in figures 15 to 17 were taken as the average slopes for angles of sideslip from approximately 0° to 5°. The derivatives may be nonlinear throughout a large sideslip range; and therefore, the data should be used only to provide approximate comparisons and to indicate trends. Deviations of lateral-force and moment coefficients from zero for symmetrical deflection of control surfaces are probably due to asymmetry of the model.

Addition of the center-line fin (E_2) to the basic body provided positive values of Cn_{β} except at high angle of attack for $M = 1.20$ (see fig. 15) and increased positive effective dihedral for all test conditions. In general, addition of the tip fins (I_2 or I_3) to the basic body with center-line fin (E_2) provided increases in Cn_{β} as shown in figure 15(a). Figure 15(b) shows positive effective dihedral for the basic body with center-line fin (E_2) and tip fin (I_3) for all test conditions whereas unstable rolling-moment characteristics are shown for the I_2 tip-fin configuration at low subsonic Mach numbers.

For most of the test conditions, roll control of the complete configuration with tip fins (I_3) is positive and is accompanied by favorable yaw due to roll. (See fig. 14).

CONCLUSIONS

An investigation was made in the Langley 8-foot transonic pressure tunnel of the static longitudinal and lateral stability and control characteristics of a manned lifting entry vehicle having a hypersonic lift-drag ratio of about 1. The investigation was made at Mach numbers from 0.20 to 1.20 and through an angle-of-attack range from approximately -2° to 24° at fixed sideslip angles of approximately 0°, 3°, and 5°. The results include the effect on the aerodynamic characteristics of uniform and differential deflection of elevons and of model components. The following conclusions are indicated:

1. Decreasing the toe-in and roll-out orientation of the tip fins resulted in a general improvement in the longitudinal stability characteristics and an increase in maximum untrimmed lift-drag ratios.

2. The complete vehicle with tip fins can be trimmed over a large angle-of-attack range with no major deficiencies in longitudinal stability near trim.

3. Addition of the center-line fin and tip fins provided, in general, directional and lateral static stability.

4. For most test conditions, roll control of the complete vehicle with tip fins toed in 10.8° and rolled out 8.5° is positive and accompanied by favorable yaw due to roll.

Langley Research Center
National Aeronautics and Space Administration,
Langley Station, Hampton, Va., December 22, 1965.

REFERENCES

1. Rainey, Robert W.; and Ladson, Charles L.: Preliminary Aerodynamic Characteristics of a Manned Lifting Entry Vehicle at a Mach Number of 6.8. NASA TM X-844, 1963.

2. Ladson, Charles L.: Aerodynamic Characteristics of a Manned Lifting Entry Vehicle at a Mach Number of 6.8. NASA TM X-915, 1964.

3. Ware, George M.: Aerodynamic Characteristics of Models of Two Thick 74° Delta Manned Lifting Entry Vehicles at Low-Subsonic Speeds. NASA TM X-914, 1964.

4. Rainey, Robert W.; and Ladson, Charles L.: Aerodynamic Characteristics of Manned Lifting Entry Vehicle at Mach Numbers From 0.2 to 1.2. NASA TM X-1015, 1964.

5. Rainey, Robert W.: Summary of an Advanced Manned Lifting Entry Vehicle Study. NASA TM X-1159, 1965.

6. Mechtly, E. A.: The International System of Units – Physical Constants and Conversion Factors. NASA SP-7012, 1964.

7. Johnston, Patrick J.: Stability Characteristics of a Manned Lifting Entry Vehicle at a Mach Number of 20.3 in Helium. NASA TM X-1156, 1965.

8. Spencer, Bernard, Jr.: An Investigation of Methods of Improving Subsonic Performance of a Manned Lifting Entry Vehicle. NASA TM X-1157, 1965.

9. Ladson, Charles L.: Aerodynamic Characteristics of a Manned Lifting Entry Vehicle With Modified Tip Fins at Mach 6.8. NASA TM X-1158, 1965.

10. Ware, George M.: Full-Scale Wind-Tunnel Investigation of the Aerodynamic Characteristics of the HL-10 Manned Lifting Entry Vehicle. NASA TM X-1160, 1965.

TABLE I.- CROSS-SECTION ORDINATES FOR HL-10 WITH TIP FINS OFF

z/l	y/l	z/l	y/l	z/l	y/l	z/l	y/l	z/l	y/l	z/l	y/l
x/l = 0.042		x/l = 0.083		x/l = 0.125		x/l = 0.167		x/l = 0.208		x/l = 0.250	
0.0541	0	0.0681	0	0.0737	0	0.0771	0	0.0792	0	0.0807	0
.0532	.0083	.0668	.0083	.0729	.0083	.0763	.0083	.0787	.0083	.0803	.0083
.0503	.0167	.0637	.0167	.0702	.0167	.0744	.0167	.0772	.0167	.0792	.0167
.0441	.0250	.0579	.0250	.0660	.0250	.0712	.0250	.0747	.0250	.0773	.0250
.0375	.0306	.0502	.0333	.0594	.0330	.0664	.0333	.0712	.0333	.0748	.0333
.0333	.0338	.0417	.0392	.0505	.0417	.0597	.0417	.0664	.0416	.0712	.0417
.0250	.0390	.0330	.0444	.0417	.0477	.0512	.0500	.0592	.0500	.0666	.0500
.0167	.0431	.0250	.0487	.0333	.0528	.0417	.0565	.0517	.0583	.0606	.0583
.0083	.0459	.0167	.0521	.0250	.0571	.0333	.0618	.0417	.0656	.0527	.0667
0	.0476	.0083	.0547	.0167	.0604	.0250	.0664	.0333	.0713	.0458	.0721
-.0536	0	0	.0568	.0083	.0632	.0167	.0701	.0250	.0760	.0417	.0754
		-.0083	.0585	0	.0656	.0083	.0732	.0167	.0800	.0333	.0811
		-.0167	.0596	-.0083	.0675	0	.0757	.0083	.0833	.0250	.0862
		-.0752	0	-.0167	.0691	-.0083	.0778	0	.0860	.0167	.0902
				-.0250	.0704	-.0167	.0796	-.0083	.0882	.0083	.0937
				-.0333	.0714	-.0250	.0811	-.0167	.0902	0	.0965
				-.0904	0	-.0333	.0823	-.0250	.0919	-.0083	.0990
						-.0417	.0833	-.0333	.0933	-.0167	.1011
						-.0500	.0840	-.0417	.0946	-.0250	.1027
						-.1026	0	-.0500	.0955	-.0333	.1044
								-.0583	.0962	-.0417	.1057
										-.0500	.1067
								-.1126	0	-.0583	.1076
										-.0667	.1083
										-.1205	0
x/l = 0.292		x/l = 0.333		x/l = 0.375		x/l = 0.417		x/l = 0.458		x/l = 0.500	
0.0817	0	0.0820	0	0.0821	0	0.0814	0	0.0800	0	0.0782	0
.0814	.0083	.0818	.0083	.0820	.0083	.0813	.0083	.0799	.0083	.0782	.0167
.0807	.0167	.0813	.0167	.0816	.0167	.0811	.0167	.0797	.0167	.0780	.0250
.0794	.0250	.0803	.0250	.0809	.0250	.0805	.0250	.0794	.0250	.0776	.0333
.0774	.0333	.0789	.0333	.0799	.0333	.0797	.0333	.0788	.0333	.0770	.0417
.0750	.0417	.0771	.0417	.0783	.0417	.0786	.0417	.0780	.0417	.0762	.0500
.0715	.0500	.0747	.0500	.0766	.0500	.0772	.0500	.0768	.0500	.0751	.0583
.0672	.0583	.0716	.0583	.0744	.0583	.0755	.0583	.0755	.0583	.0738	.0667
.0617	.0667	.0677	.0667	.0714	.0667	.0733	.0667	.0739	.0667	.0723	.0750
.0546	.0750	.0627	.0750	.0679	.0750	.0706	.0750	.0720	.0750	.0705	.0833
.0500	.0789	.0564	.0833	.0633	.0833	.0674	.0833	.0694	.0833	.0682	.0917
.0417	.0858	.0485	.0917	.0576	.0917	.0633	.0917	.0664	.0917	.0655	.1000
.0333	.0918	.0417	.0968	.0503	.1000	.0582	.1000	.0629	.1000	.0620	.1083
.0250	.0969	.0333	.1027	.0415	.1083	.0517	.1083	.0581	.1083	.0579	.1167
.0167	.1010	.0250	.1078	.0333	.1136	.0437	.1167	.0526	.1167	.0529	.1250
.0083	.1044	.0167	.1119	.0250	.1187	.0375	.1211	.0453	.1250	.0467	.1333
0	.1072	.0083	.1152	.0167	.1229	.0333	.1241	.0363	.1333	.0390	.1417
-.0083	.1098	0	.1179	.0083	.1262	.0250	.1296	.0292	.1379	.0333	.1458
-.0167	.1119	-.0083	.1204	0	.1292	.0167	.1339	.0250	.1407	.0250	.1521
-.0250	.1137	-.0167	.1227	-.0083	.1315	.0083	.1375	.0167	.1454	.0167	.1571
-.0333	.1156	-.0250	.1250	-.0167	.1337	0	.1406	.0083	.1491	.0083	.1612
-.0417	.1170	-.0333	.1267	-.0250	.1358	-.0083	.1431	0	.1521	0	.1643
-.0500	.1182	-.0417	.1282	-.0333	.1377	-.0167	.1453	-.0083	.1549	-.0083	.1672
-.0583	.1192	-.0500	.1296	-.0417	.1394	-.0250	.1472	-.0167	.1571	-.0167	.1694
-.0667	.1198	-.0583	.1306	-.0500	.1408	-.0333	.1492	-.0250	.1592	-.0250	.1715
-.0750	.1202	-.0667	.1317	-.0583	.1420	-.0417	.1508	-.0333	.1611	-.0333	.1733
-.1268	0	-.0750	.1321	-.0667	.1429	-.0500	.1523	-.0417	.1627	-.0417	.1750
		-.1312	0	-.0750	.1437	-.0583	.1536	-.0500	.1642	-.0500	.1763
				-.0833	.1442	-.0667	.1546	-.0583	.1654	-.0583	.1775
				-.1334	0	-.0750	.1554	-.0667	.1664	-.0667	.1785
						-.0833	.1559	-.0750	.1672	-.0750	.1792
						-.1340	0	-.0833	.1677	-.1285	0
								-.1322	0		

TABLE I.- CROSS-SECTION ORDINATES FOR HL-10 WITH TIP FINS OFF – Concluded

z/l	y/l	z/l	y/l	z/l	y/l	z/l	y/l	z/l	y/l	z/l	y/l
x/l = 0.542		x/l = 0.583		x/l = 0.625		x/l = 0.667		x/l = 0.708		x/l = 0.750	
0.0759	0	0.0741	0	0.0716	0	0.0687	0	0.0654	0	0.0617	0
.0759	.0166	.0741	.0104	.0716	.0104	.0686	.0208	.0653	.0417	.0616	.0625
.0758	.0249	.0740	.0271	.0716	.0271	.0686	.0375	.0651	.0583	.0615	.0791
.0756	.0332	.0735	.0437	.0713	.0437	.0684	.0541	.0650	.0750	.0611	.0958
.0752	.0415	.0726	.0604	.0707	.0604	.0678	.0708	.0643	.0916	.0606	.1125
.0747	.0498	.0710	.0771	.0696	.0771	.0669	.0875	.0634	.1083	.0596	.1291
.0740	.0581	.0671	.0937	.0678	.0937	.0655	.1041	.0617	.1250	.0581	.1458
.0730	.0664	.0668	.1020	.0655	.1104	.0634	.1208	.0596	.1416	.0561	.1624
.0718	.0747	.0651	.1104	.0637	.1187	.0601	.1374	.0582	.1499	.0533	.1791
.0705	.0830	.0626	.1187	.0616	.1270	.0580	.1458	.0563	.1583	.0488	.1958
.0688	.0913	.0596	.1270	.0591	.1354	.0553	.1541	.0542	.1666	.0458	.2041
.0666	.0996	.0563	.1354	.0558	.1437	.0522	.1624	.0517	.1749	.0421	.2124
.0642	.1079	.0521	.1437	.0521	.1520	.0483	.1708	.0487	.1833	.0372	.2207
.0611	.1162	.0471	.1520	.0478	.1604	.0439	.1791	.0446	.1916	.0333	.2256
.0575	.1245	.0412	.1604	.0429	.1687	.0385	.1874	.0398	.1999	.0292	.2307
.0530	.1328	.0337	.1687	.0365	.1770	.0317	.1958	.0340	.2083	.0250	.2347
.0476	.1411	.0250	.1756	.0292	.1842	.0250	.2015	.0292	.2130	.0167	.2409
.0410	.1494	.0167	.1813	.0250	.1878	.0167	.2080	.0250	.2168	.0083	.2447
.0326	.1577	.0083	.1860	.0167	.1941	.0083	.2128	.0167	.2235	0	.2470
.0249	.1629	0	.1897	.0083	.1991	0	.2167	.0083	.2283	-.0083	.2491
.0166	.1685	-.0083	.1926	0	.2028	-.0083	.2197	0	.2317	-.0167	.2504
.0083	.1729	-.0167	.1949	-.0083	.2057	-.0167	.2218	-.0083	.2343	-.0250	.2511
0	.1764	-.0250	.1970	-.0167	.2080	-.0250	.2237	-.0167	.2363	-.0785	0
-.0083	.1790	-.0333	.1988	-.0250	.2101	-.0333	.2254	-.0250	.2378		
-.0166	.1815	-.0417	.2003	-.0333	.2118	-.0417	.2264	-.0333	.2390		
-.0249	.1834	-.0500	.2017	-.0417	.2132	-.0986	0	-.0889	0		
-.0332	.1853	-.0583	.2028	-.0500	.2143						
-.0415	.1869	-.1156	0	-.1073	0						
-.0498	.1882										
-.0581	.1893										
-.0664	.1902										
-.1229	0										
x/l = 0.792		x/l = 0.833		x/l = 0.875		x/l = 0.917		x/l = 0.958		x/l = 1.000	
0.0578	0	0.0536	0	0.0487	0	0.0440	0	0.0392	0	0.0344	0
.0577	.0937	.0534	.1666	-.0452	0	-.0341	0	-.0227	0	-.0125	0
.0576	.1104	.0532	.1833								
.0573	.1270	.0528	.1999								
.0569	.1437	.0521	.2166								
.0561	.1604	.0510	.2332								
.0549	.1770	.0482	.2499								
.0532	.1937	.0455	.2582								
.0506	.2103	.0400	.2666								
.0486	.2187	.0333	.2707								
.0460	.2270	.0250	.2736								
.0425	.2353	.0167	.2749								
.0375	.2437	.0083	.2753								
.0333	.2481	0	.2753								
.0250	.2551	-.0563	0								
.0167	.2588										
.0083	.2611										
0	.2624										
-.0083	.2631										
-.0167	.2634										
-.0673	0										

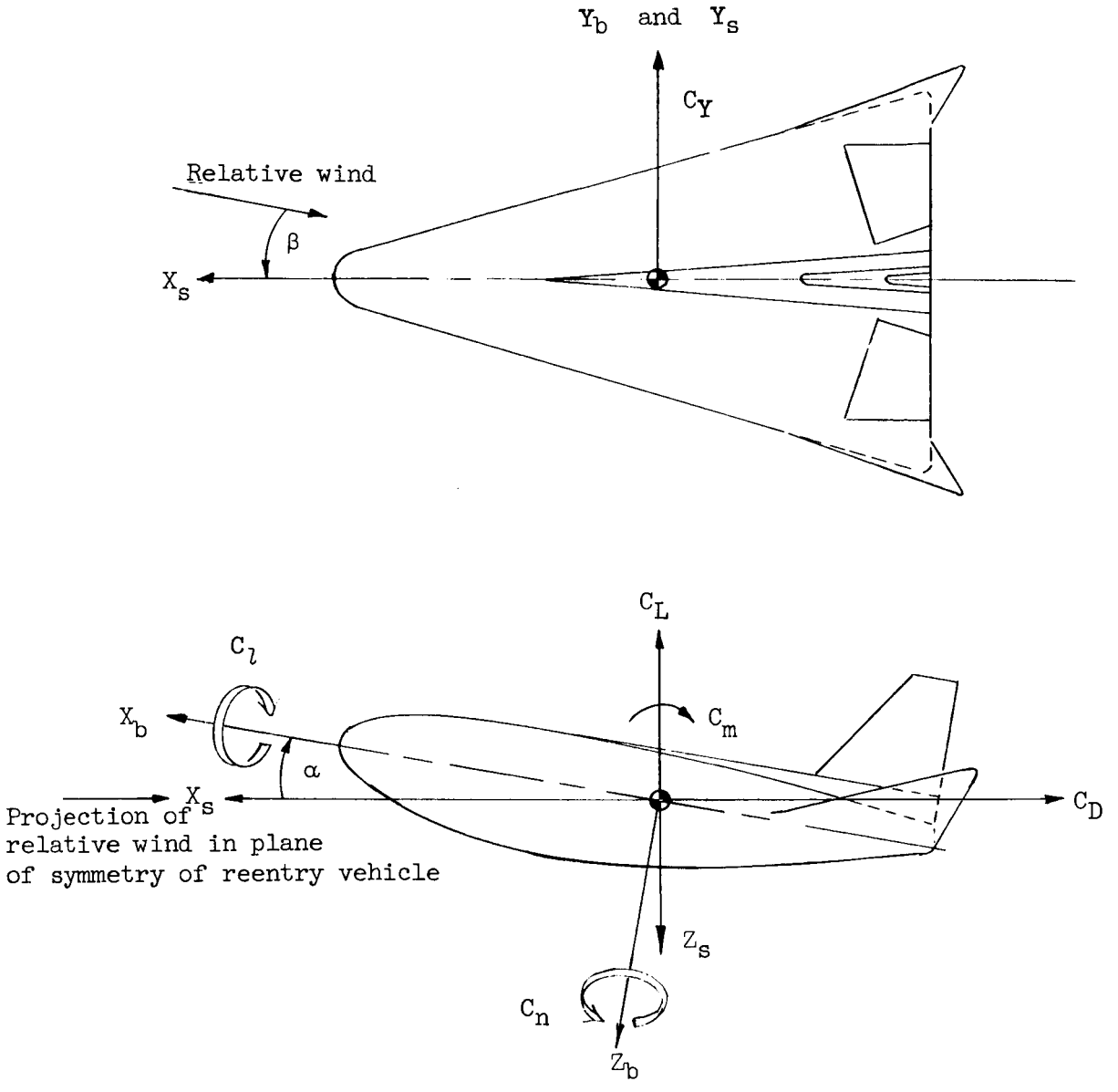

Figure 1. Stability and body axes. Arrows indicate positive direction of forces, moments, and angles.

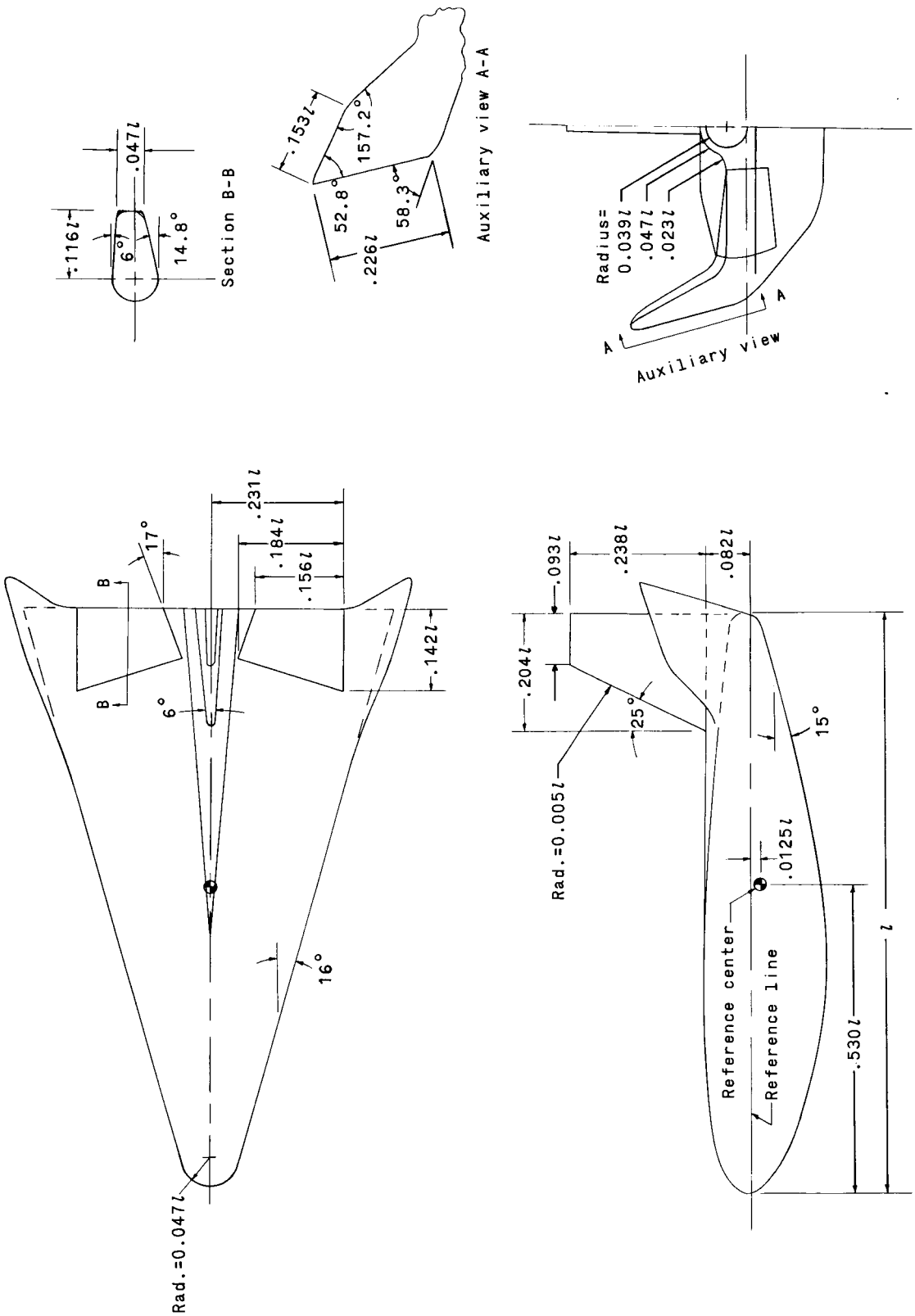

(a) Sketch of HL-10 model. Dimensions given in terms of model length, l = 40.64 cm (16.00 in.).

Figure 2.- Drawings and photograph of HL-10 model.

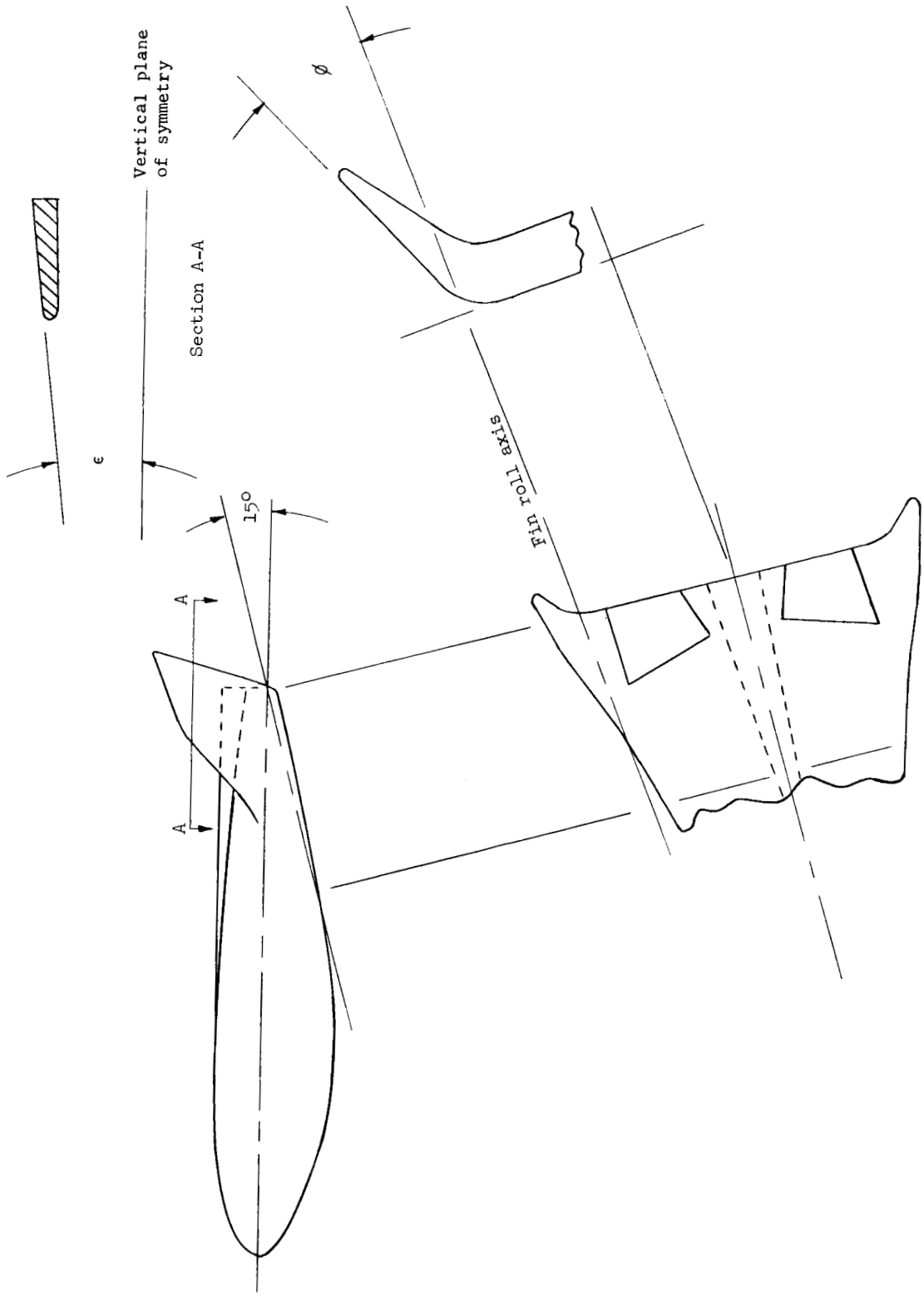

(b) Tip-fin orientation.

Figure 2.- Continued.

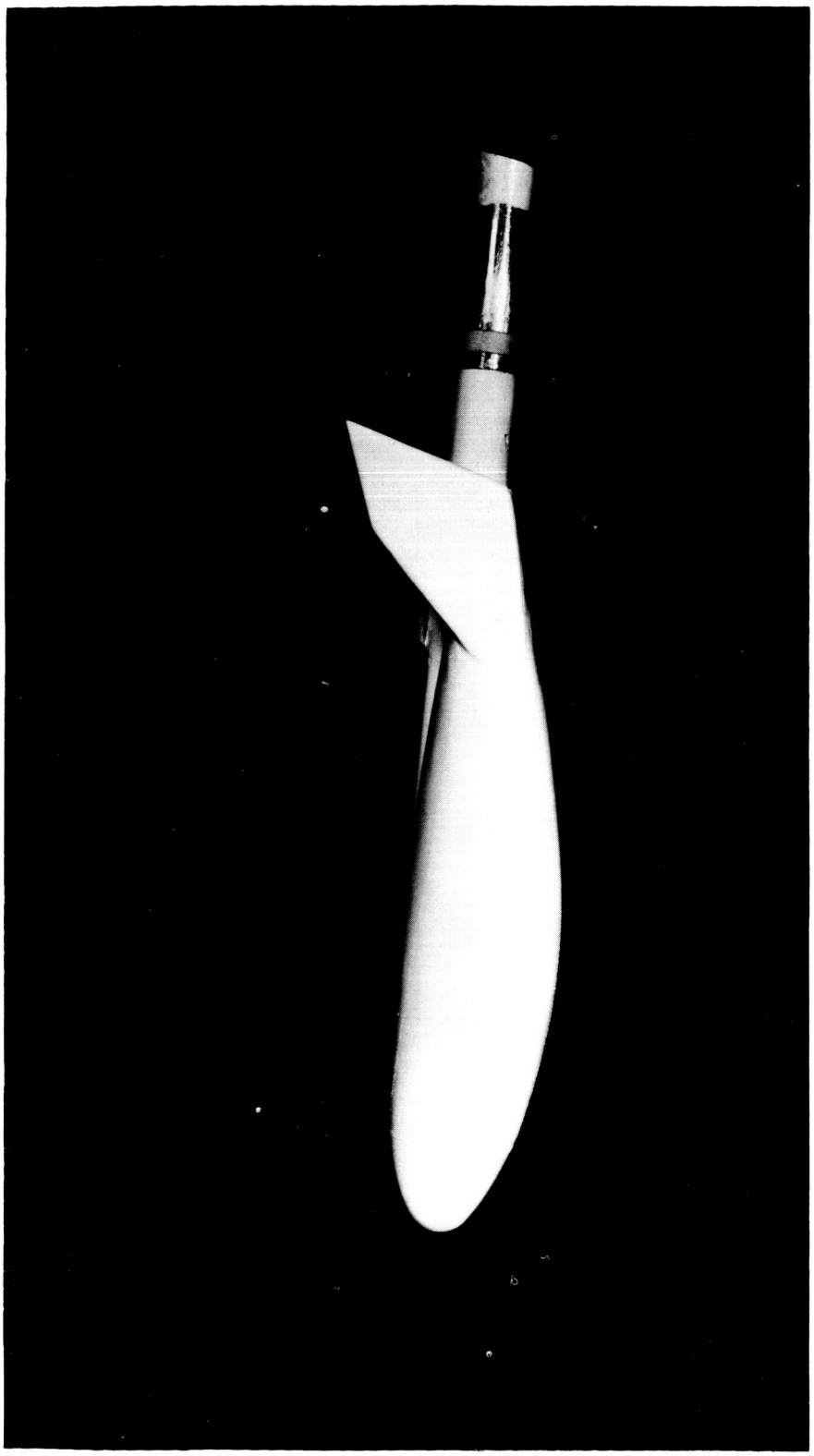

L-64-9883

(c) Photograph of model with center-line dorsal fin E_2 and tip dorsal fins.

Figure 2.- Concluded.

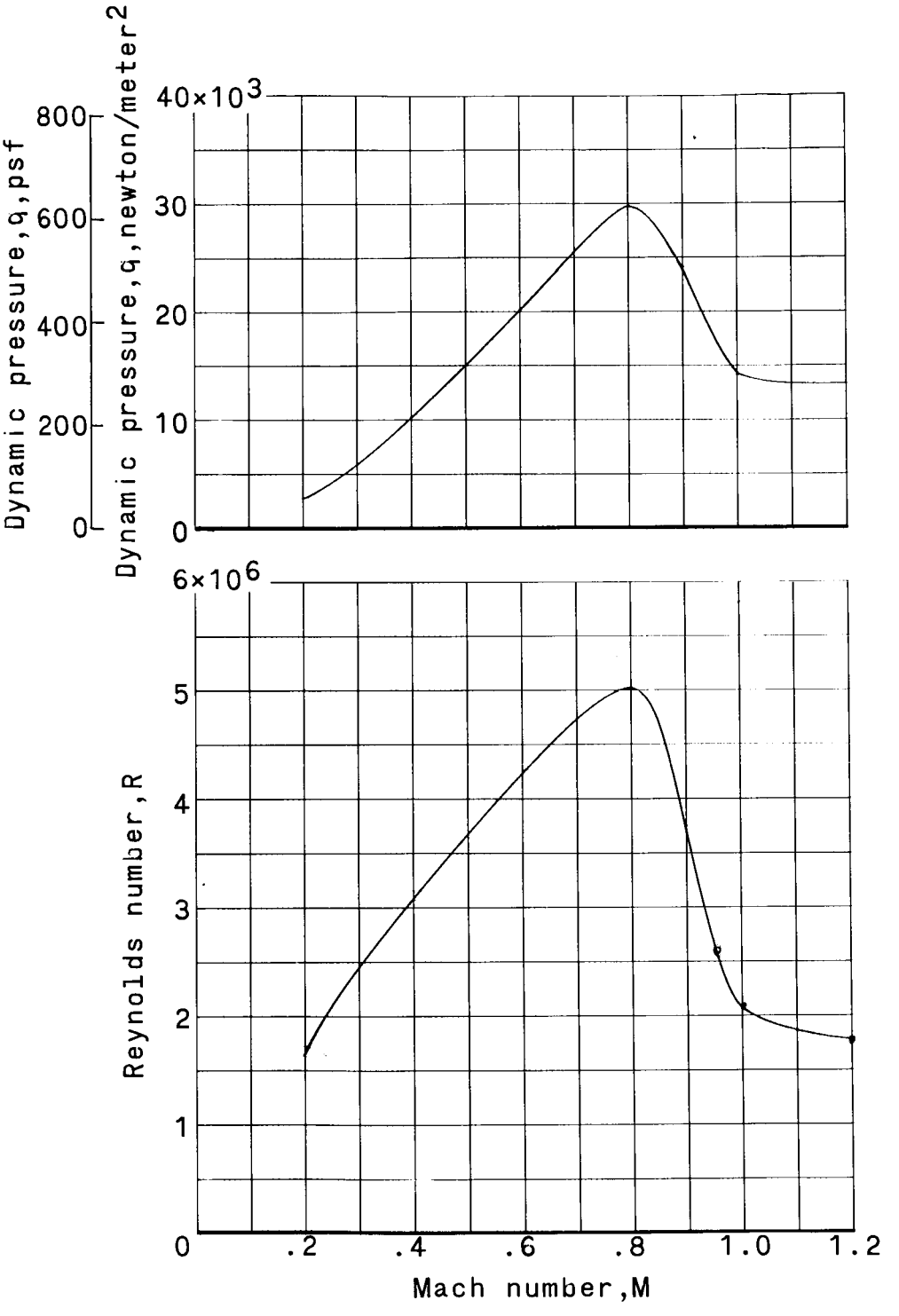

Figure 3.- Variation with Mach number of test Reynolds number based on reference body length, l = 40.640 cm (16.000 in.), and of test dynamic pressure.

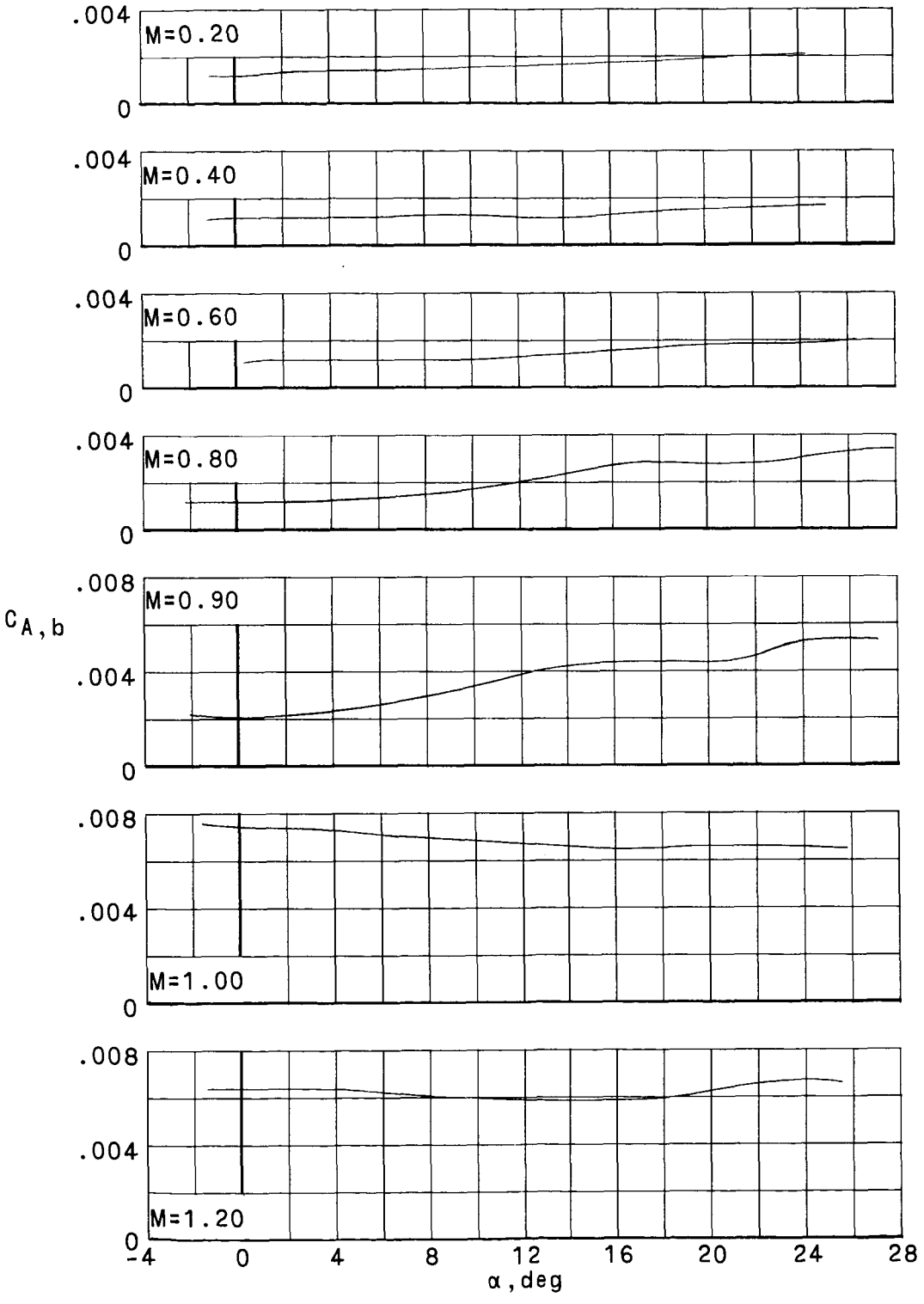

Figure 4.- Base-axial-force adjustment for basic body with center-line fin (E_2) and tip fins (I_3).

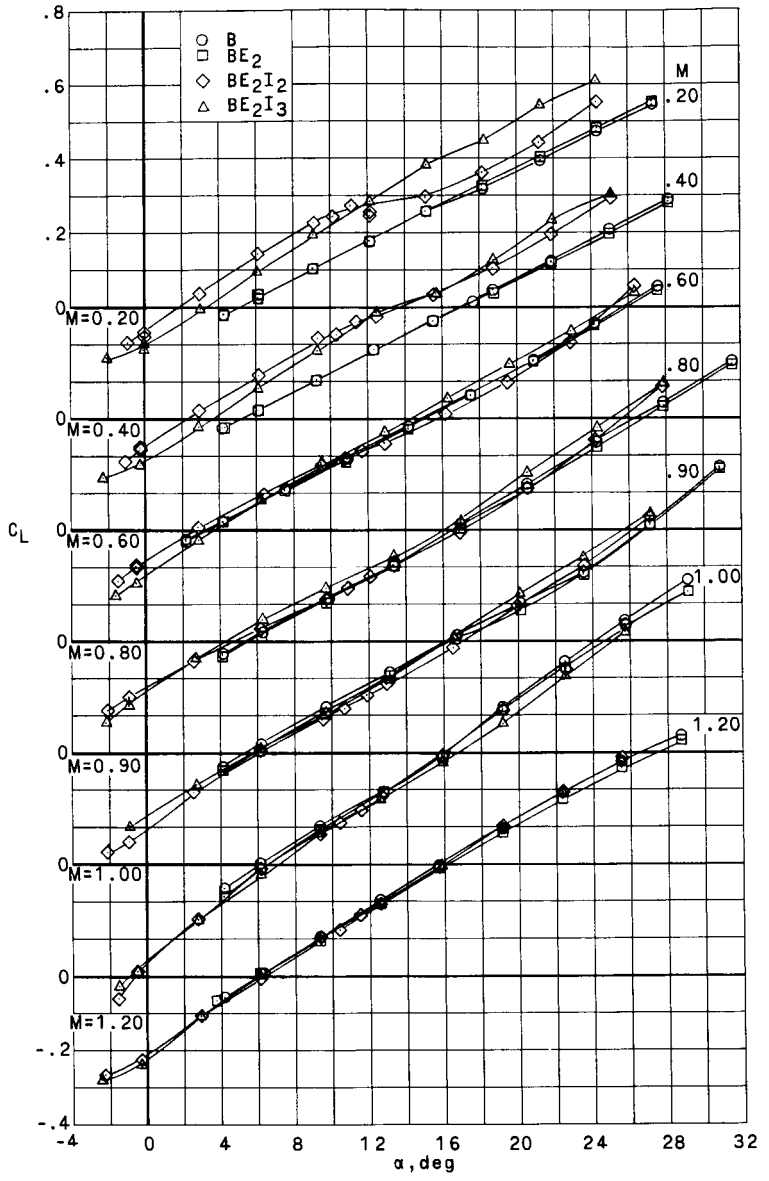

(a) C_L against α.

Figure 5.- Effect of model components on longitudinal aerodynamic characteristics. $\delta_e = \delta_a = 0^0$; $\beta \approx 0^0$.

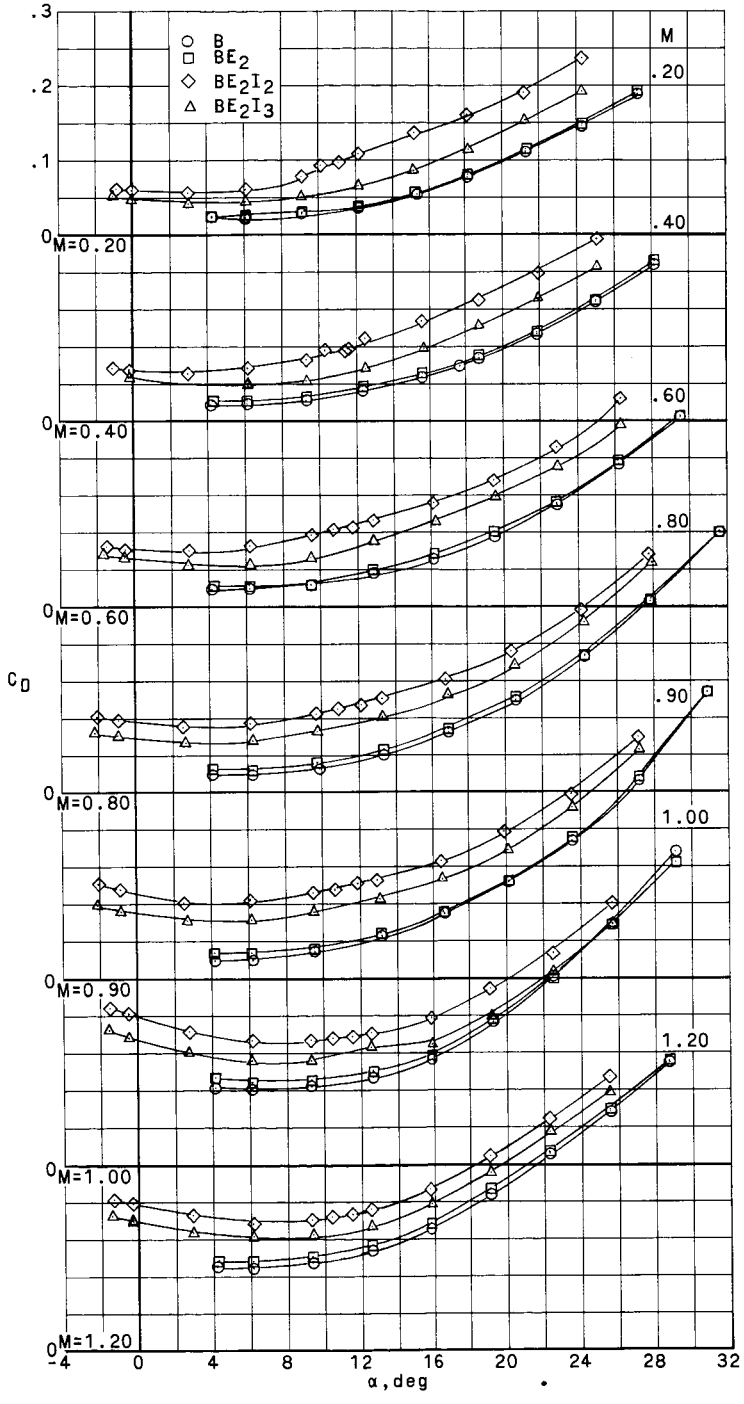

(b) C_D against α.

Figure 5.- Continued.

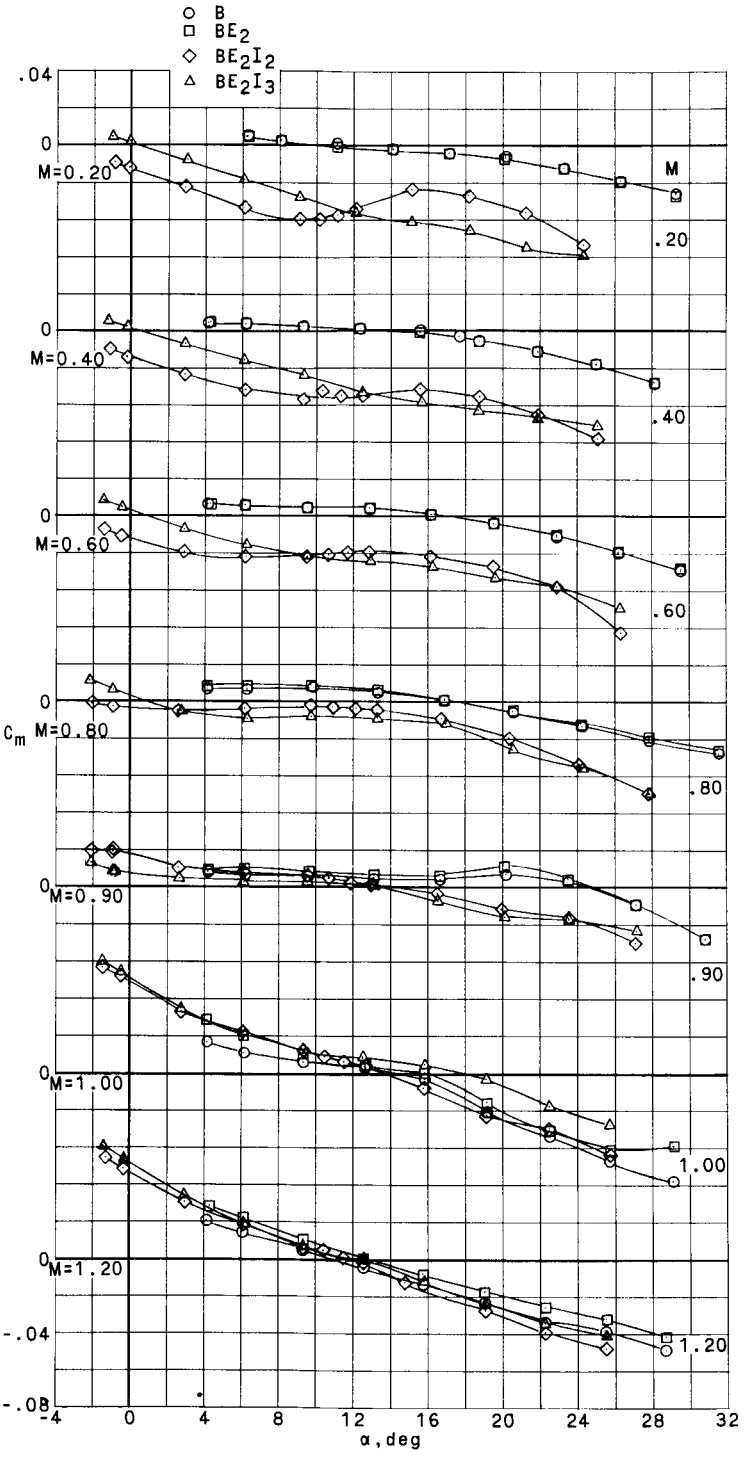

(c) C_m against α.

Figure 5.- Continued.

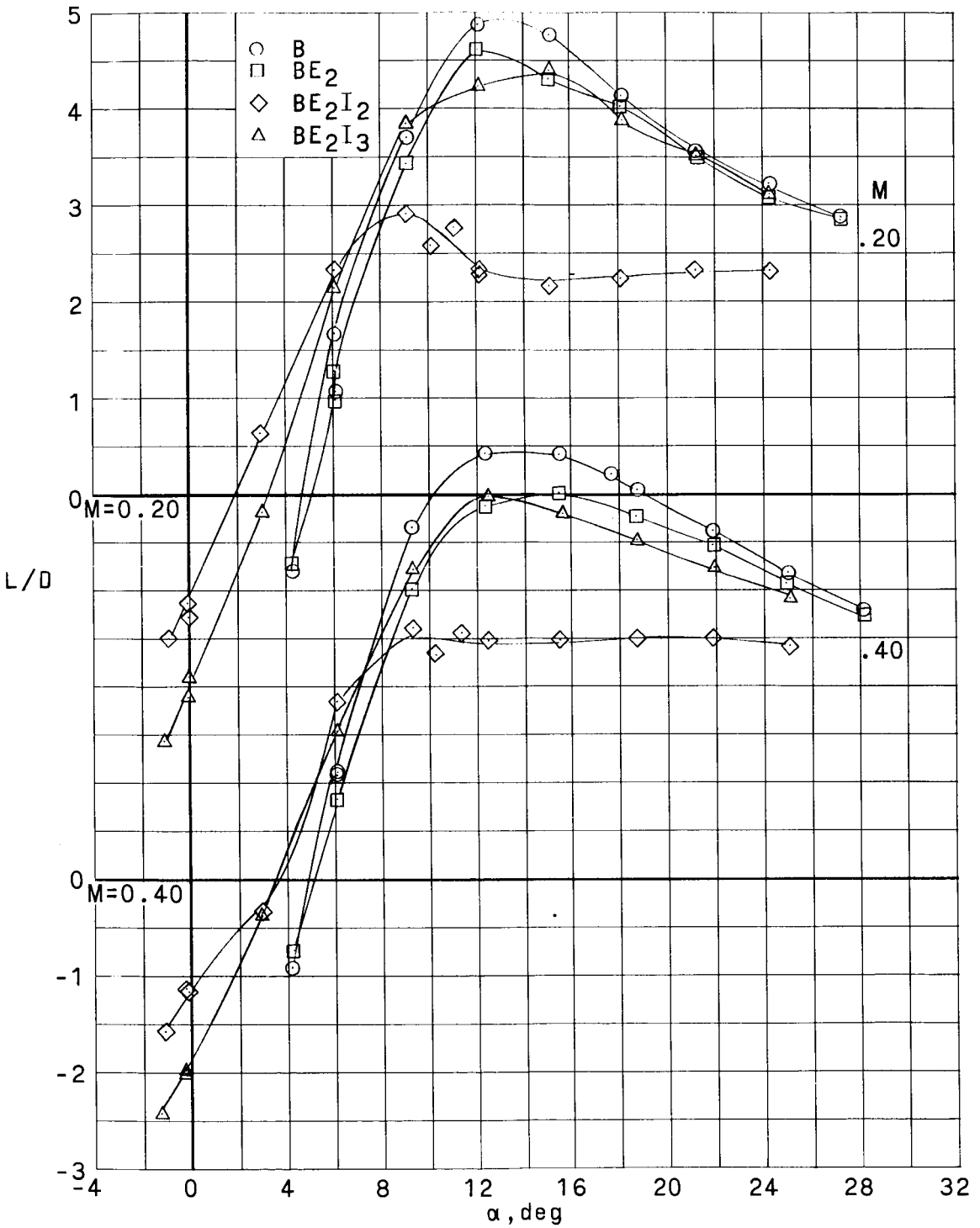

(d) L/D against α.

Figure 5.- Continued.

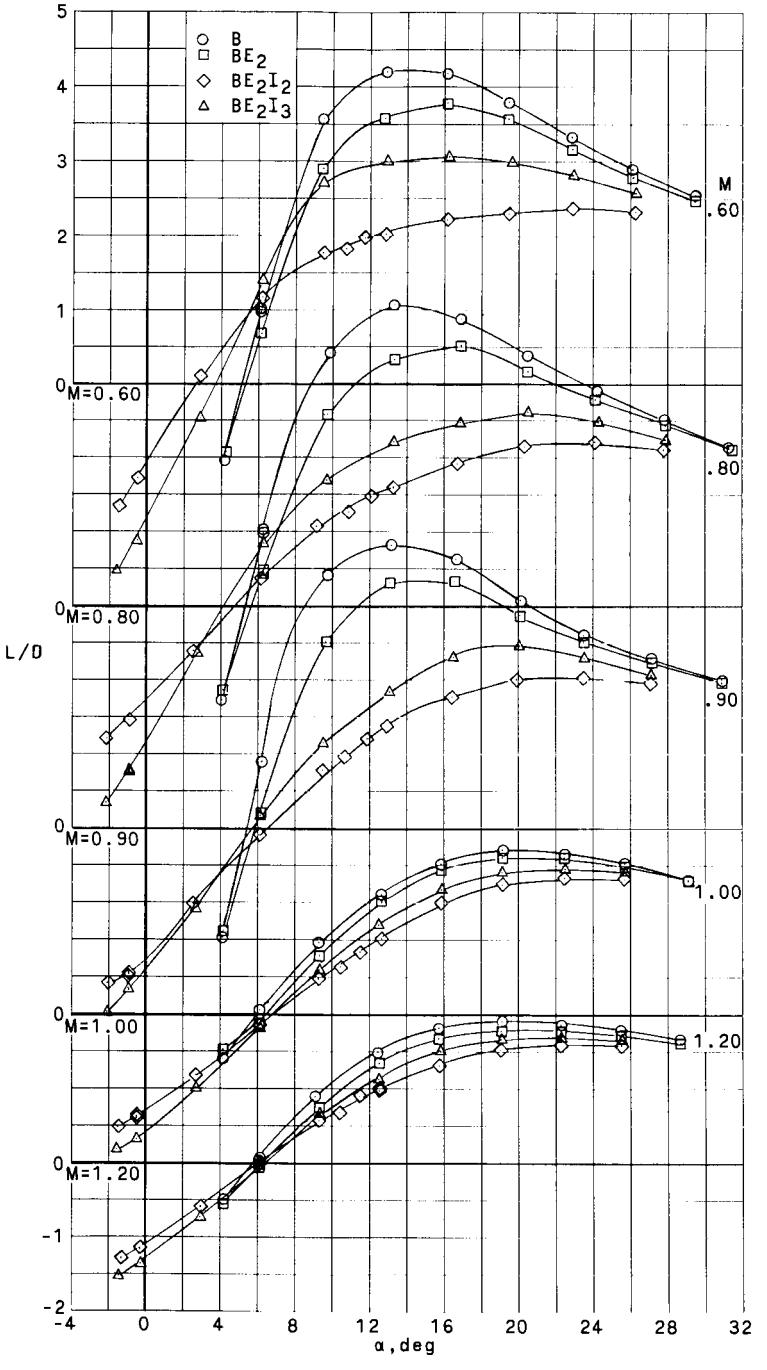

(d) L/D against α. Concluded.

Figure 5.- Concluded.

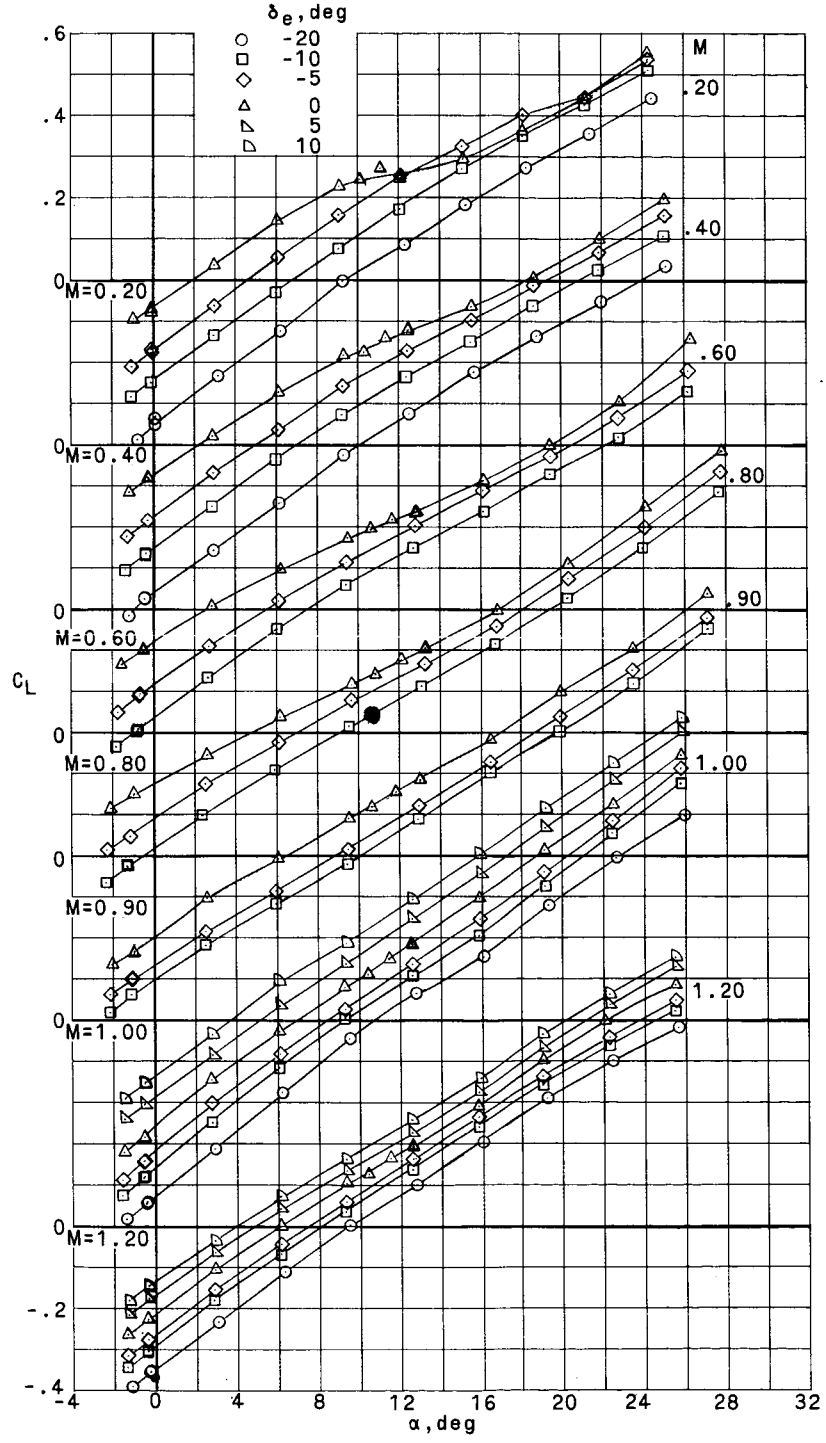

(a) C_L against α.

Figure 6.- Effect of uniform deflection on longitudinal aerodynamic characteristics. BE_2I_2; $\delta_a = 0^0$; $\beta \approx 0^0$.

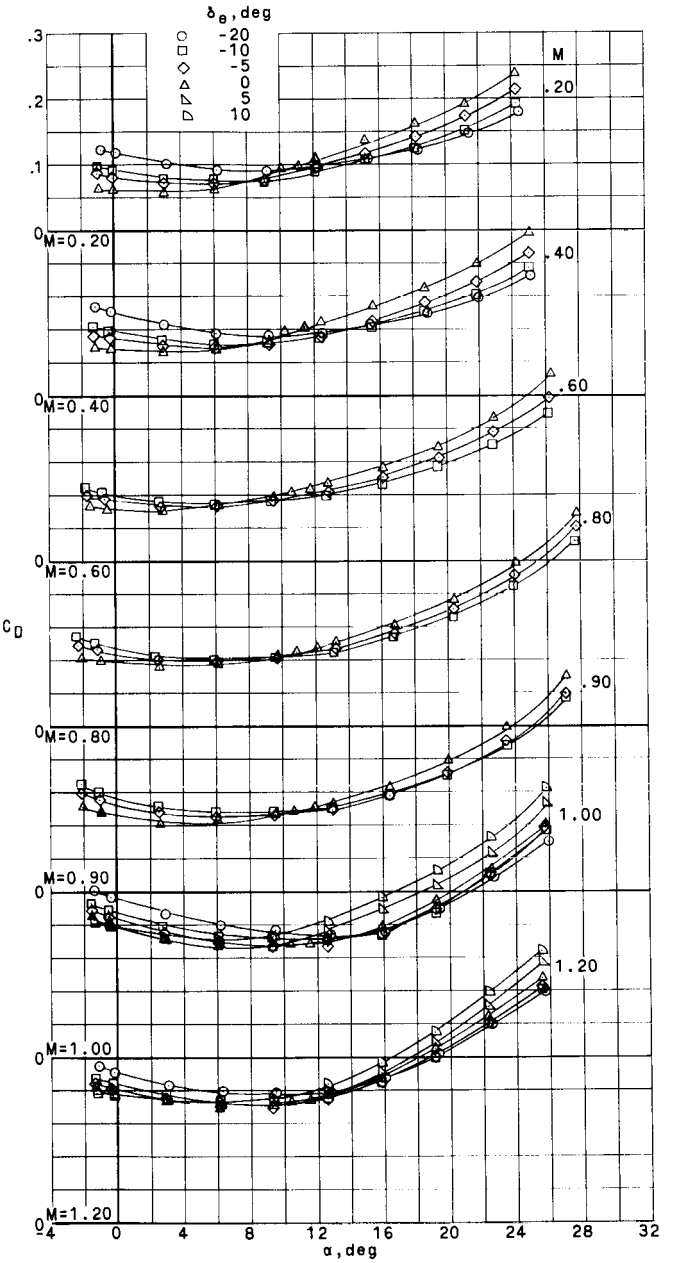

(b) C_D against α.

Figure 6.- Continued.

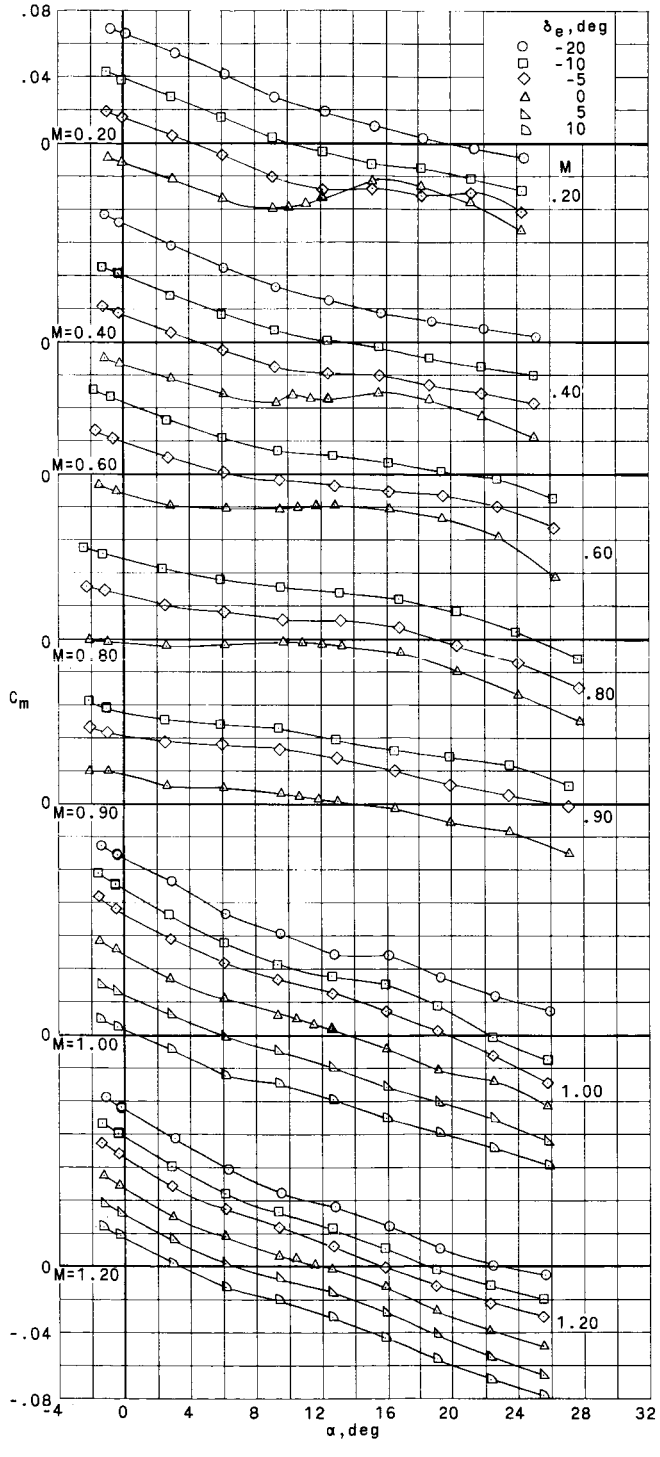

(c) C_m against α.

Figure 6.- Continued.

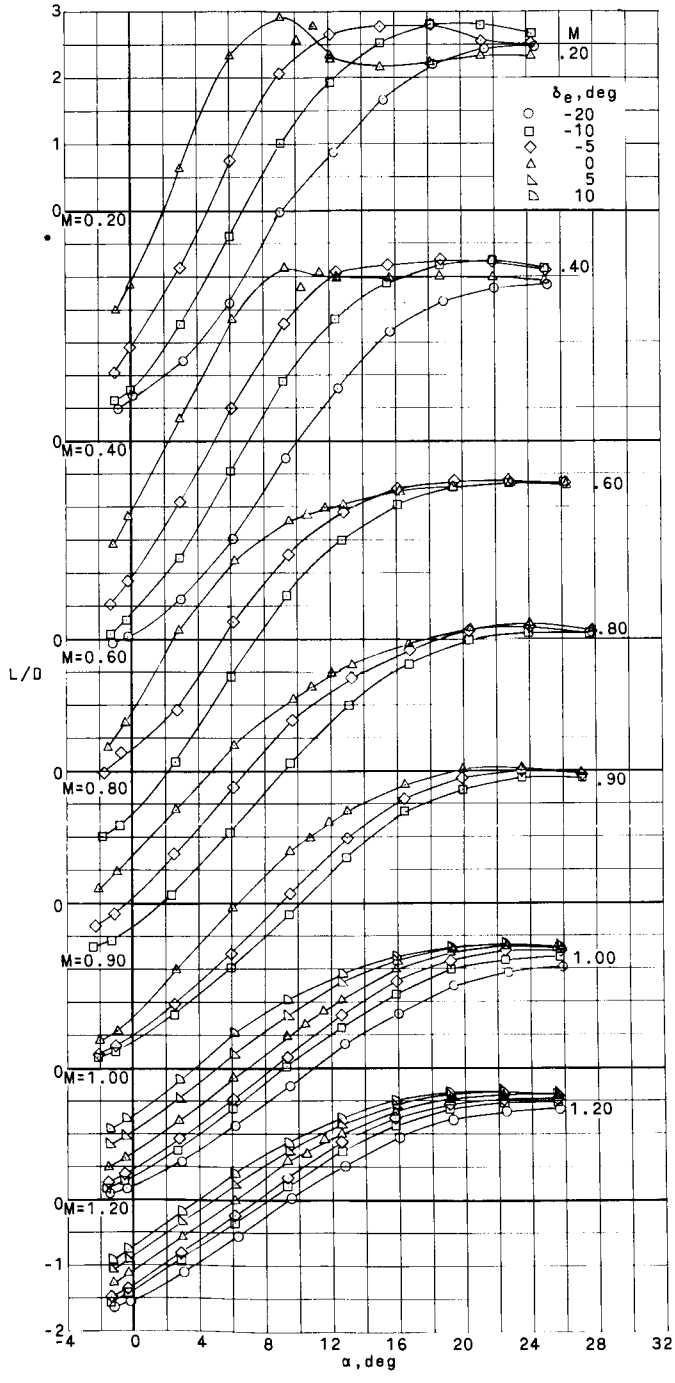

(d) L/D against α.

Figure 6.- Concluded.

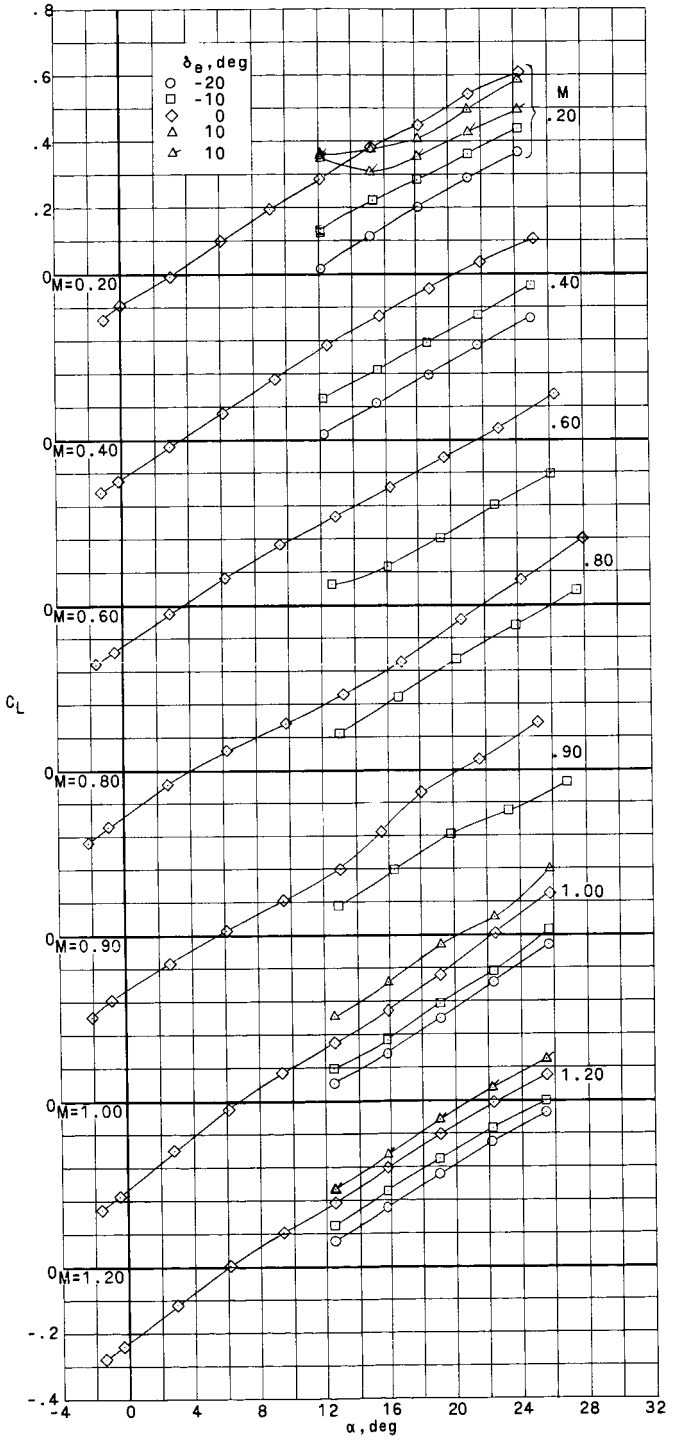

(a) C_L against α.

Figure 7.- Effect of uniform elevon deflection on longitudinal aerodynamic characteristics. BE_2F_3; $\delta_a = 0^0$; $\beta \approx 0^0$. (Flagged symbols indicate transition grit off.)

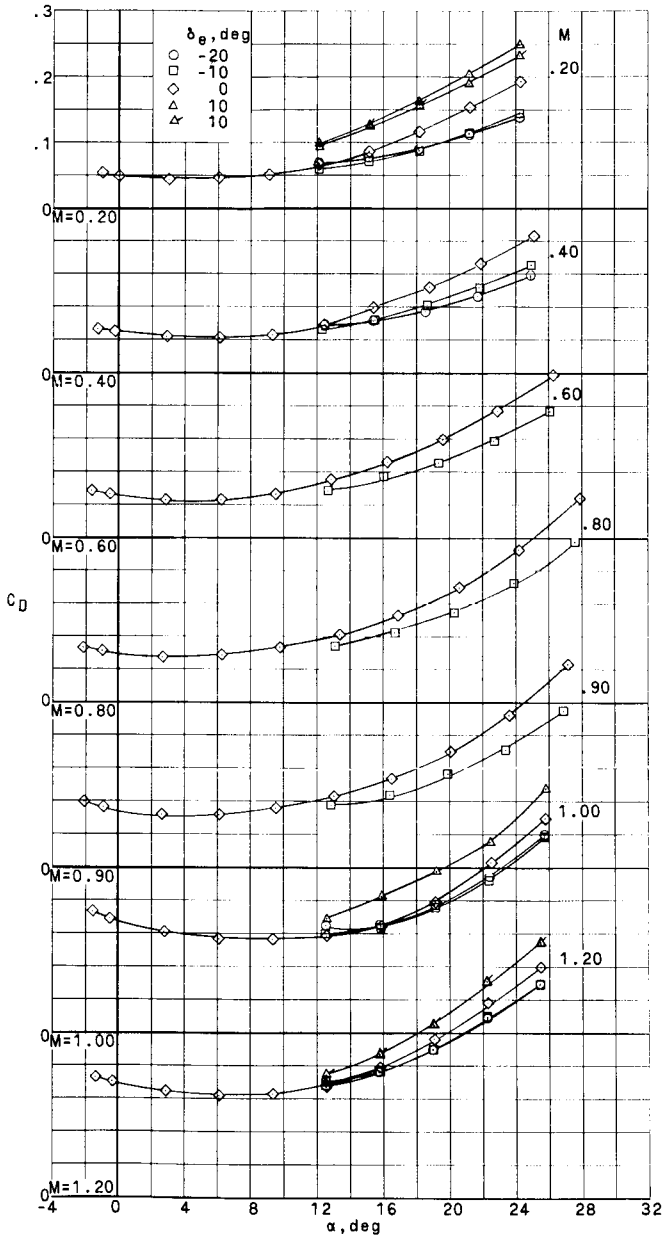

(b) C_D against α.

Figure 7.- Continued.

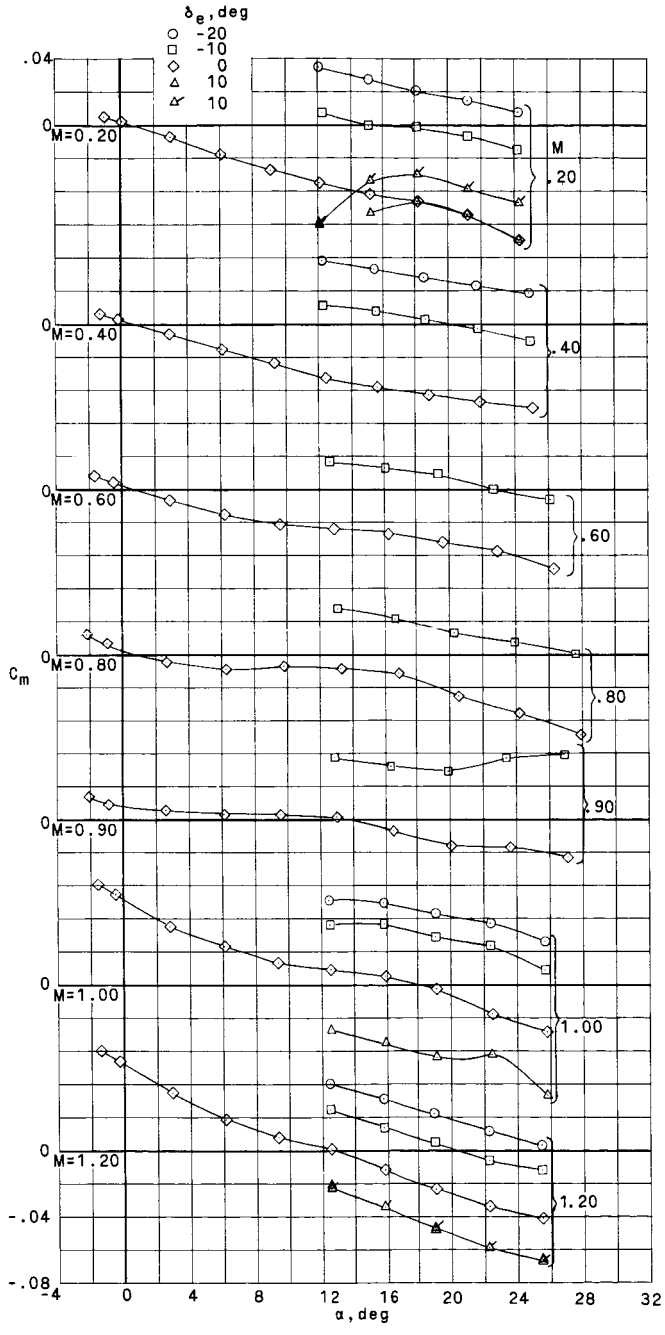

(c) C_m against α.

Figure 7.- Continued.

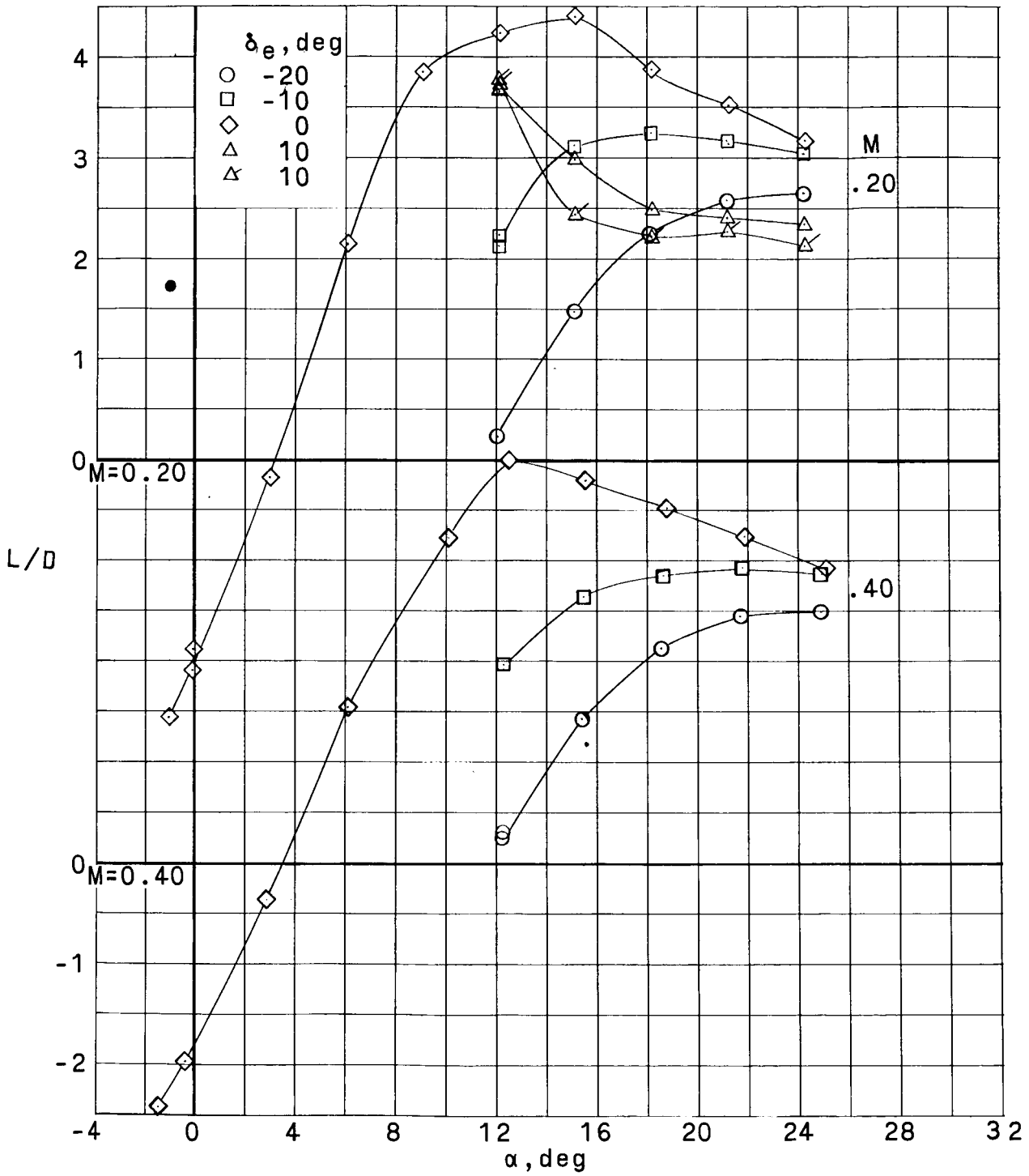

(d) L/D against α.

Figure 7.- Continued.

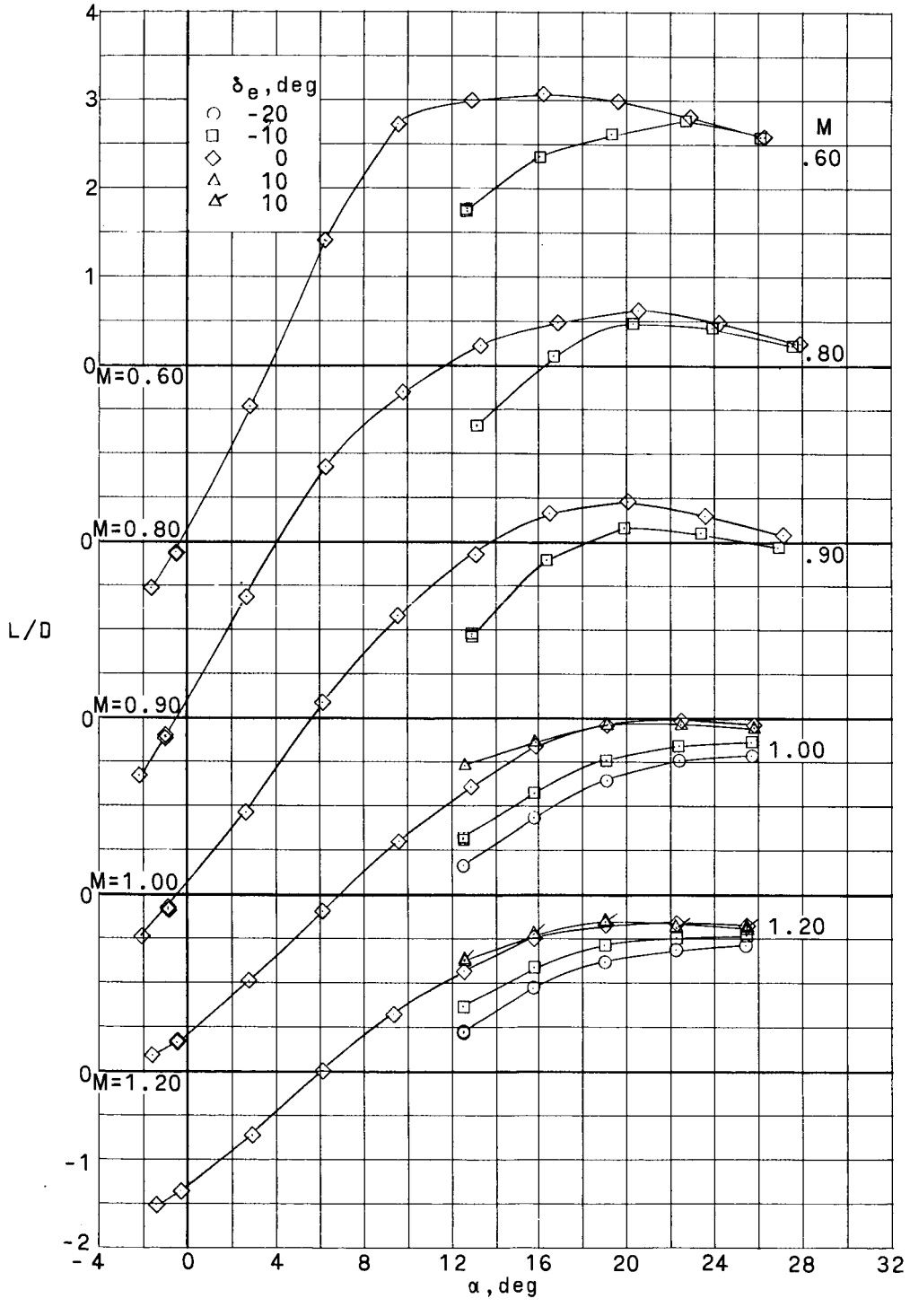

(d) L/D against α. Concluded.

Figure 7.- Concluded.

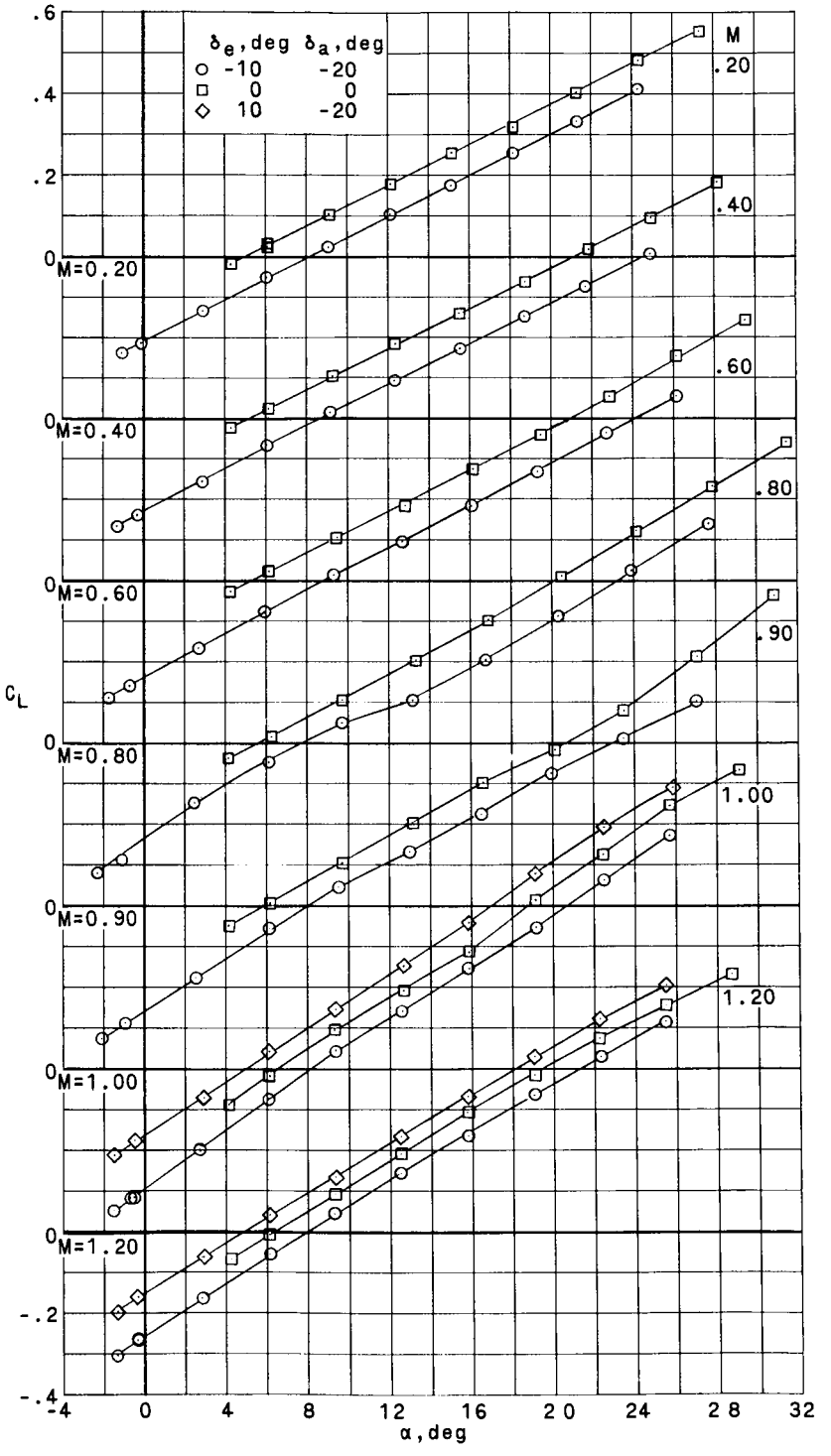

(a) C_L against α.

Figure 8.- Effect of differential elevon deflection on longitudinal aerodynamic characteristics. BE_2; $\beta \approx 0^0$.

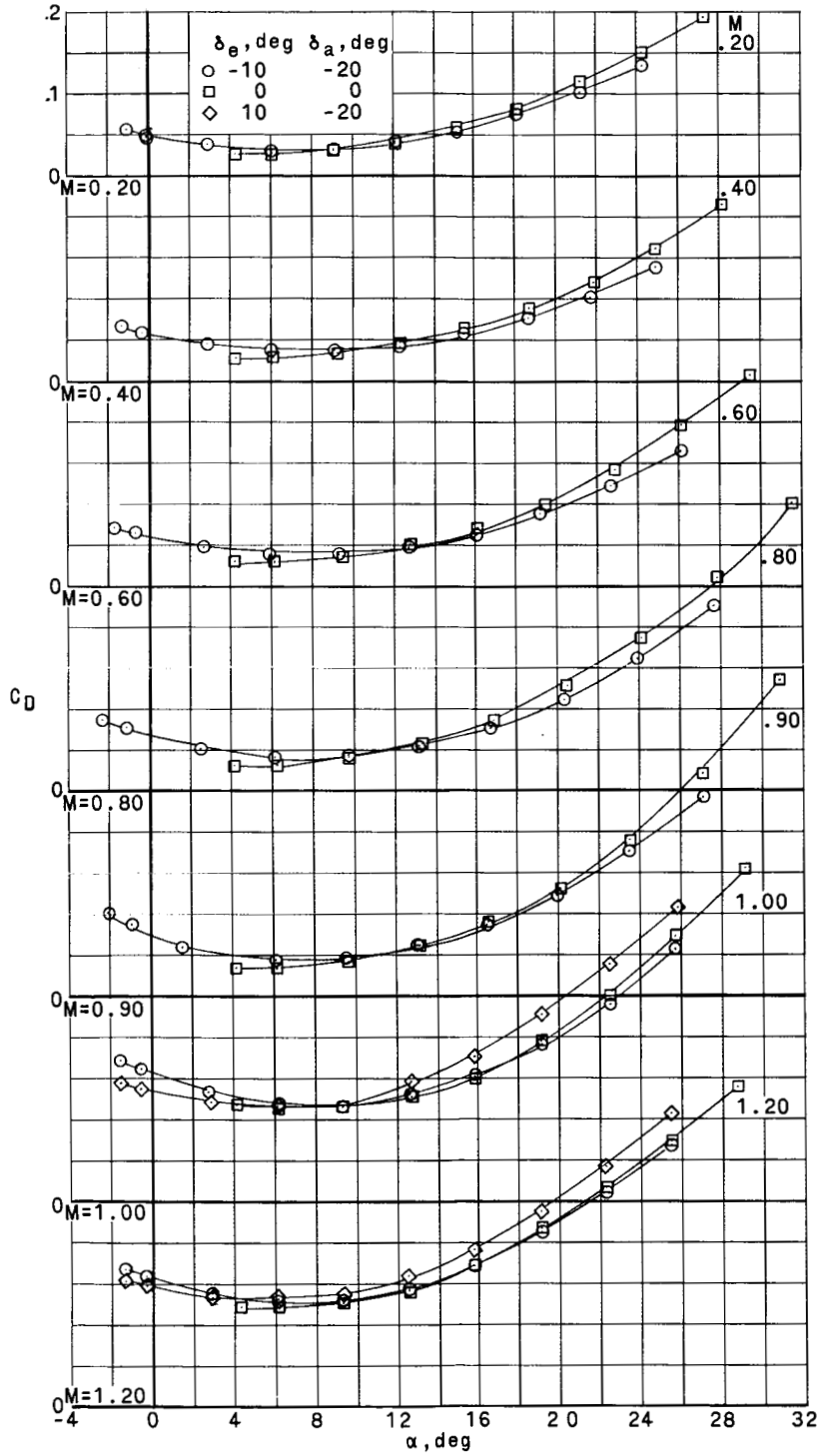

(b) C_D against α.

Figure 8.- Continued.

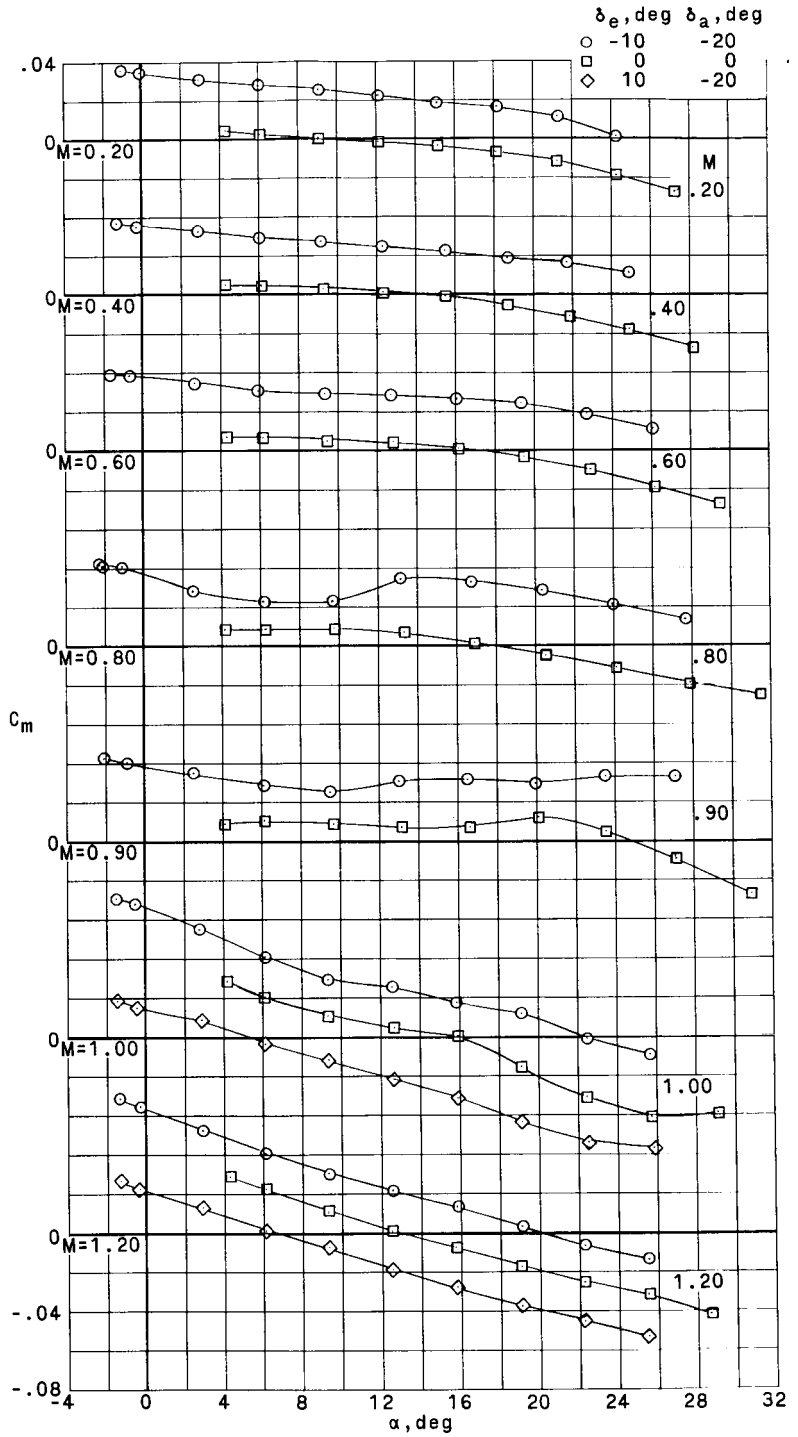

(c) C_m against α.

Figure 8.- Continued.

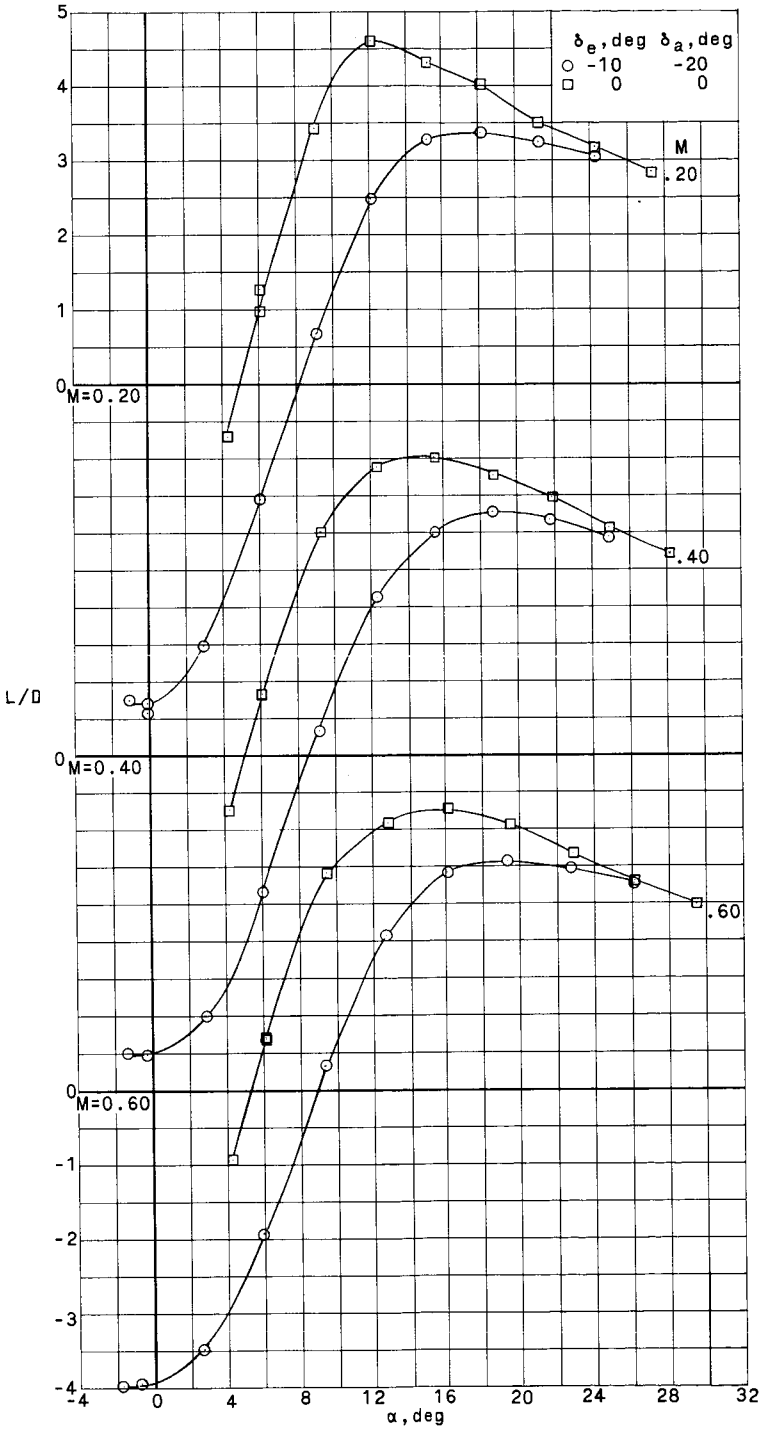

(d) L/D against α.

Figure 8.- Continued.

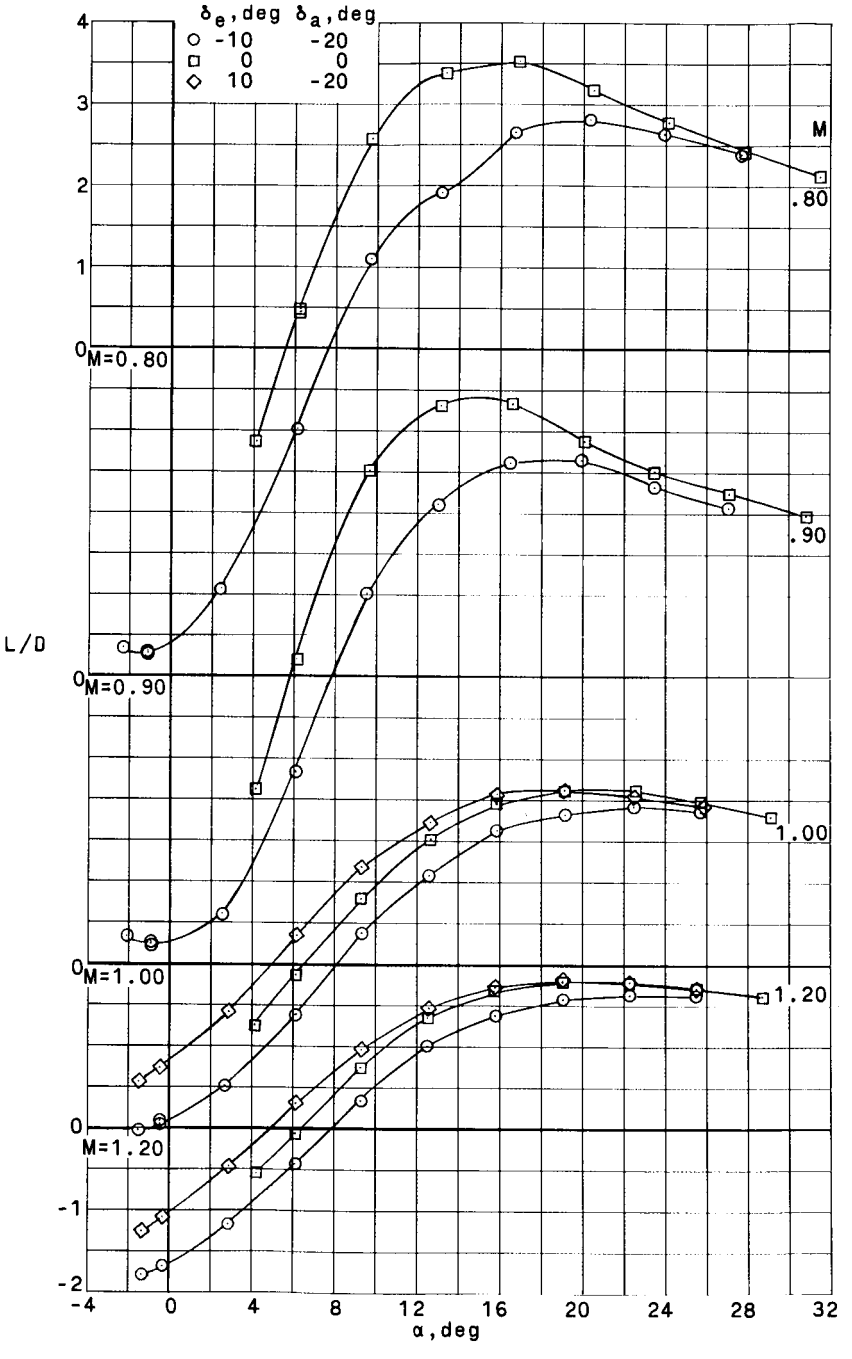

(d) L/D against α. Concluded.

Figure 8.- Concluded.

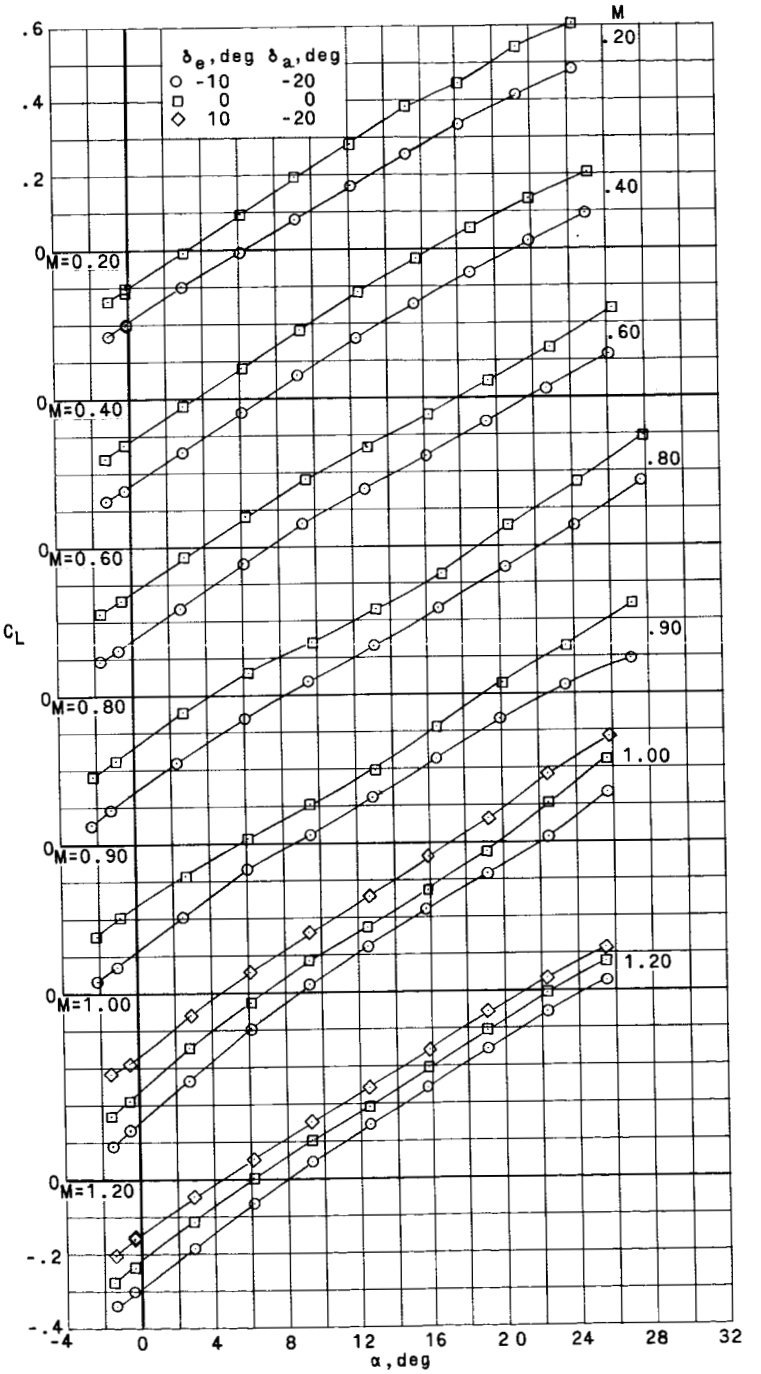

(a) C_L against α.

Figure 9.- Effect of differential elevon deflection on longitudinal aerodynamic characteristics. BE_2I_3; $\beta \approx 0^o$.

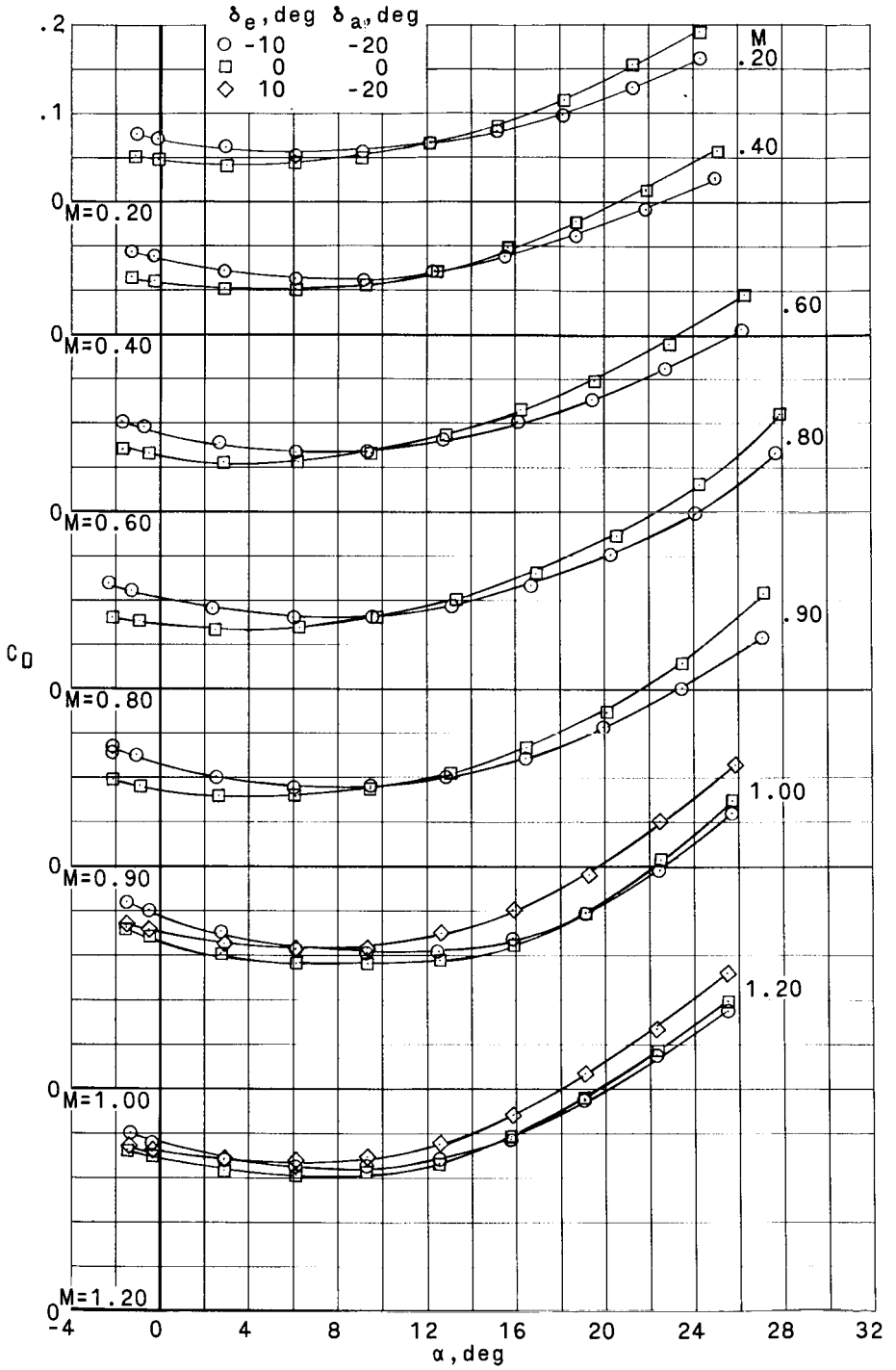

(b) C_D against α.

Figure 9.- Continued.

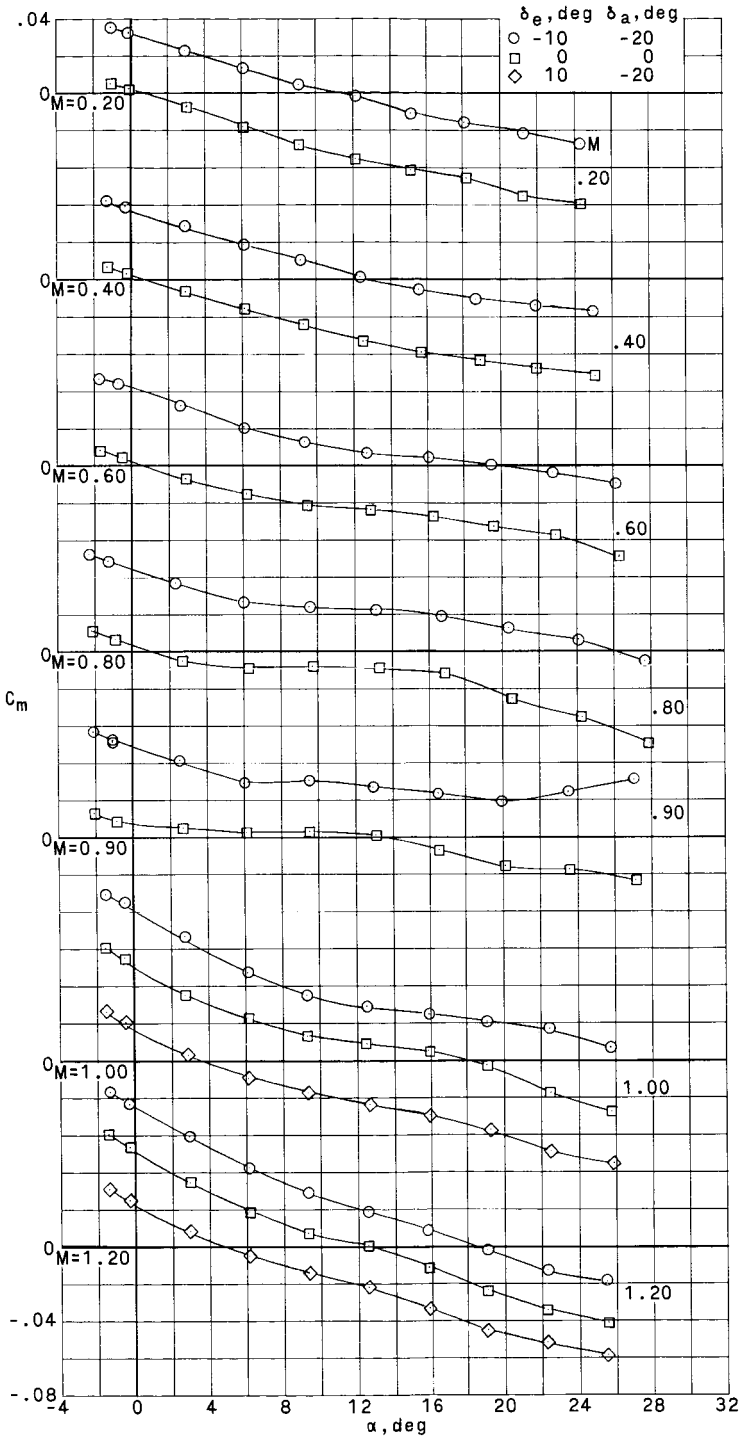

(c) C_m against α.

Figure 9.- Continued.

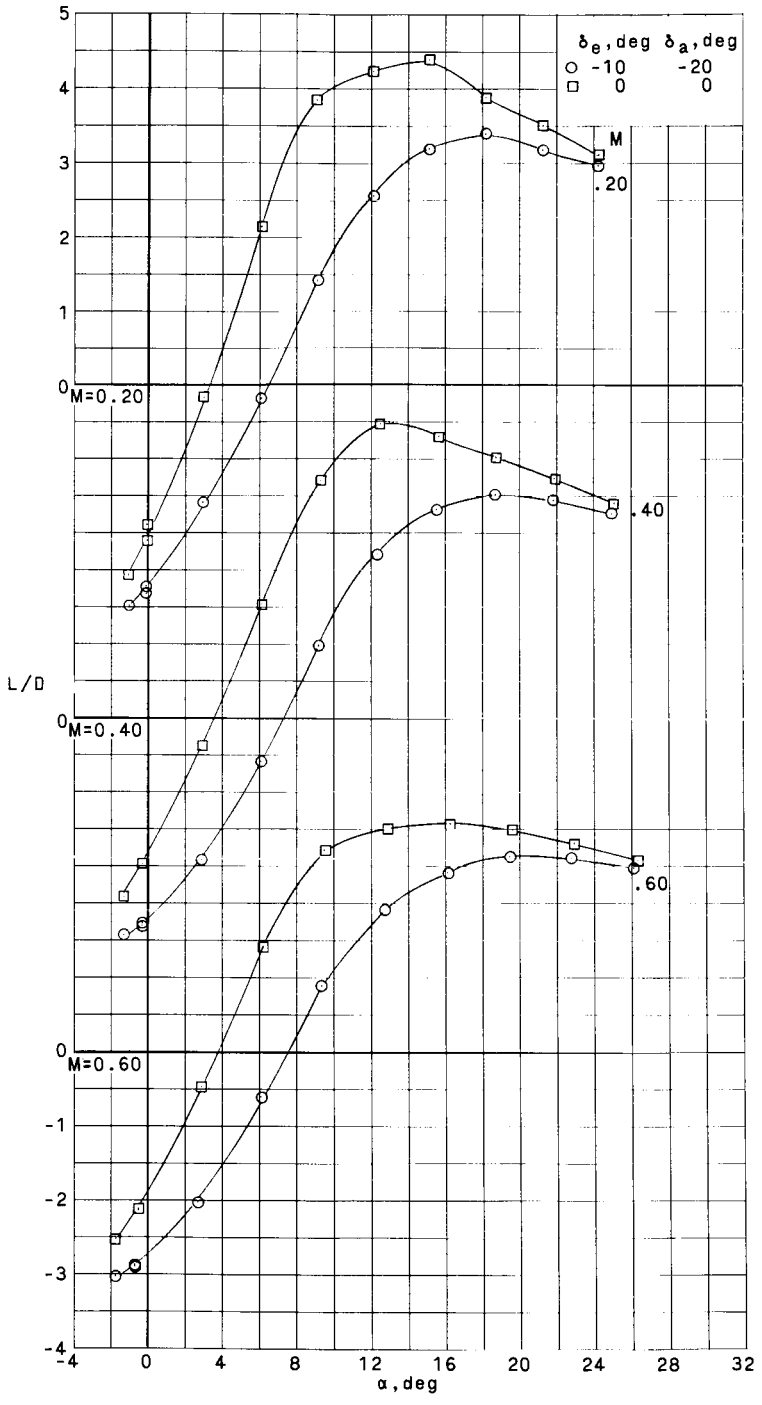

(d) L/D against α.

Figure 9.- Continued.

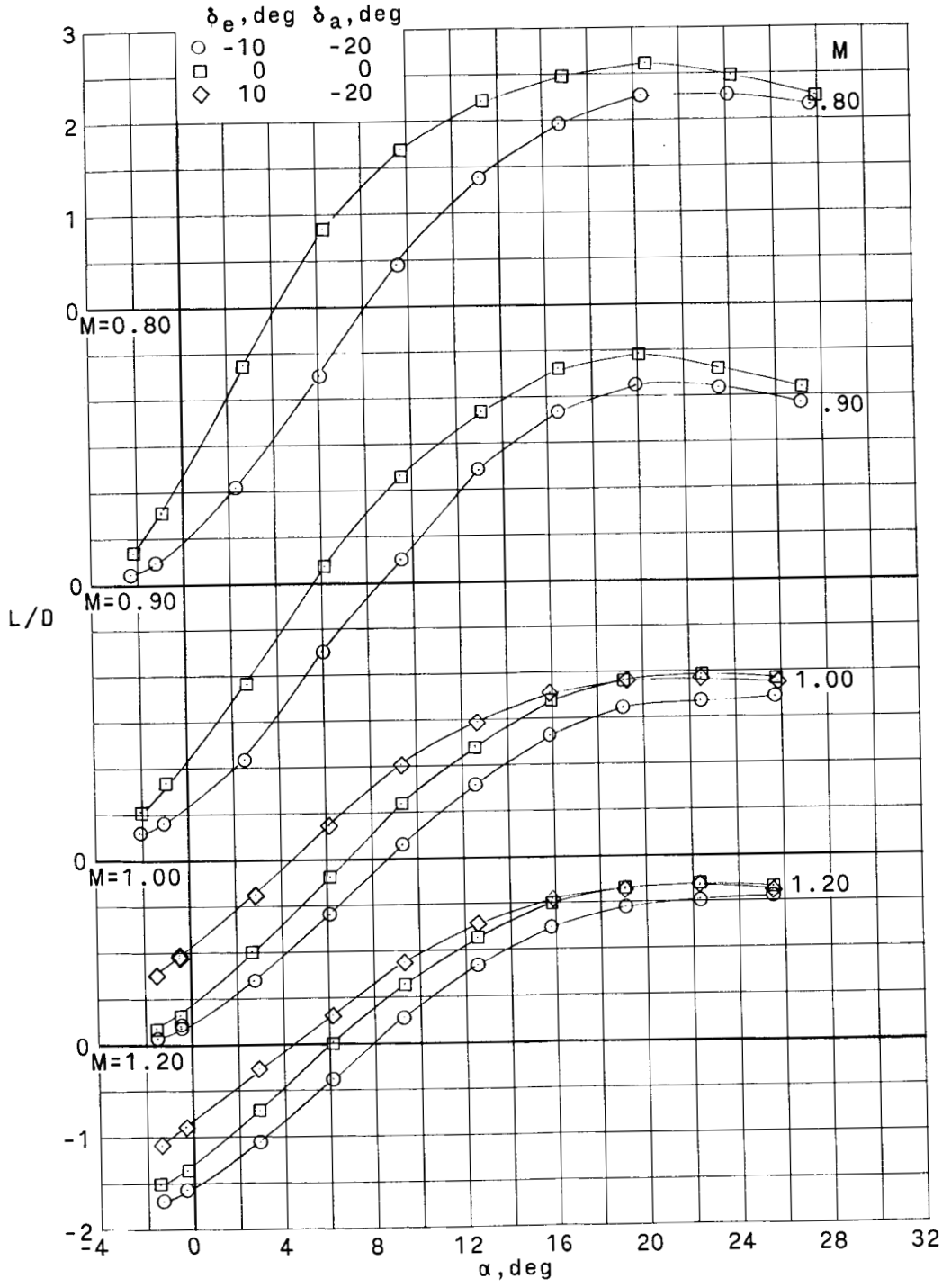

(d) L/D against α. Concluded.

Figure 9.- Concluded.

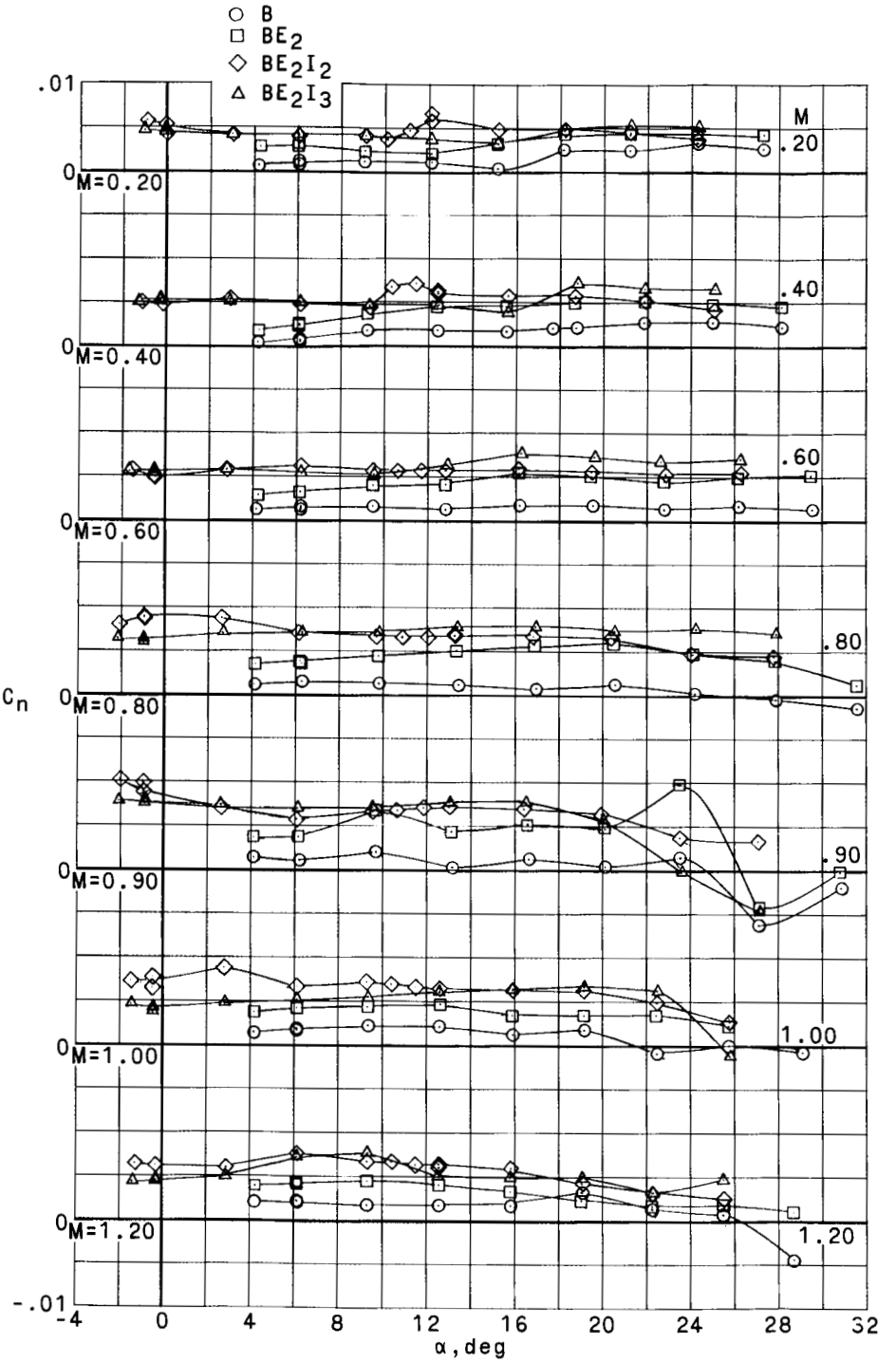

(a) C_n against α, $\beta \approx 0^0$.

Figure 10.- Effect of model components on lateral aerodynamic characteristics. $\delta_e = \delta_a = 0^0$.

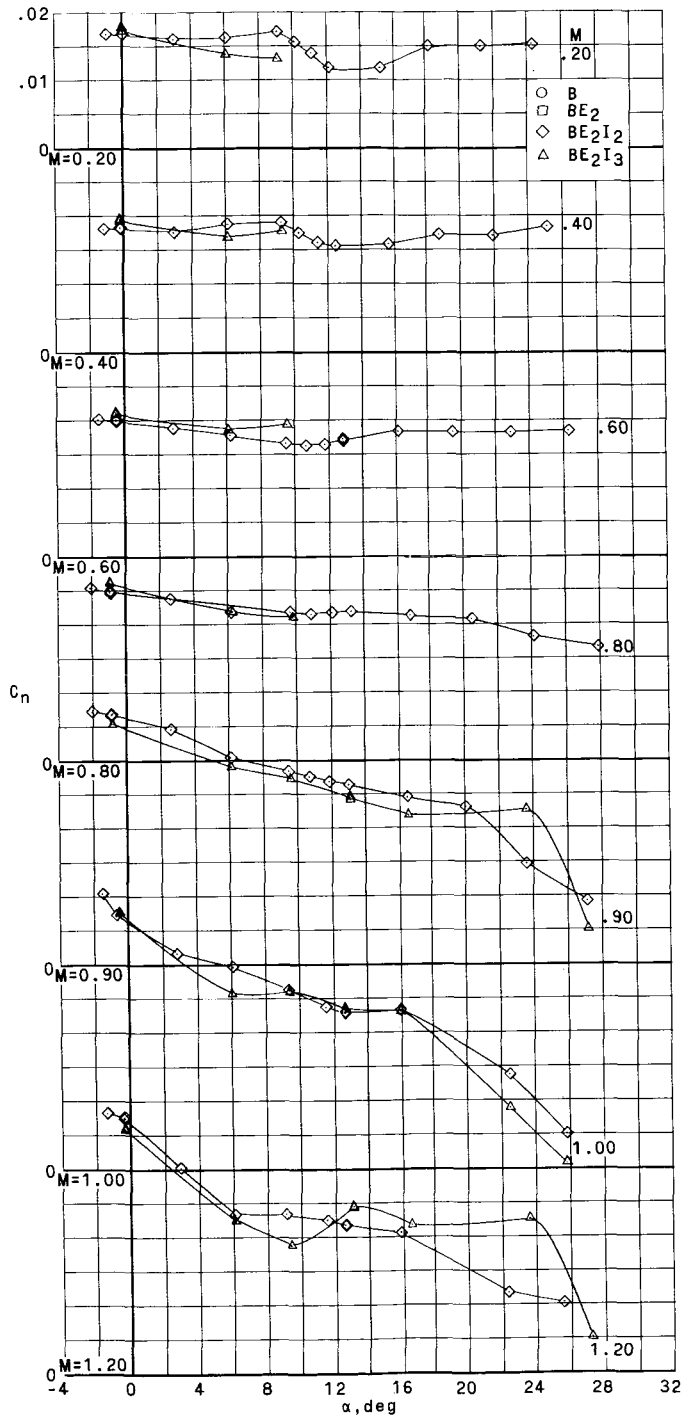

(b) C_n against α, $\beta \approx 3^0$.

Figure 10.- Continued.

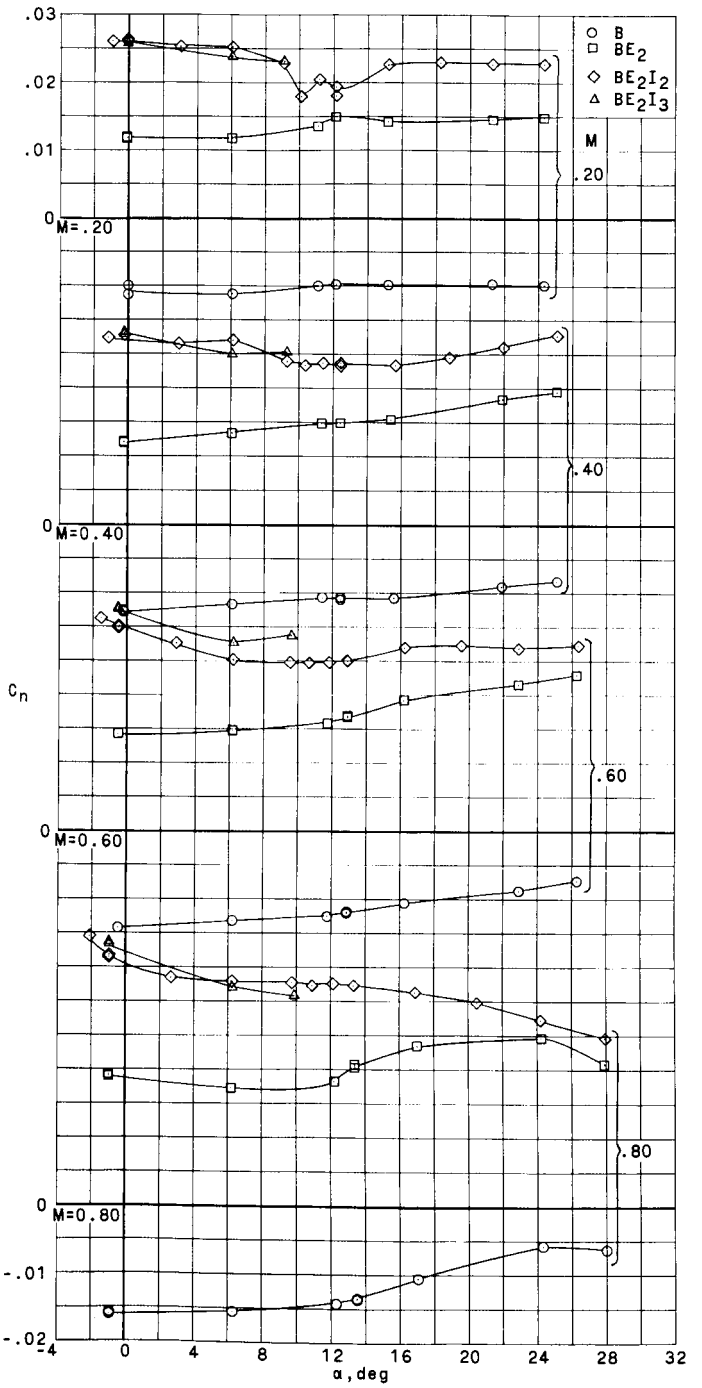

(c) C_n against α, $\beta \approx 5^0$.

Figure 10.- Continued.

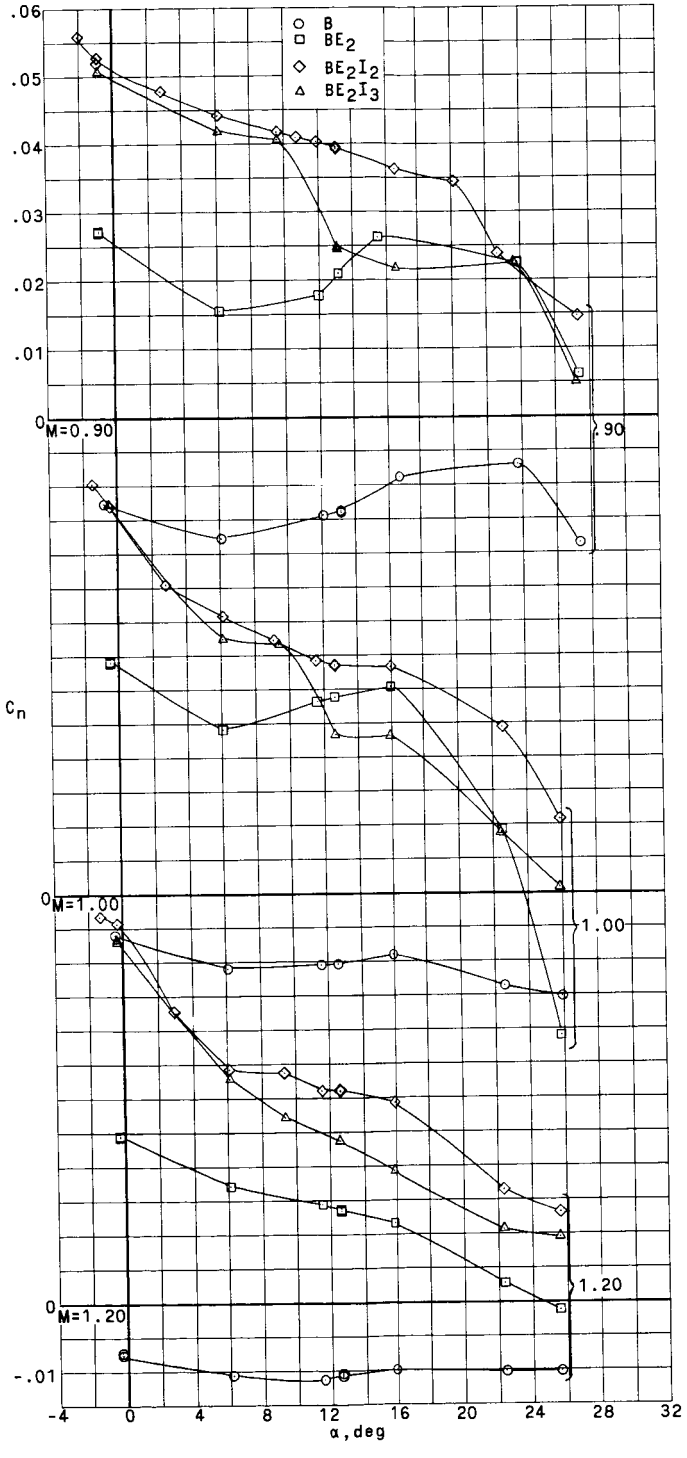

(c) C_n against α, $\beta \approx 5^0$. Concluded.

Figure 10.- Continued.

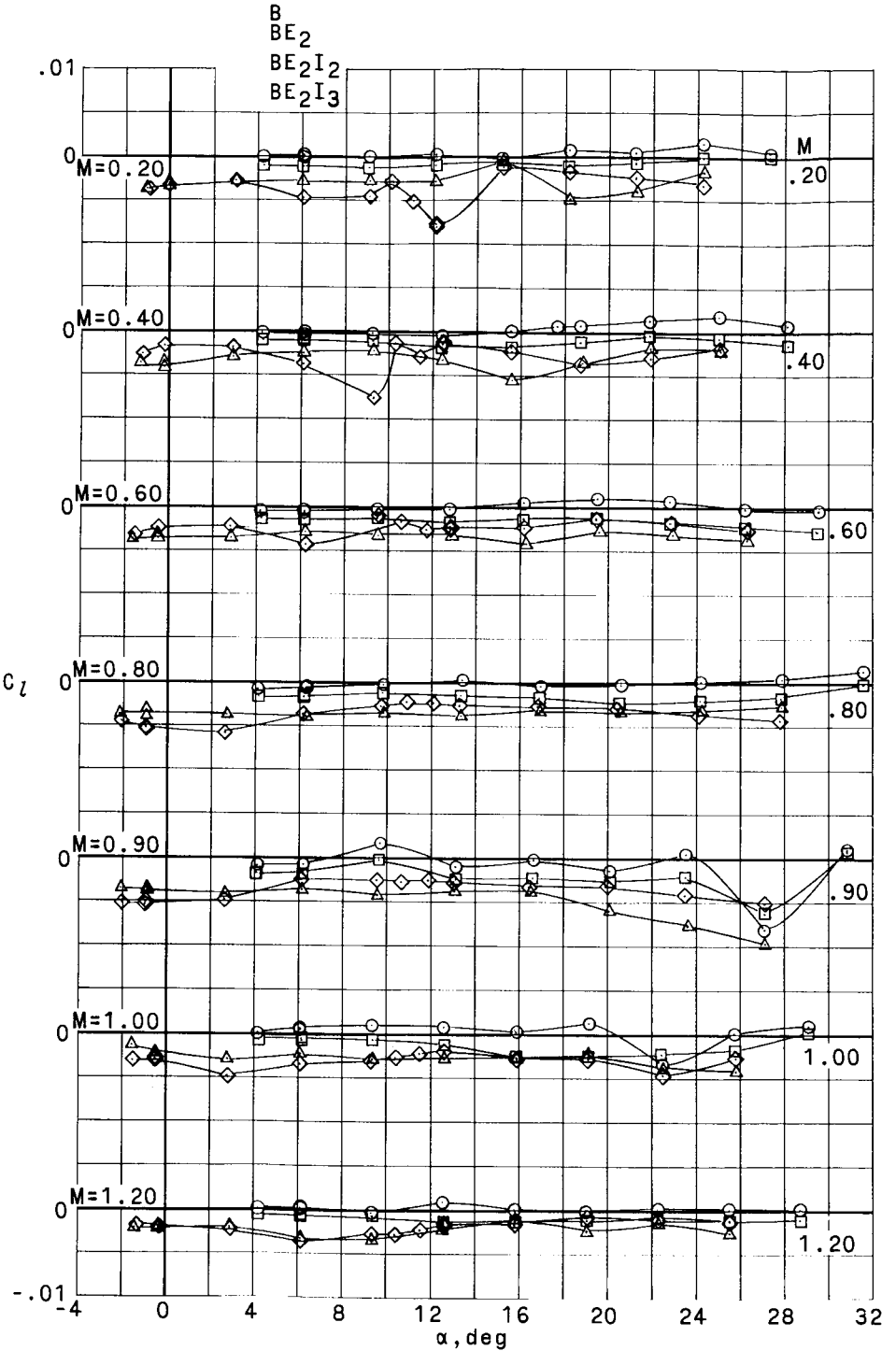

(d) C_l against α, $\beta \approx 0^0$.

Figure 10.- Continued.

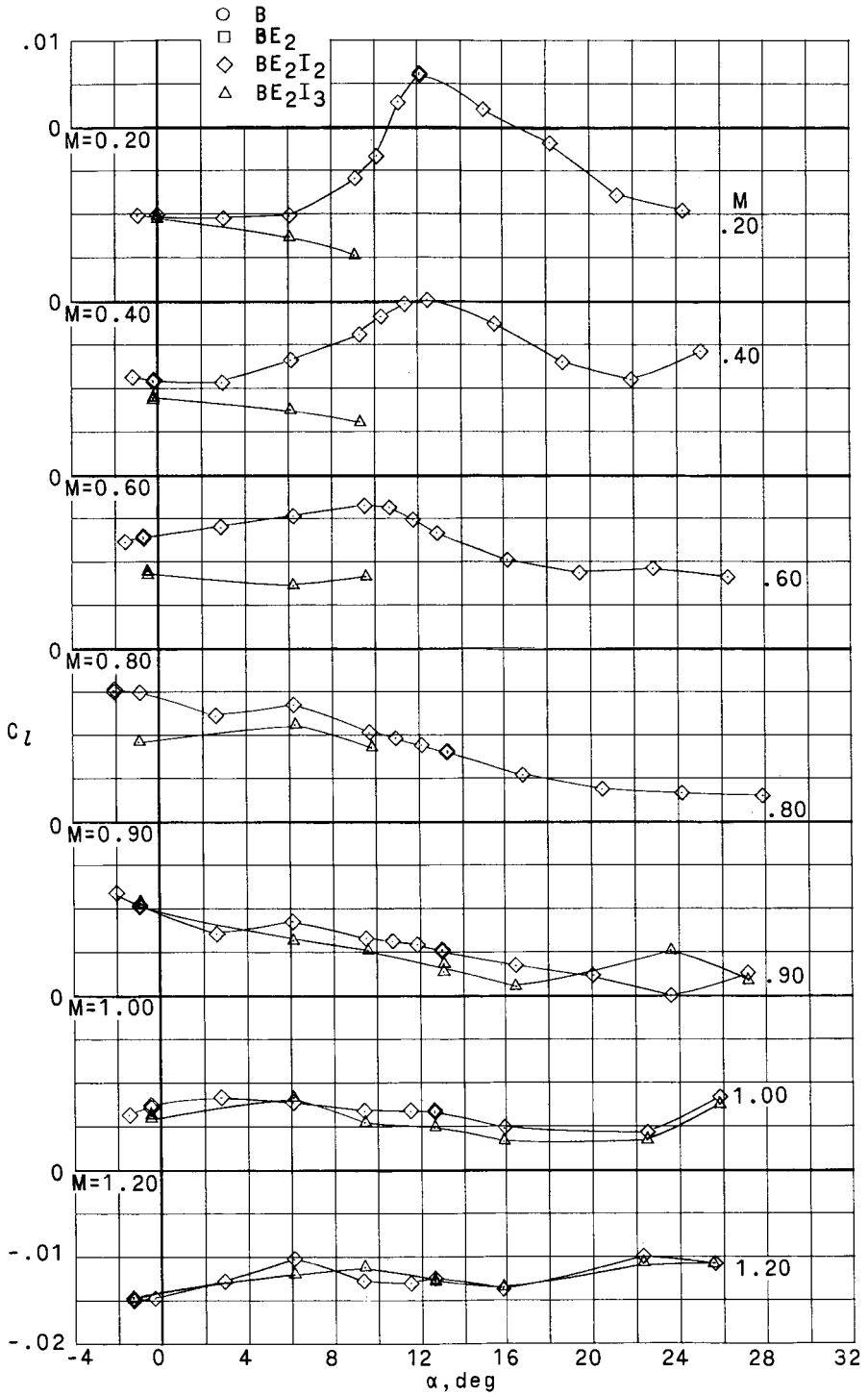

(e) C_l against α, $\beta \approx 3^0$.

Figure 10.- Continued.

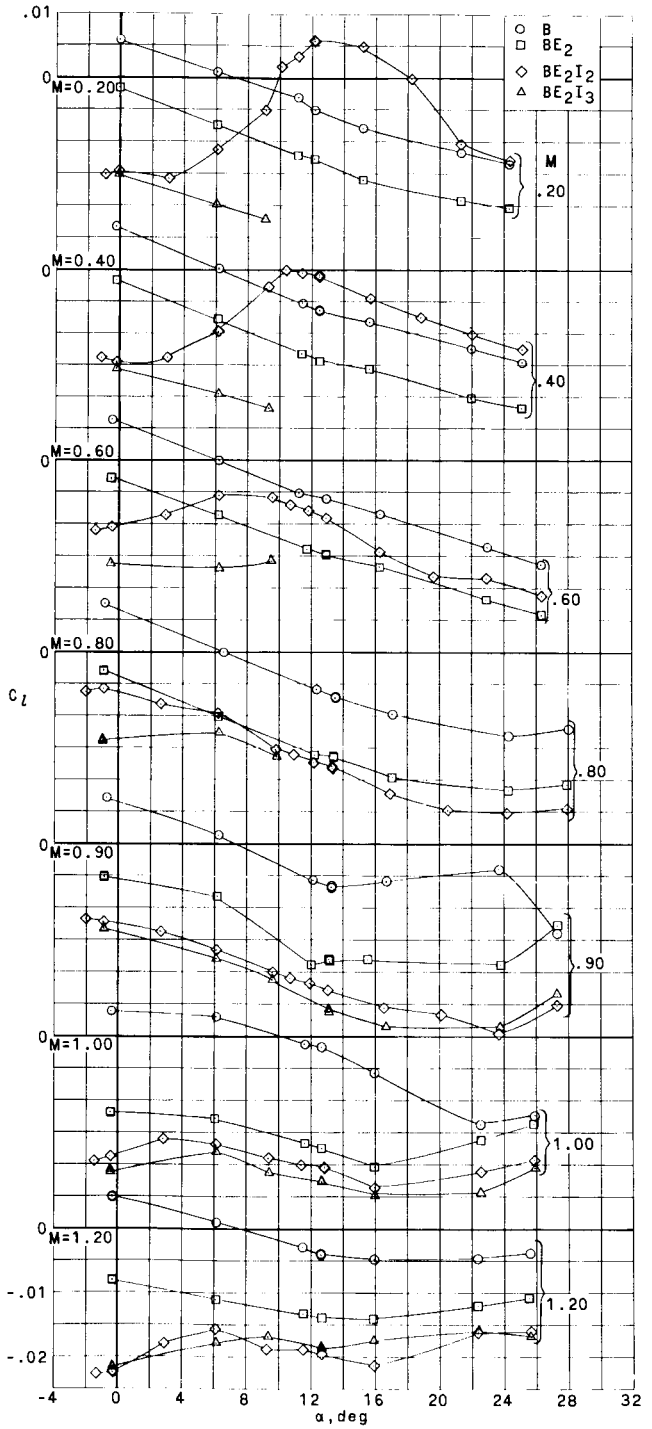

(f) C_l against α, $\beta \approx 5^0$.

Figure 10.- Continued.

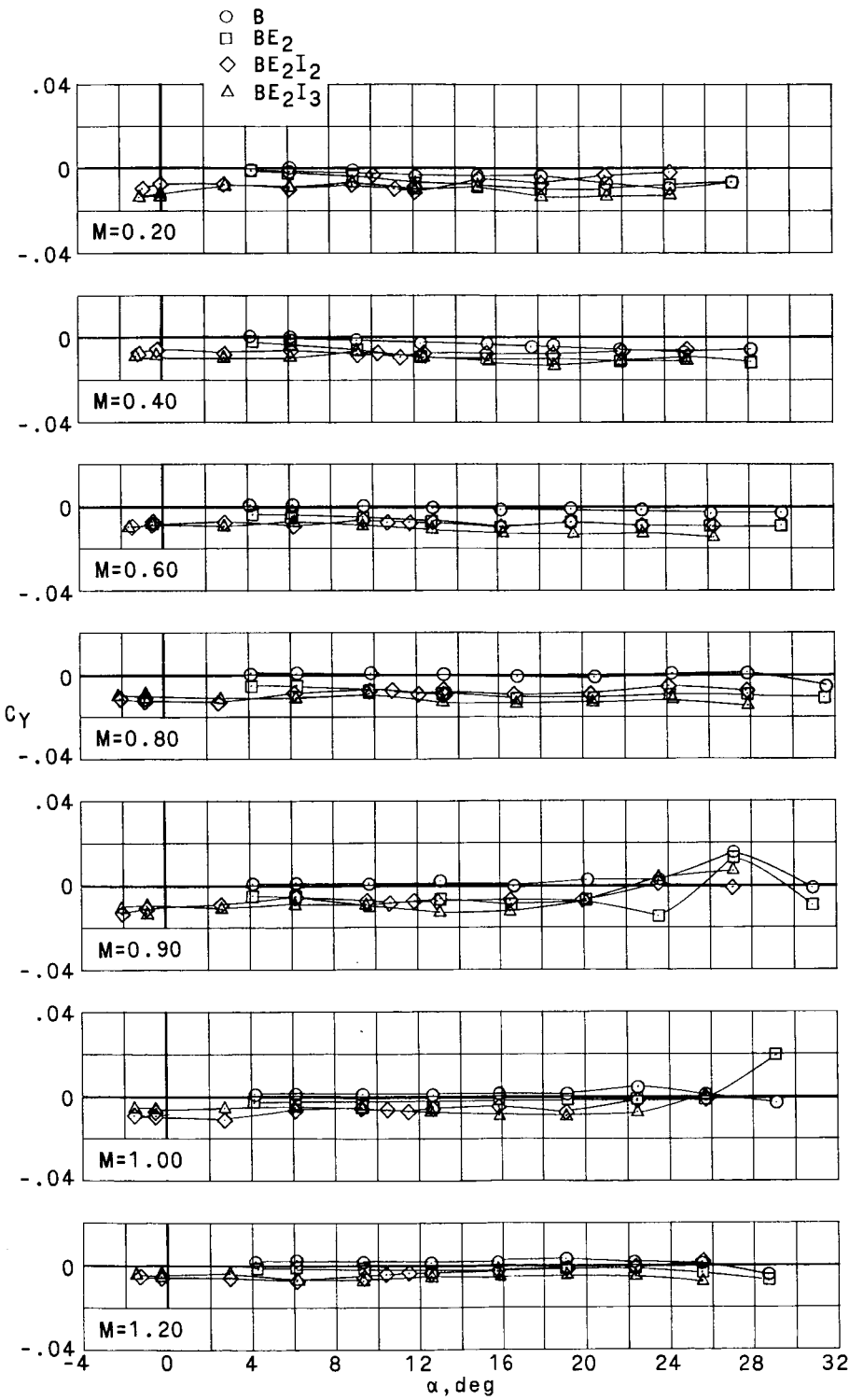

(g) C_Y against α, $\beta \approx 0^0$.

Figure 10.- Continued.

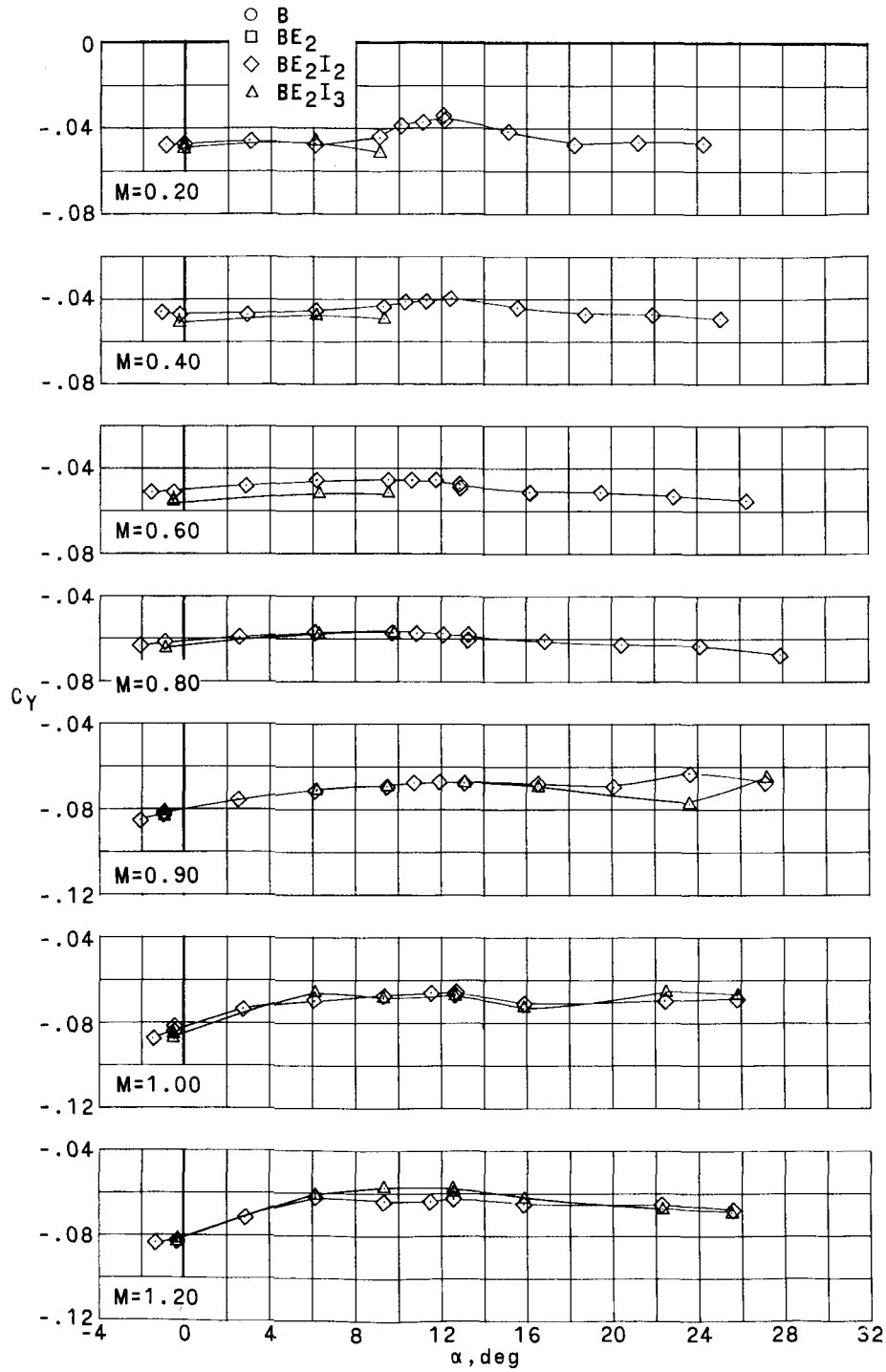

(h) C_Y against α, $\beta \approx 3^0$.

Figure 10.- Continued.

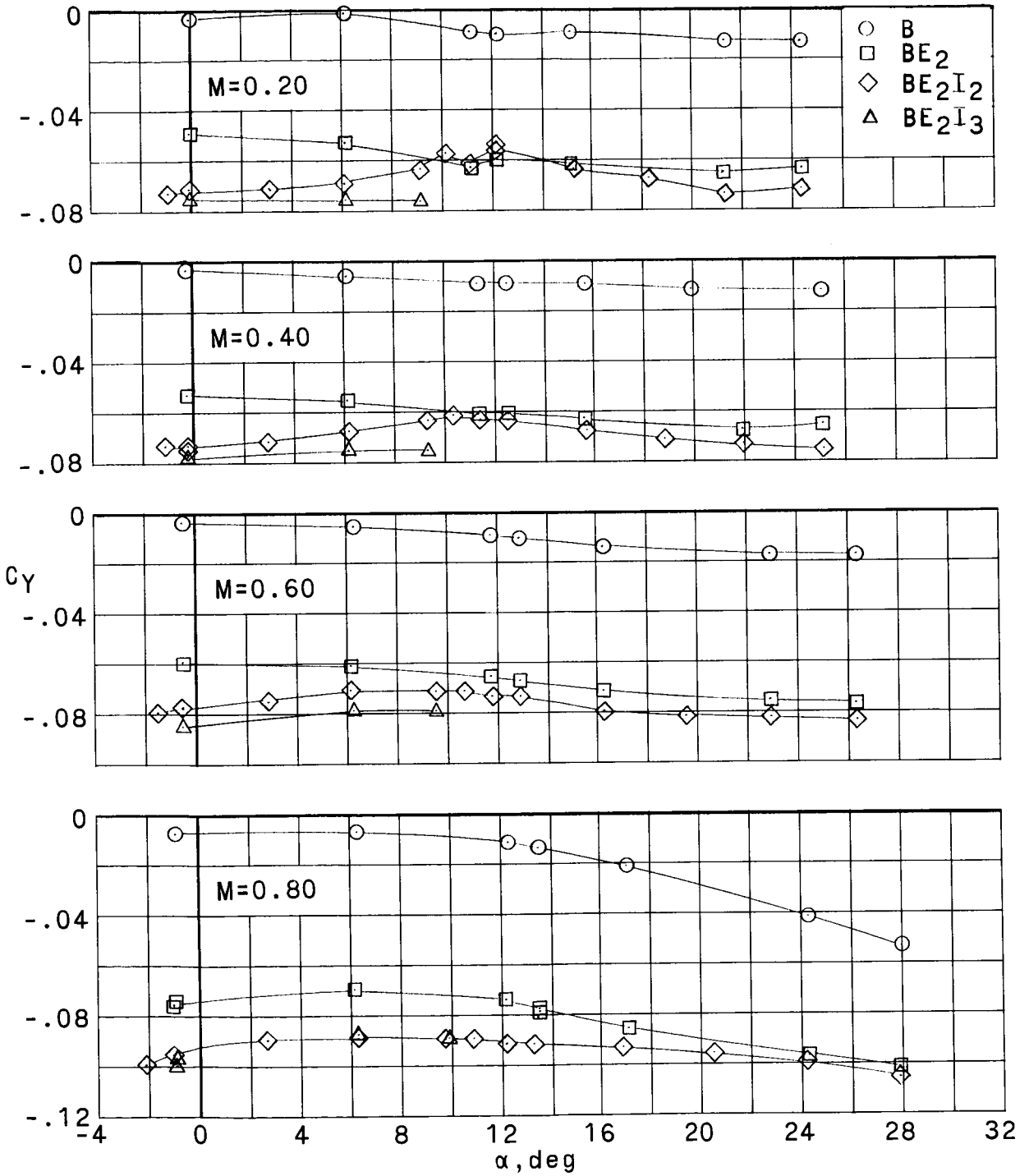

(i) C_Y against α, $\beta \approx 5^0$.

Figure 10.- Continued.

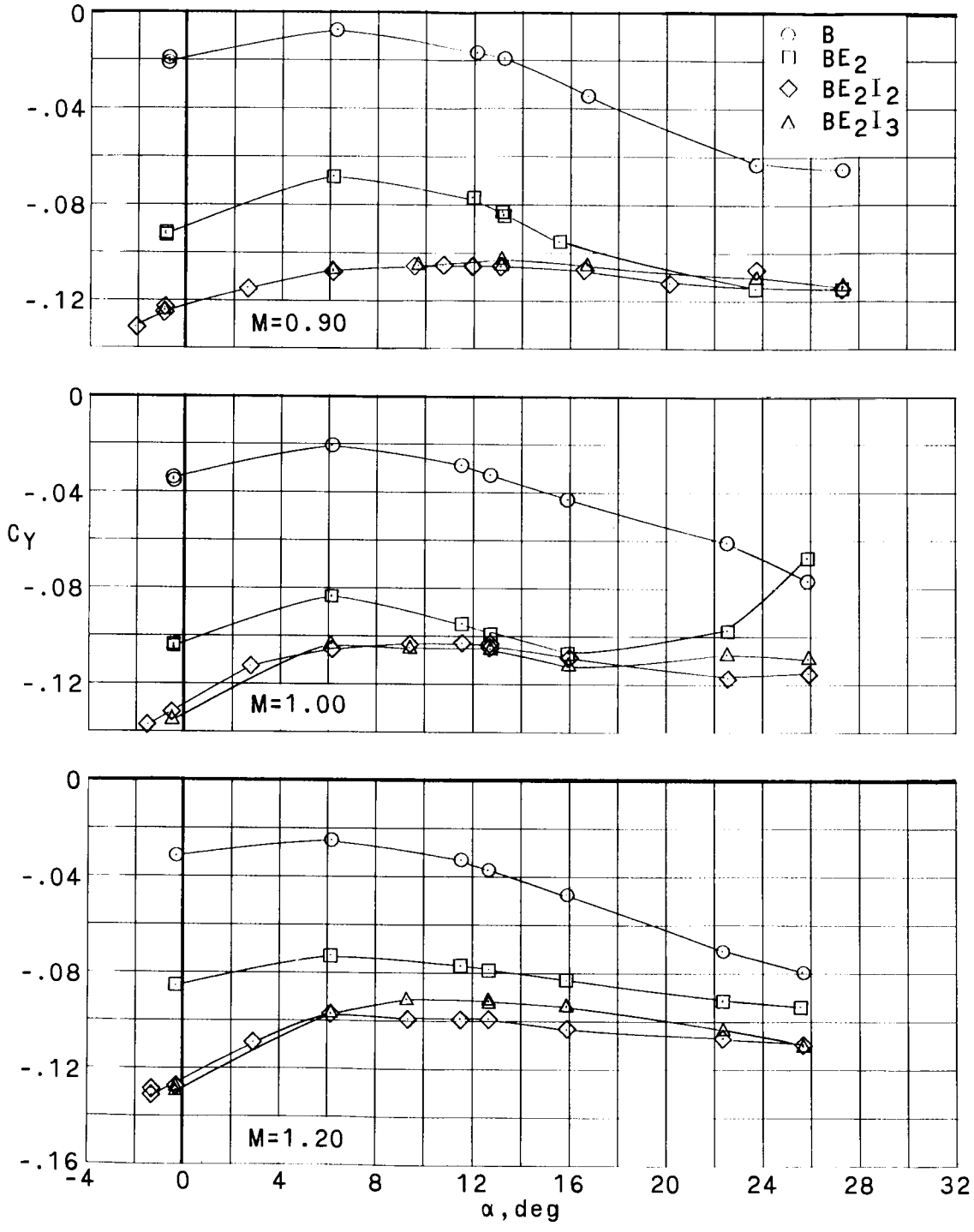

(i) C_Y against α, $\beta \approx 5^0$. Concluded.

Figure 10.- Concluded.

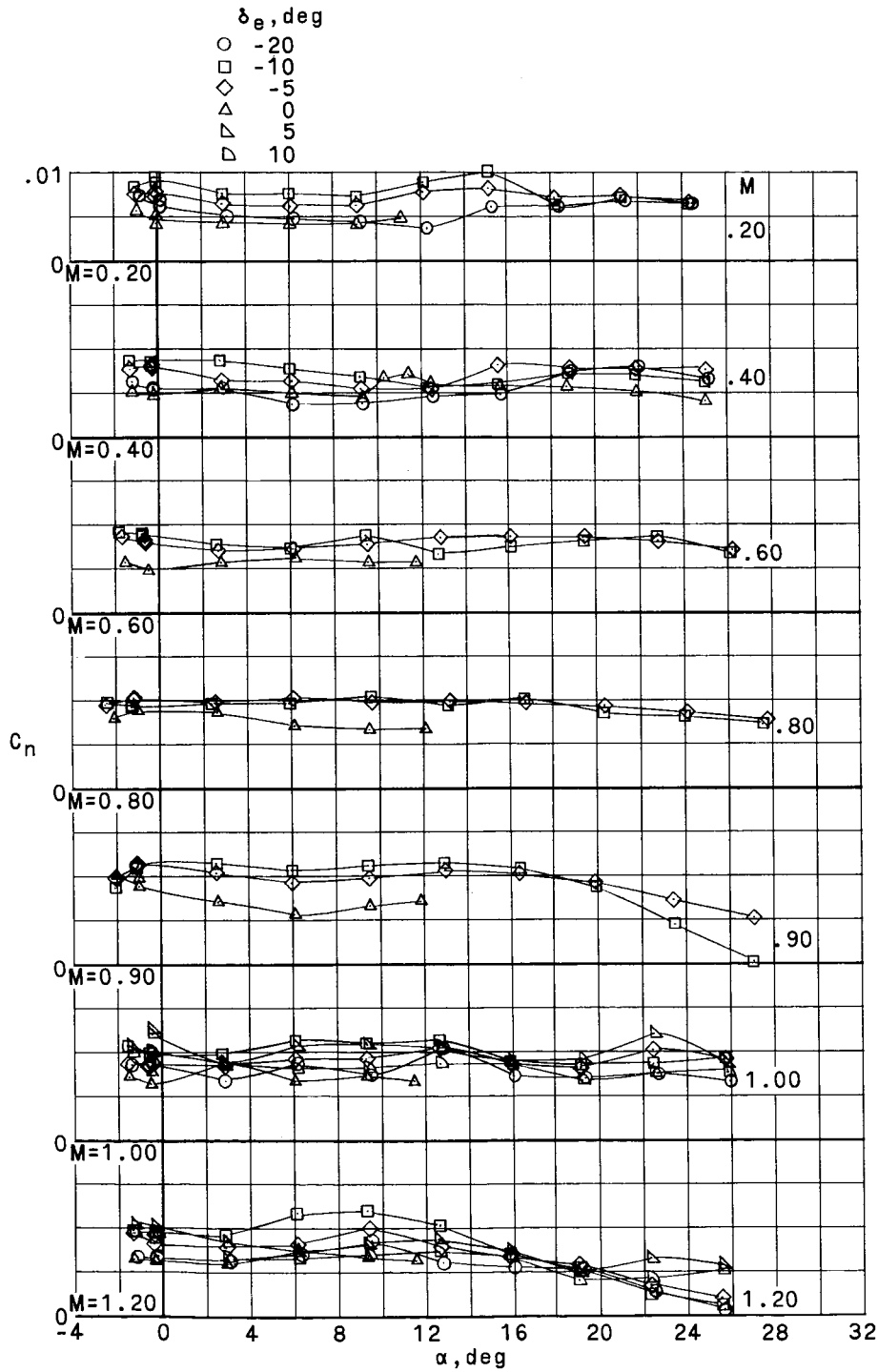

(a) C_n against α, $\beta \approx 0^0$.

Figure 11.- Effect of uniform elevon deflection on lateral aerodynamic characteristics. BE_2I_2; $\delta_a = 0^0$.

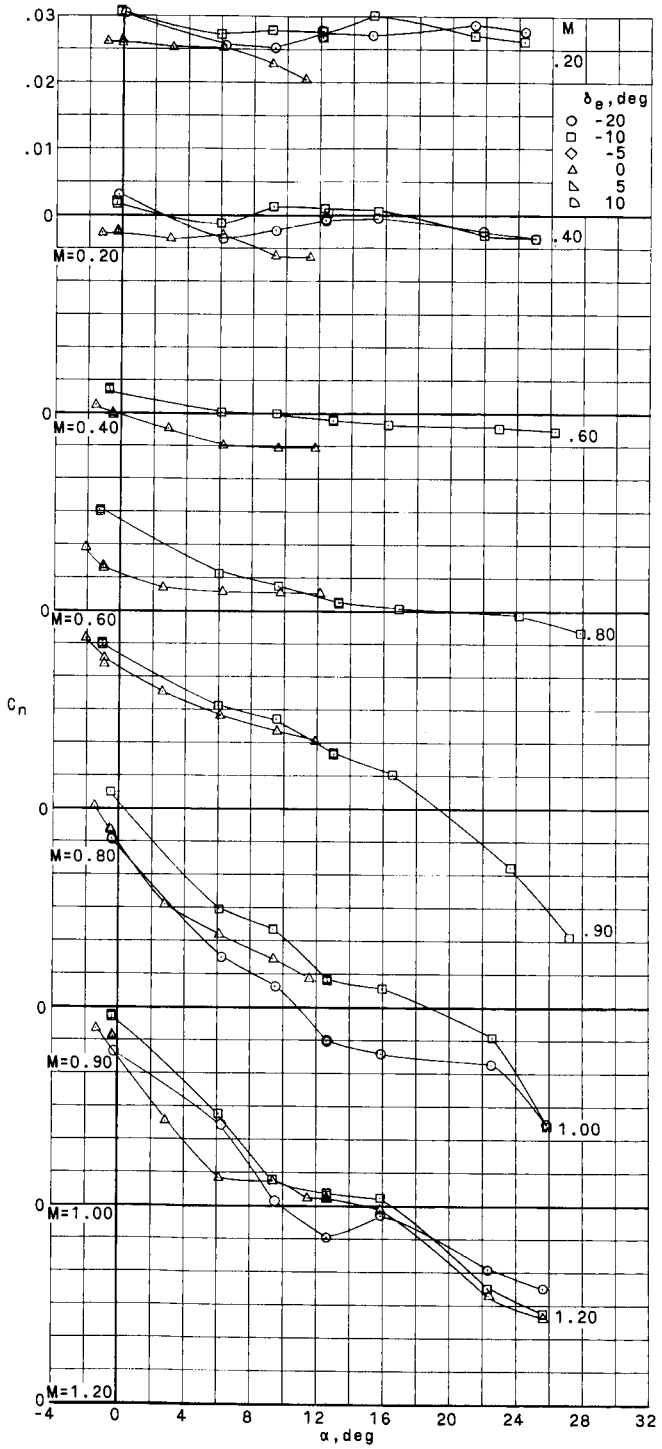

(b) C_n against α, $\beta \approx 5^0$.

Figure 11.- Continued.

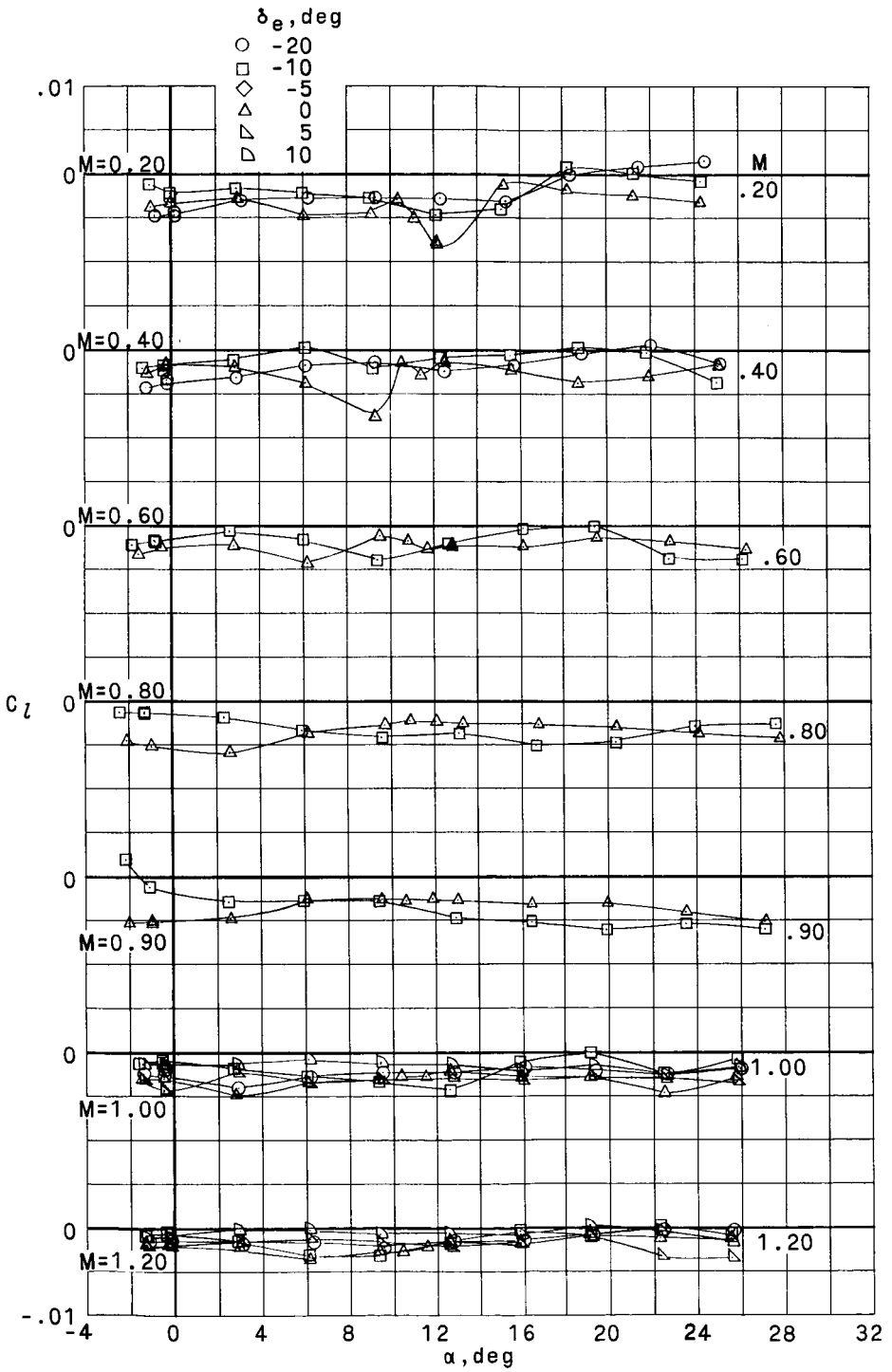

(c) C_l against α, $\beta \approx 0^0$.

Figure 11.- Continued.

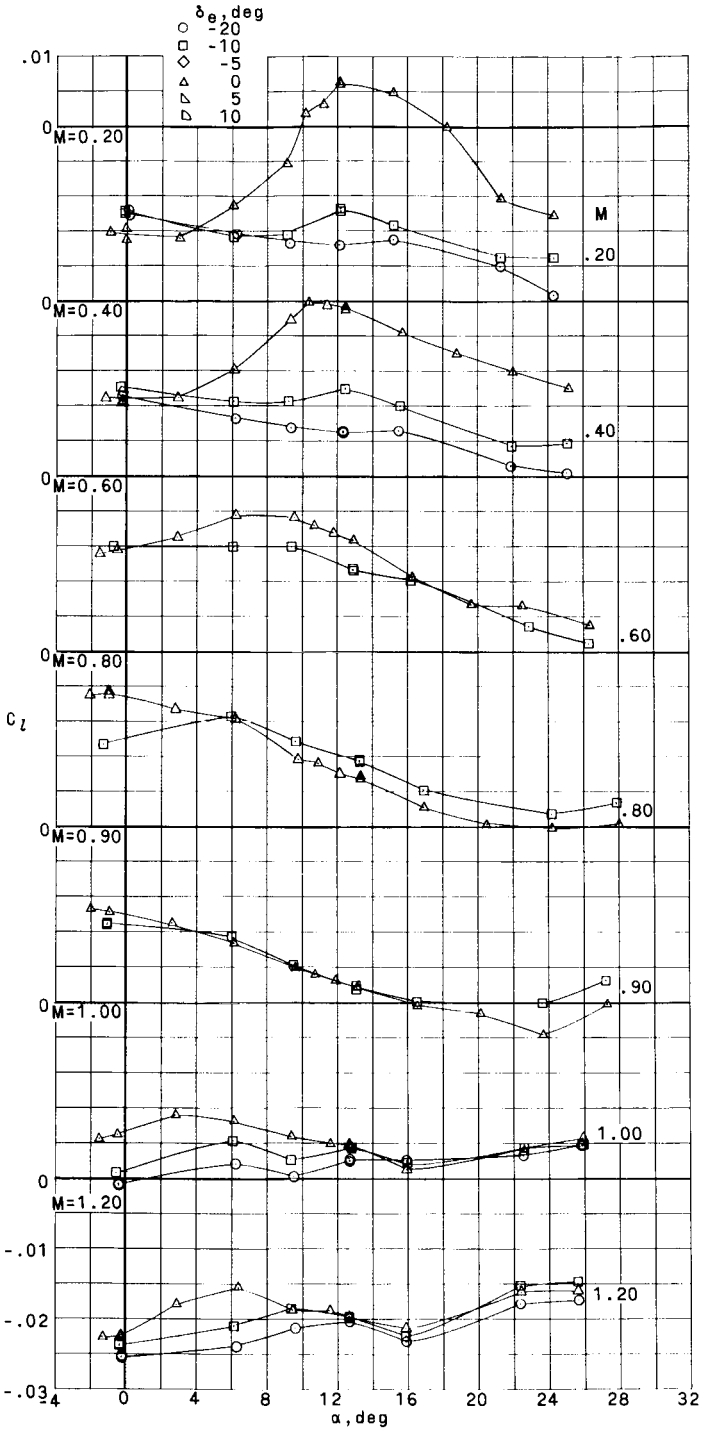

(d) C_l against α, $\beta \approx 5^0$.

Figure 11.- Continued.

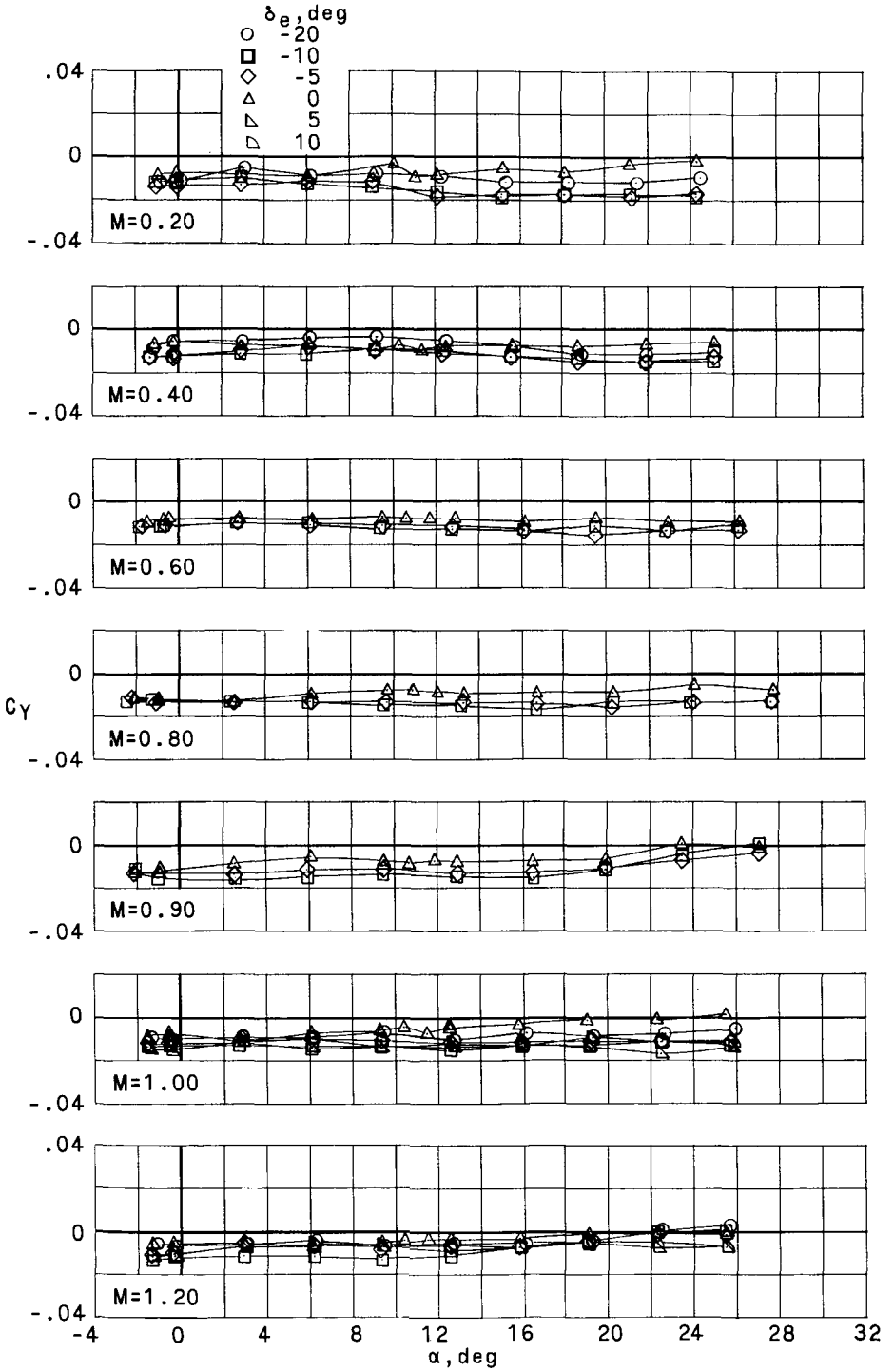

(e) C_Y against α, $\beta \approx 0^0$.

Figure 11.- Continued.

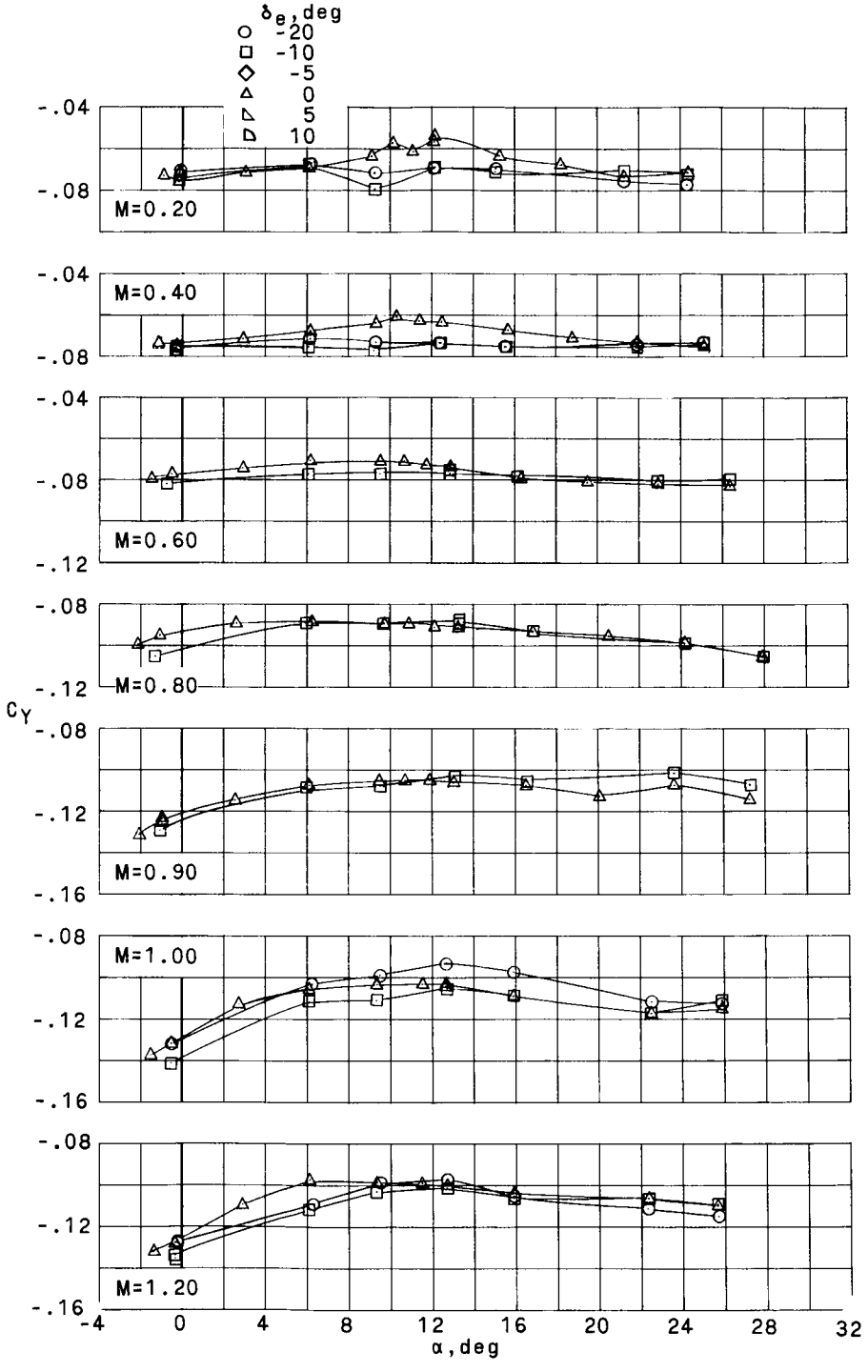

(f) C_Y against α, $\beta \approx 5^0$.

Figure 11.- Concluded.

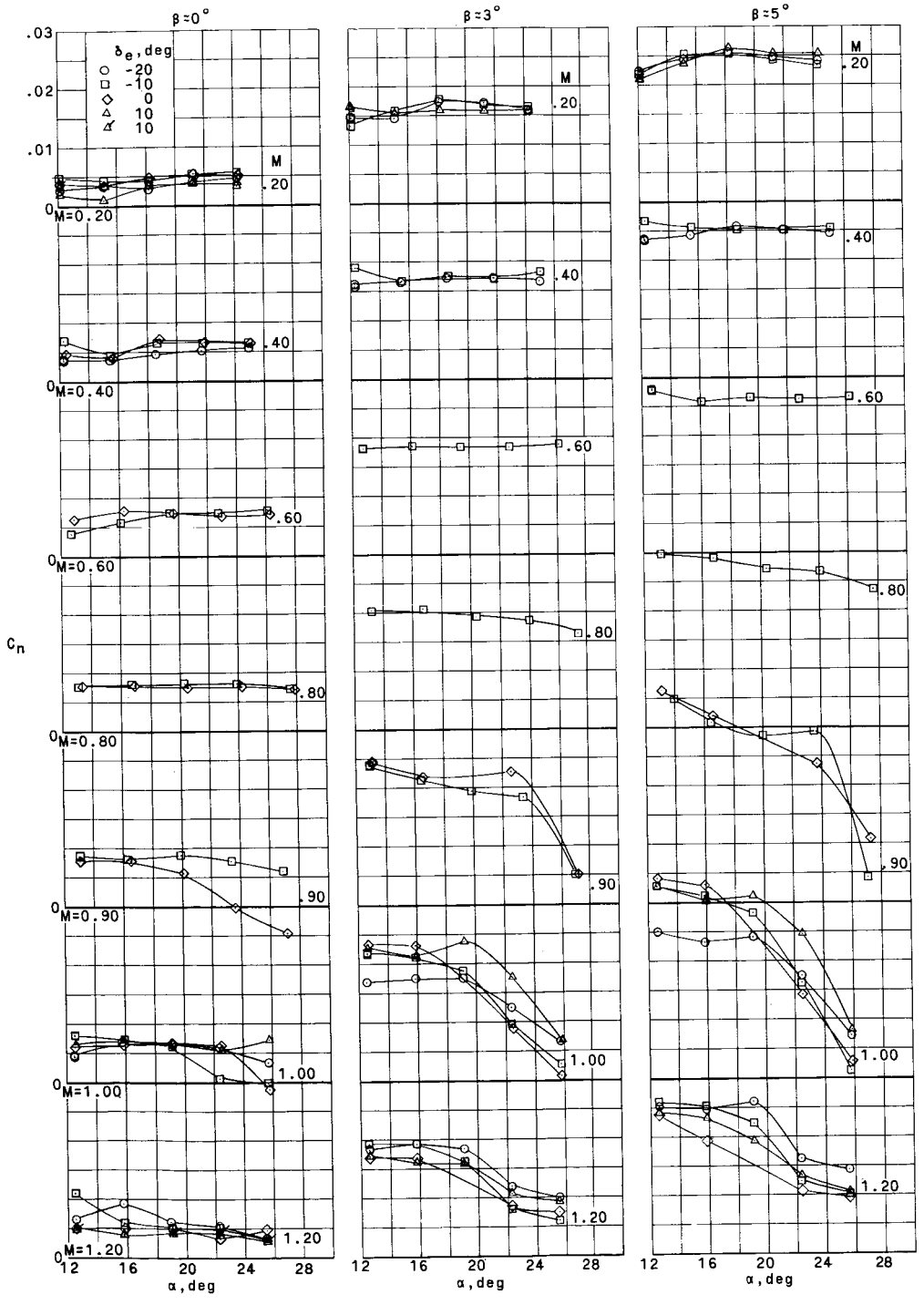

(a) C_n against α.

Figure 12.- Effects of uniform elevon deflections on lateral aerodynamic characteristics. BE_2I_3; $\delta_a = 0^0$. (Flagged symbols indicate transition grit off.)

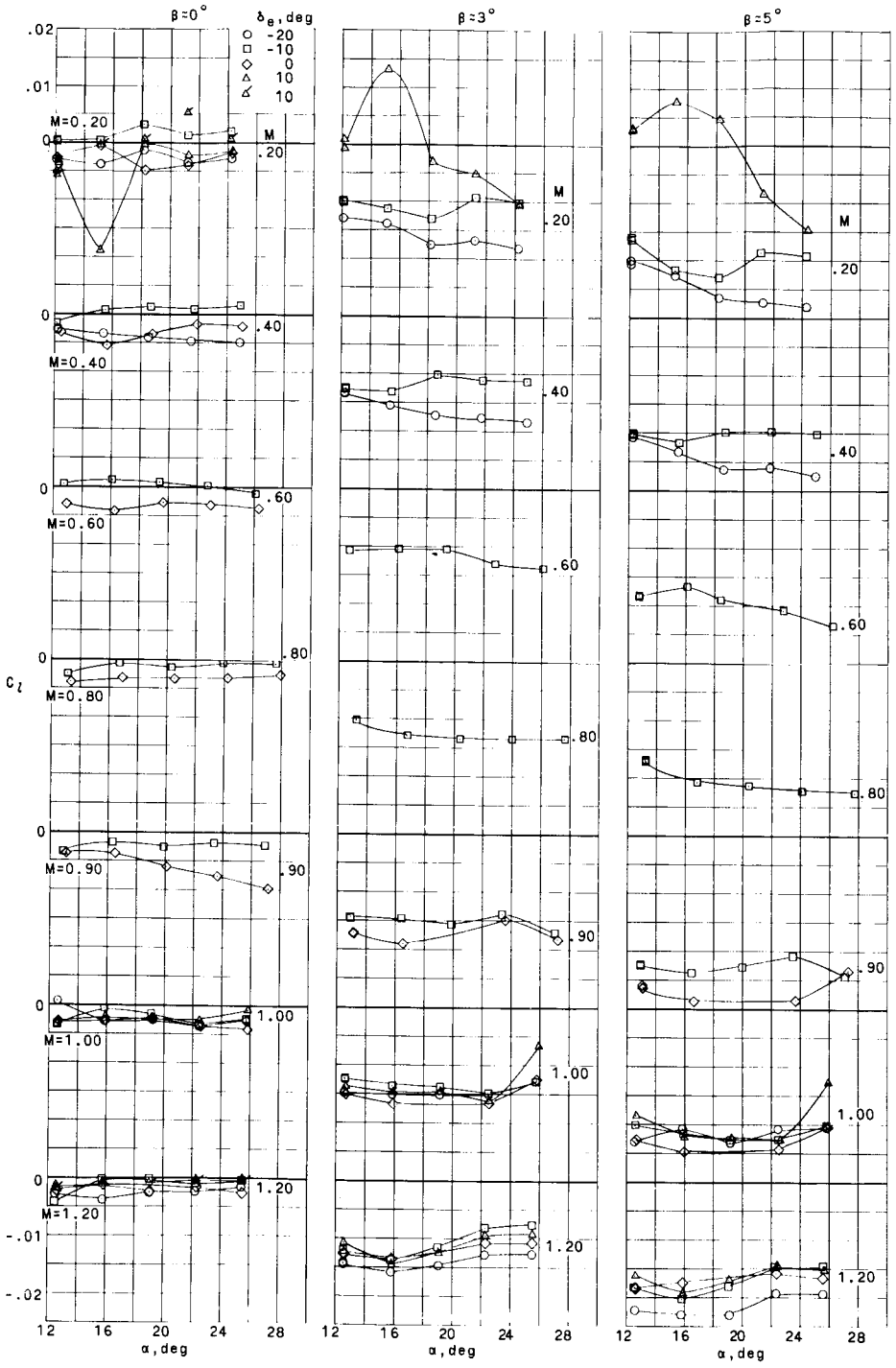

(b) C_l against α.

Figure 12.- Continued.

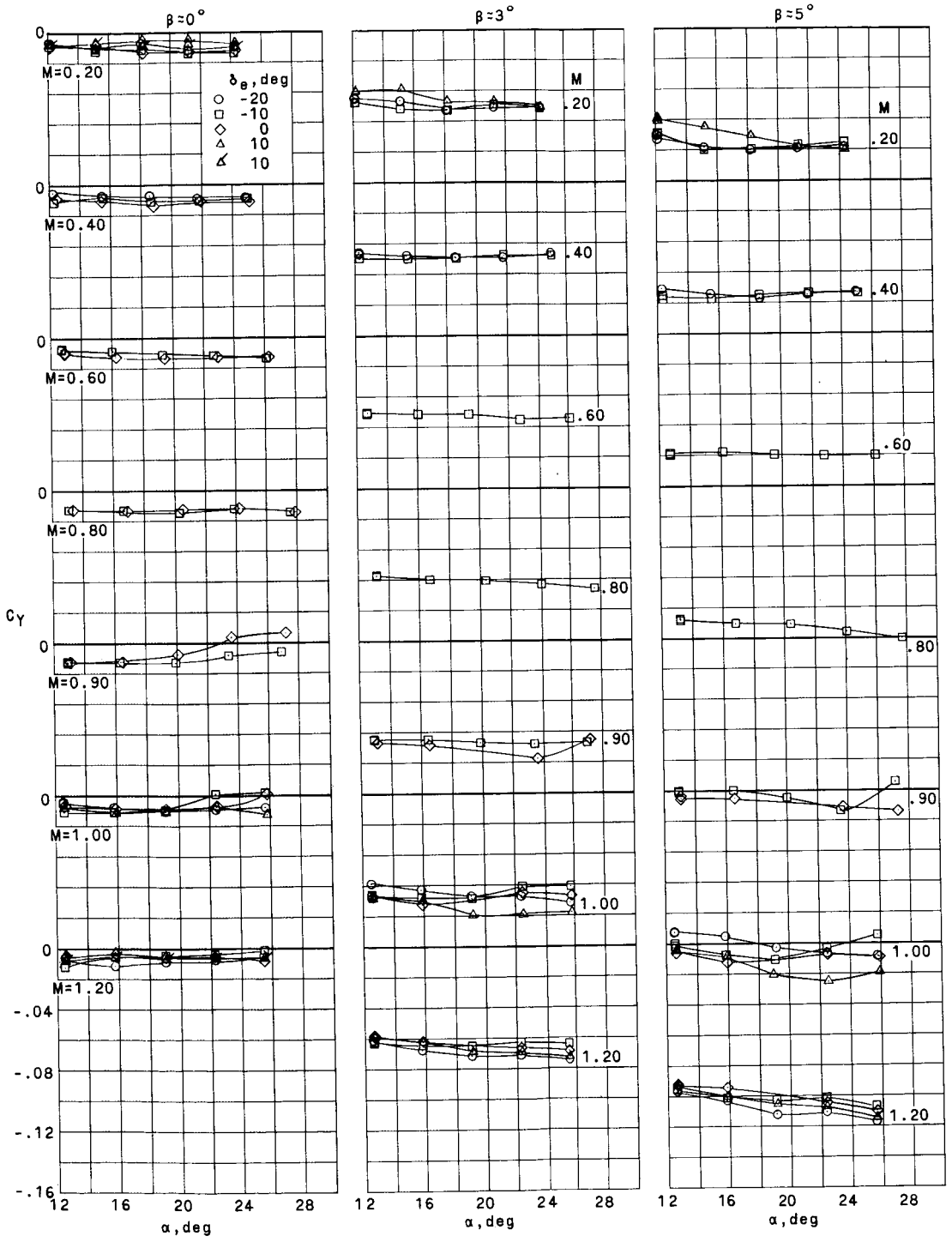

(c) C_Y against α.

Figure 12.- Concluded.

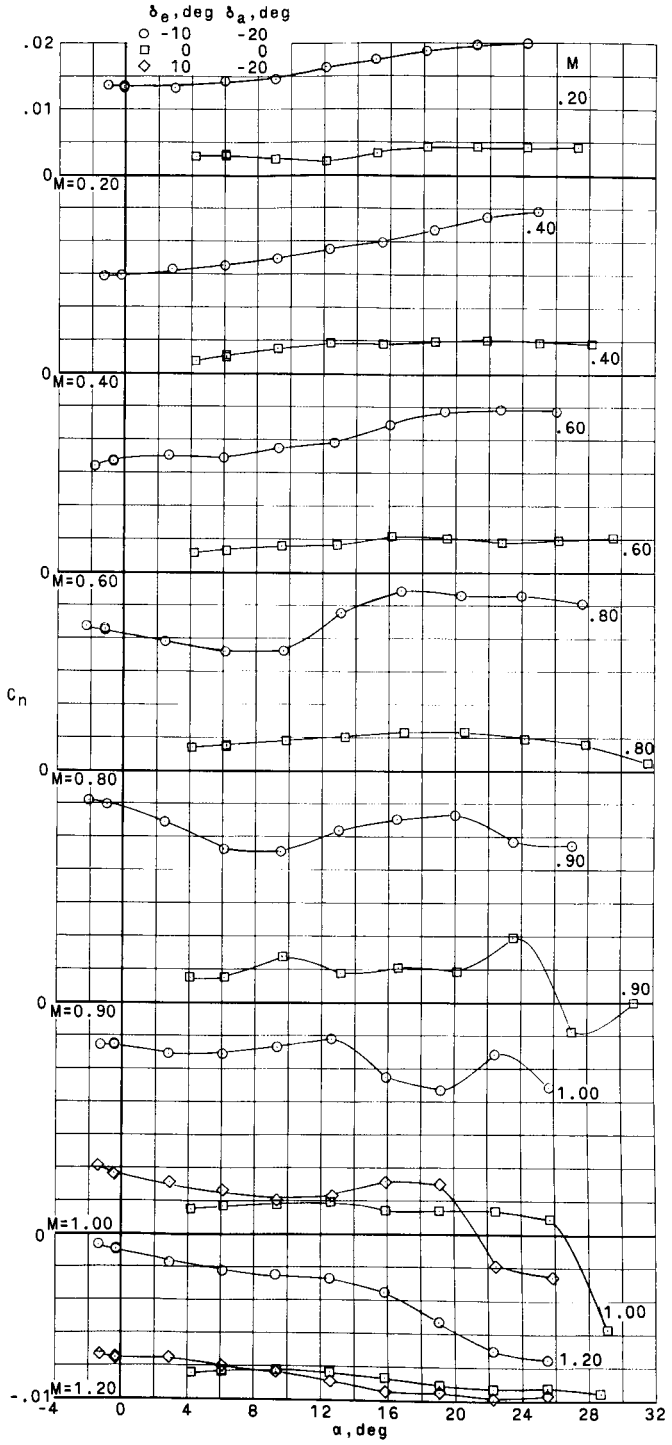

(a) C_n against α.

Figure 13.- Effect of differential elevon deflection on lateral aerodynamic characteristics. BE_2; $\beta \approx 0^0$.

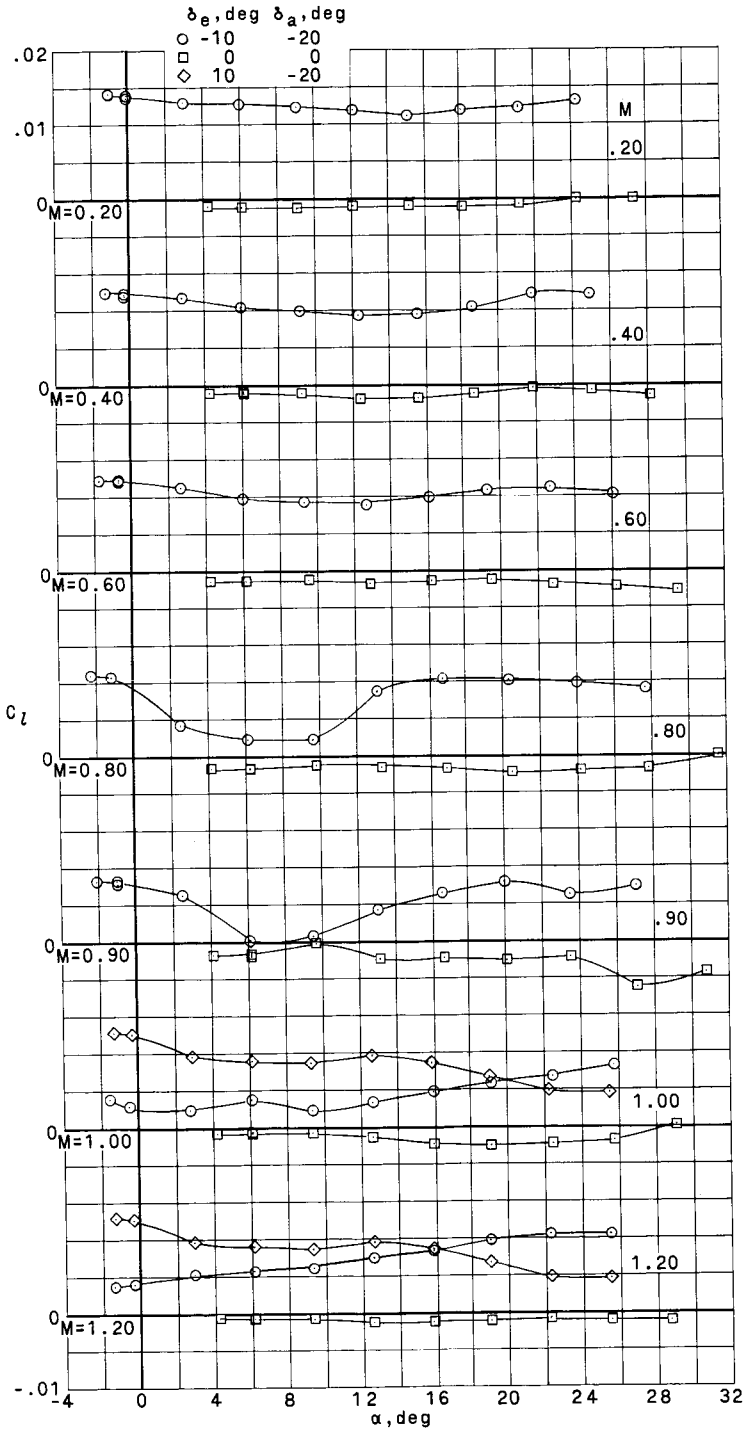

(b) C_l against α.

Figure 13.- Continued.

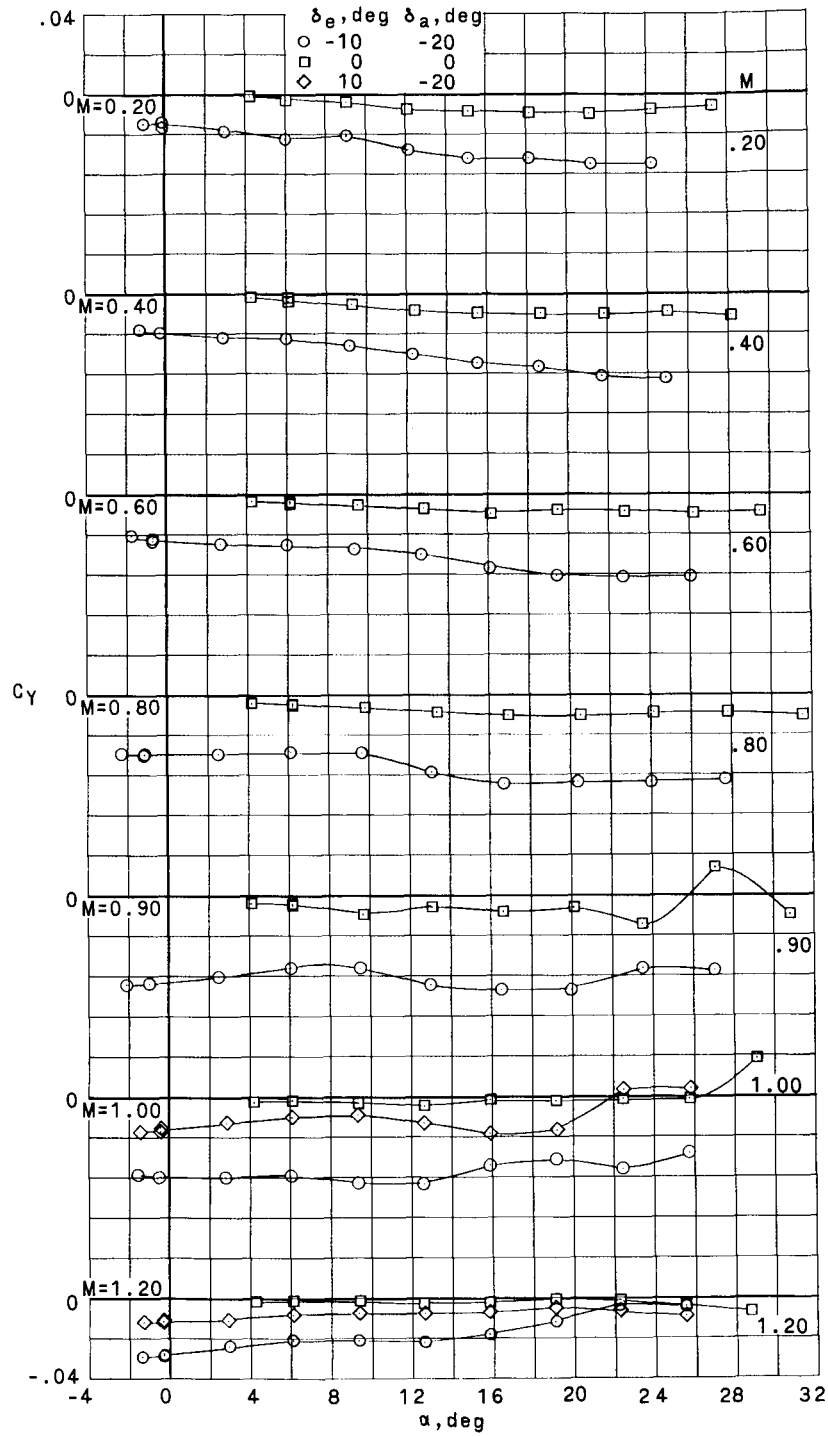

(c) C_Y against α.

Figure 13.- Concluded.

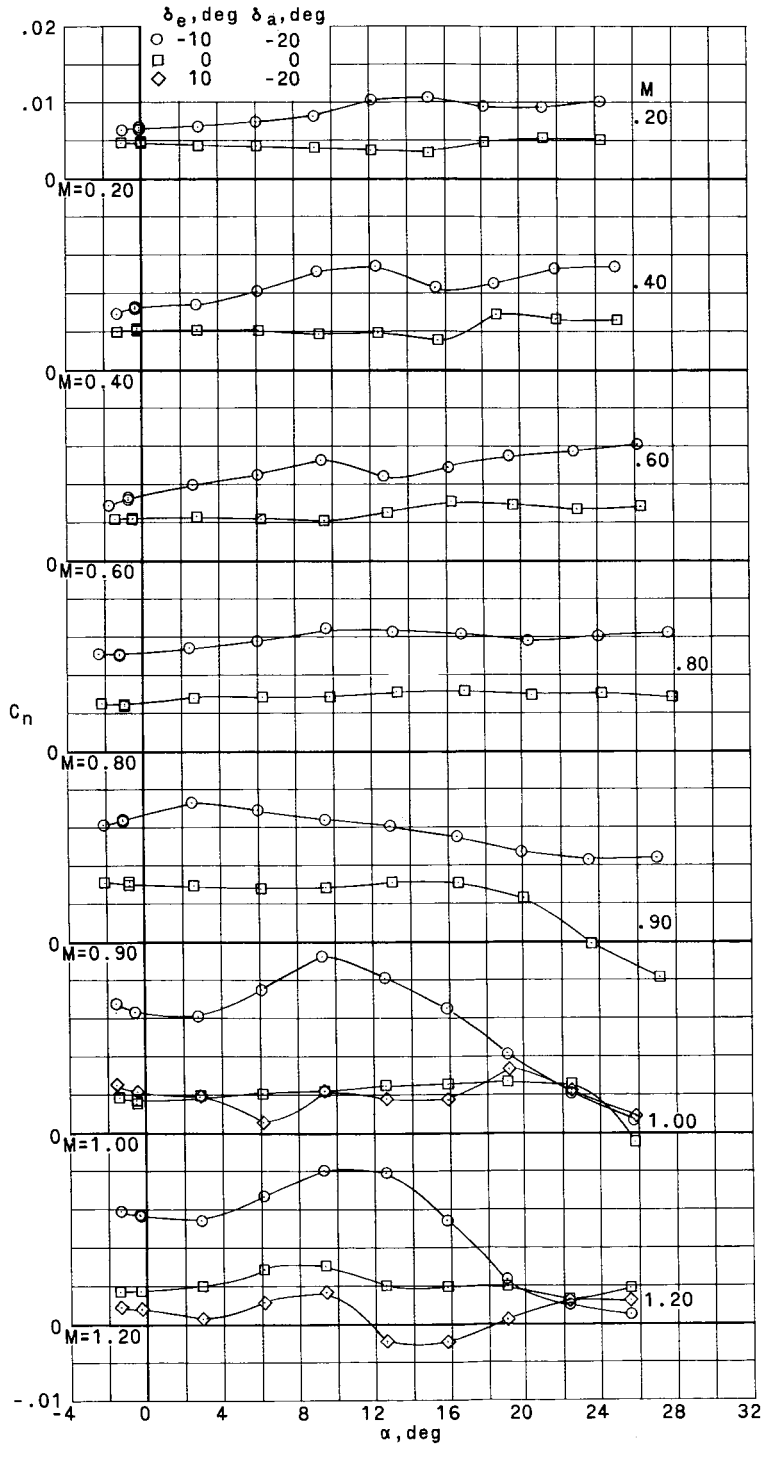

(a) C_n against α.

Figure 14.- Effects of differential elevon deflection on lateral aerodynamic characteristics. BE_2I_3; $\beta \approx 0^0$.

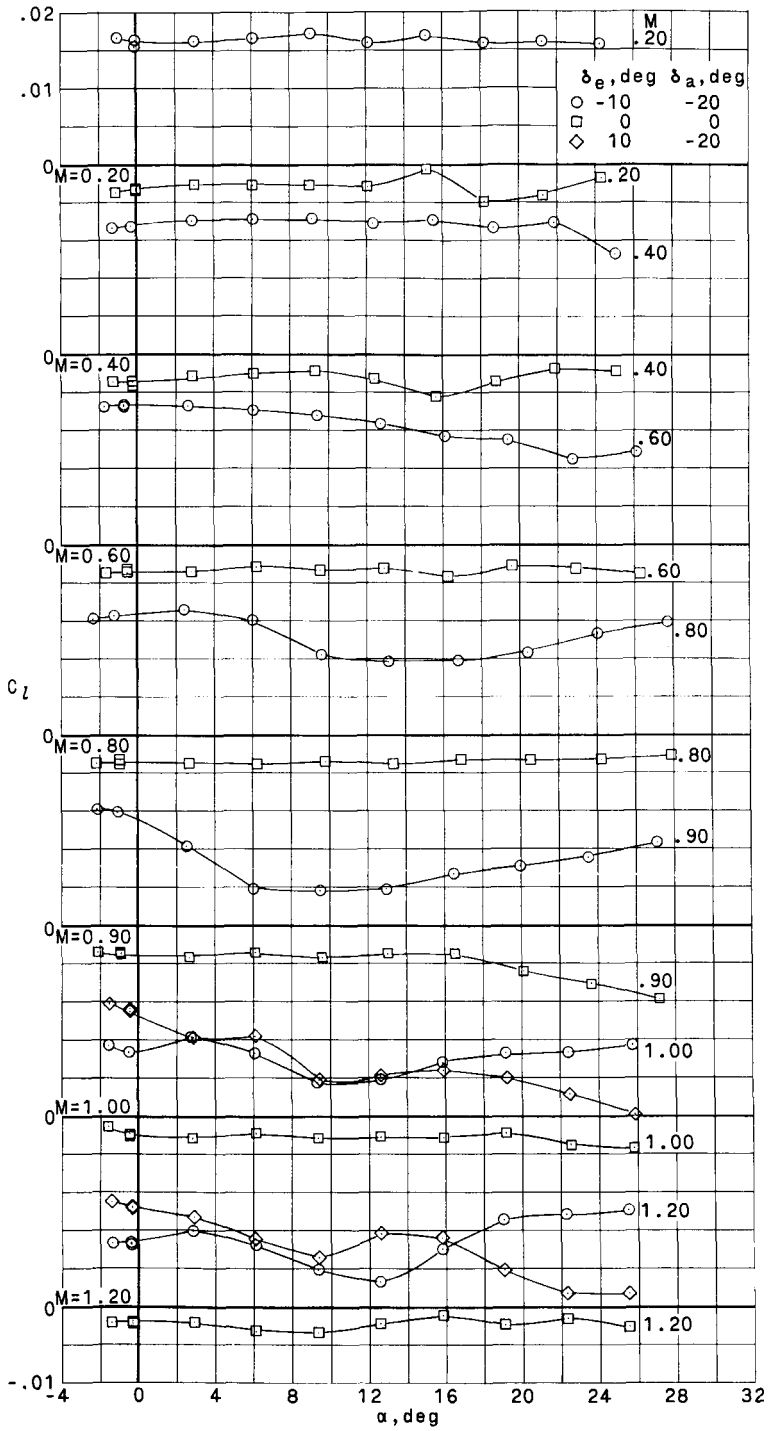

(b) C_l against α.

Figure 14.- Continued.

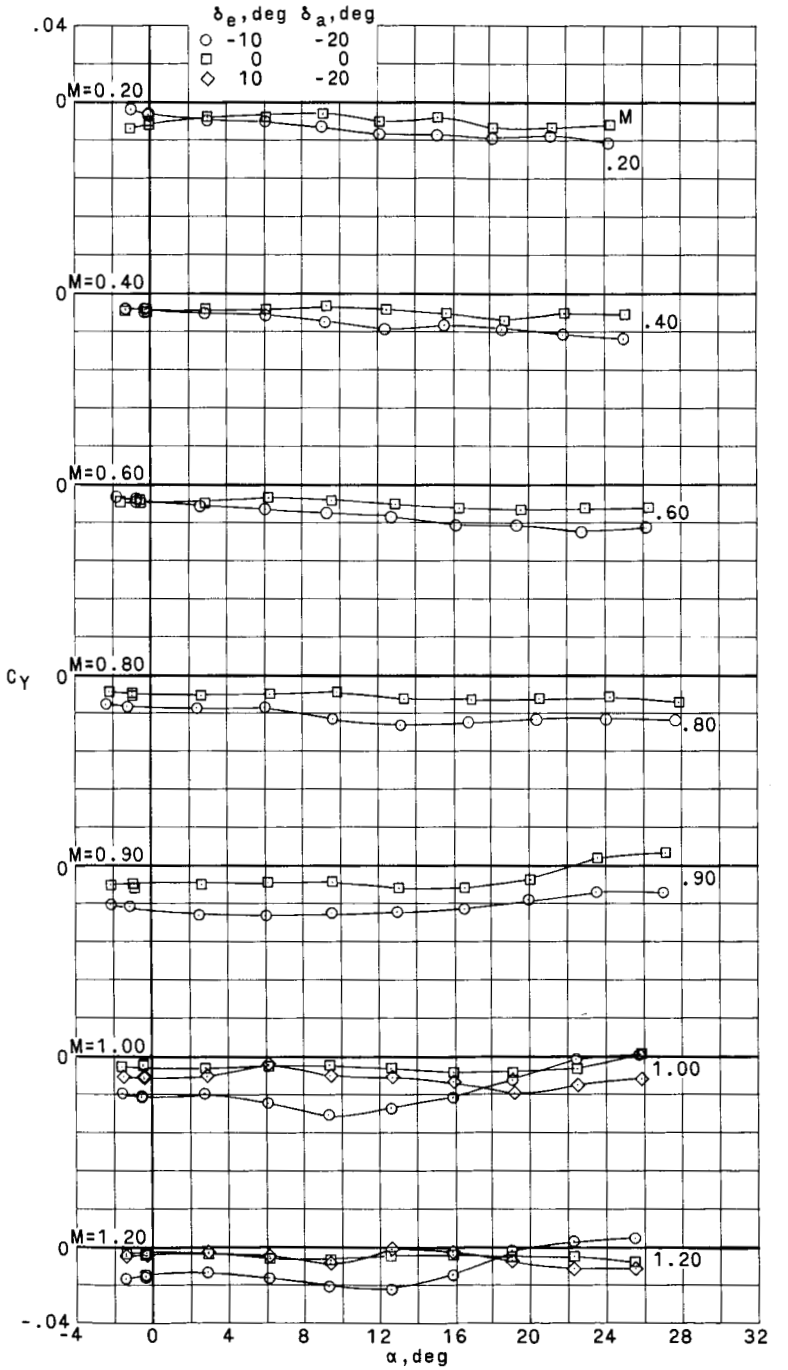

(c) C_Y against α.

Figure 14.- Concluded.

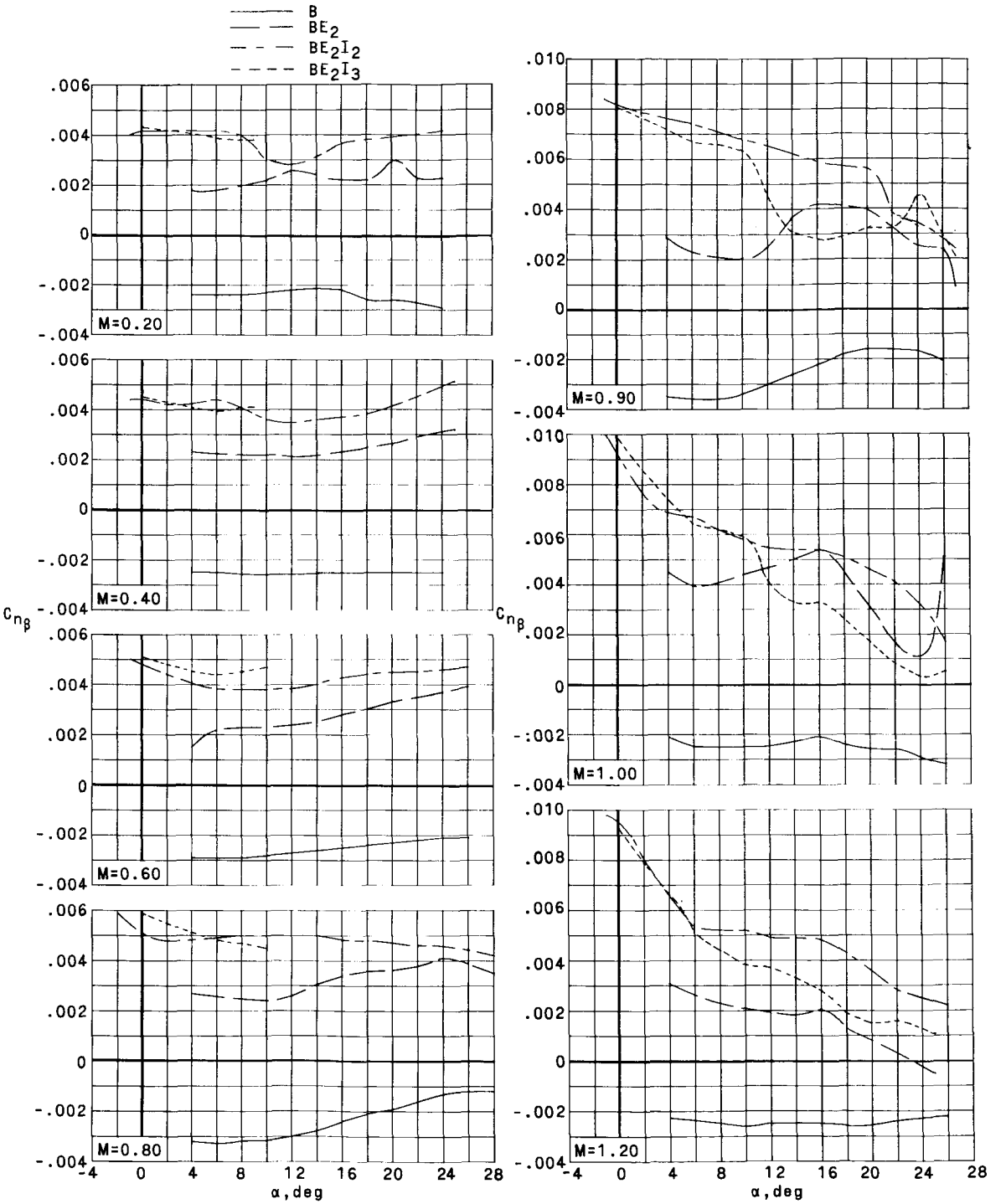

(a) C_{n_β} against α.

Figure 15.- Effect of model components on lateral-stability derivatives.

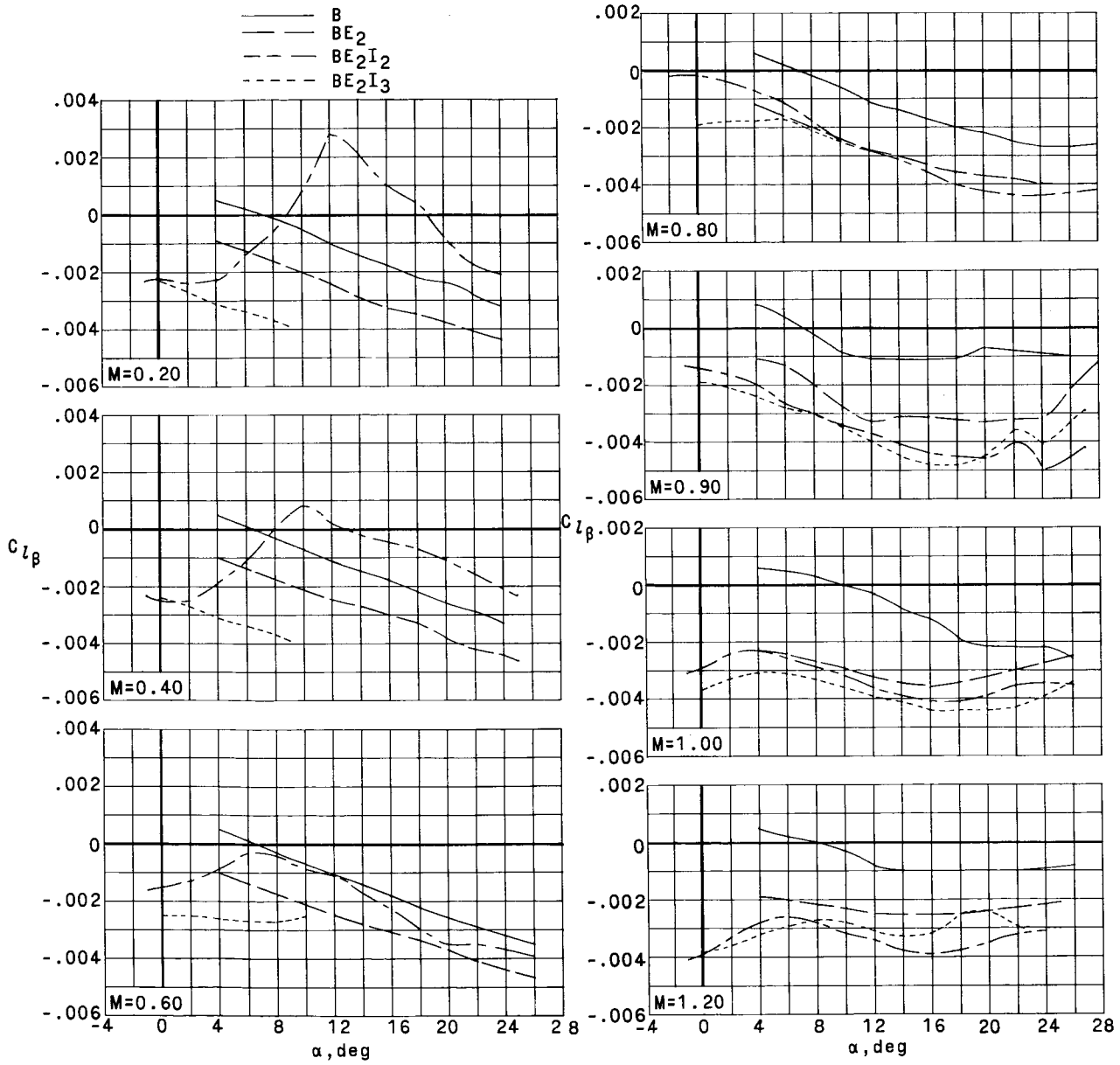

(b) C_{l_β} against α.

Figure 15.- Concluded.

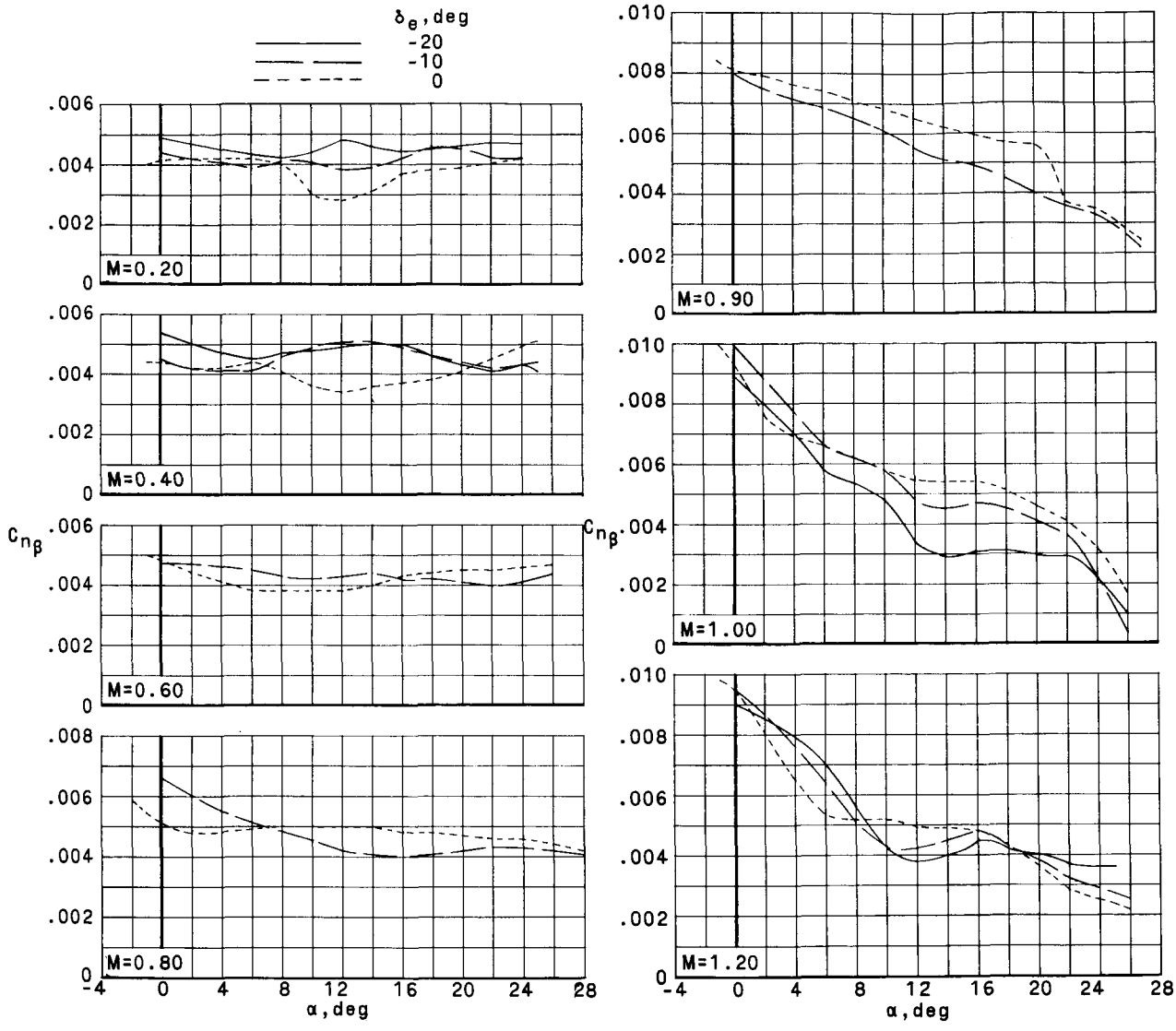

(a) C_{n_β} against α.

Figure 16.- Effect of uniform elevon deflection on lateral-stability derivatives. BE_2I_2; $\delta_a = 0^o$.

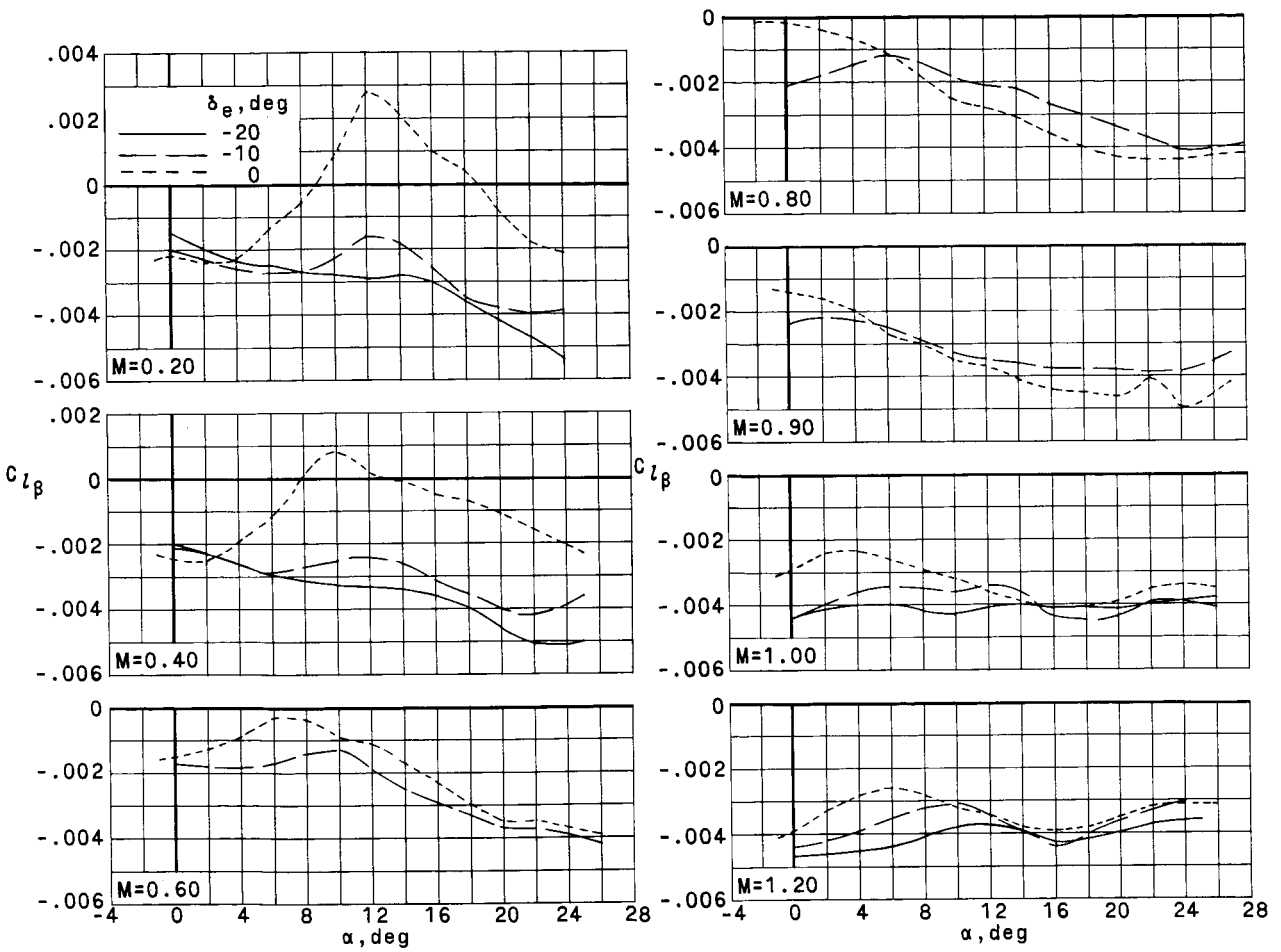

(b) C_{l_β} against α.

Figure 16.- Concluded.

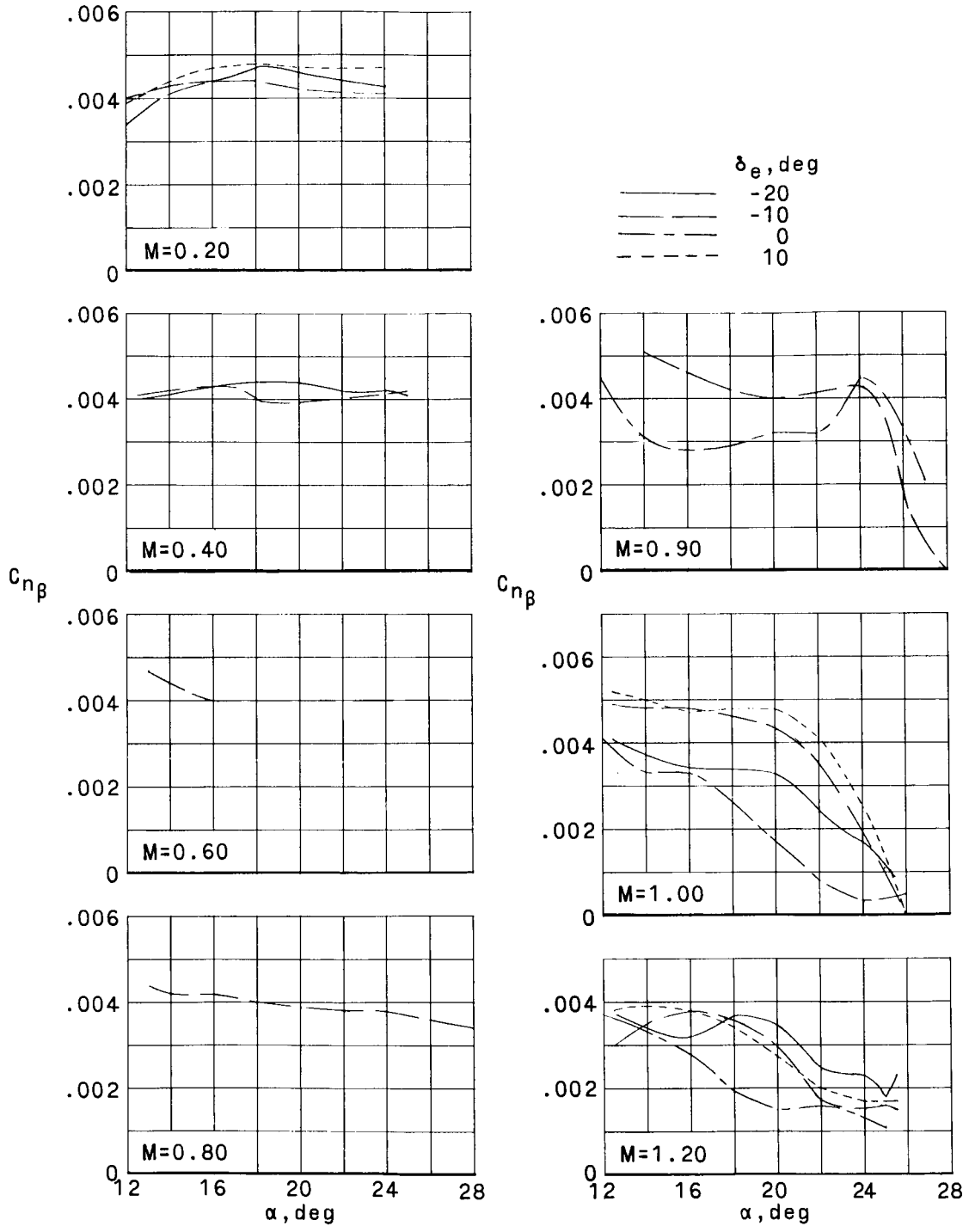

(a) C_{n_β} against α.

Figure 17.- Effect of uniform elevon deflection on lateral-stability derivatives. BE_2I_3; $\delta_a = 0^o$.

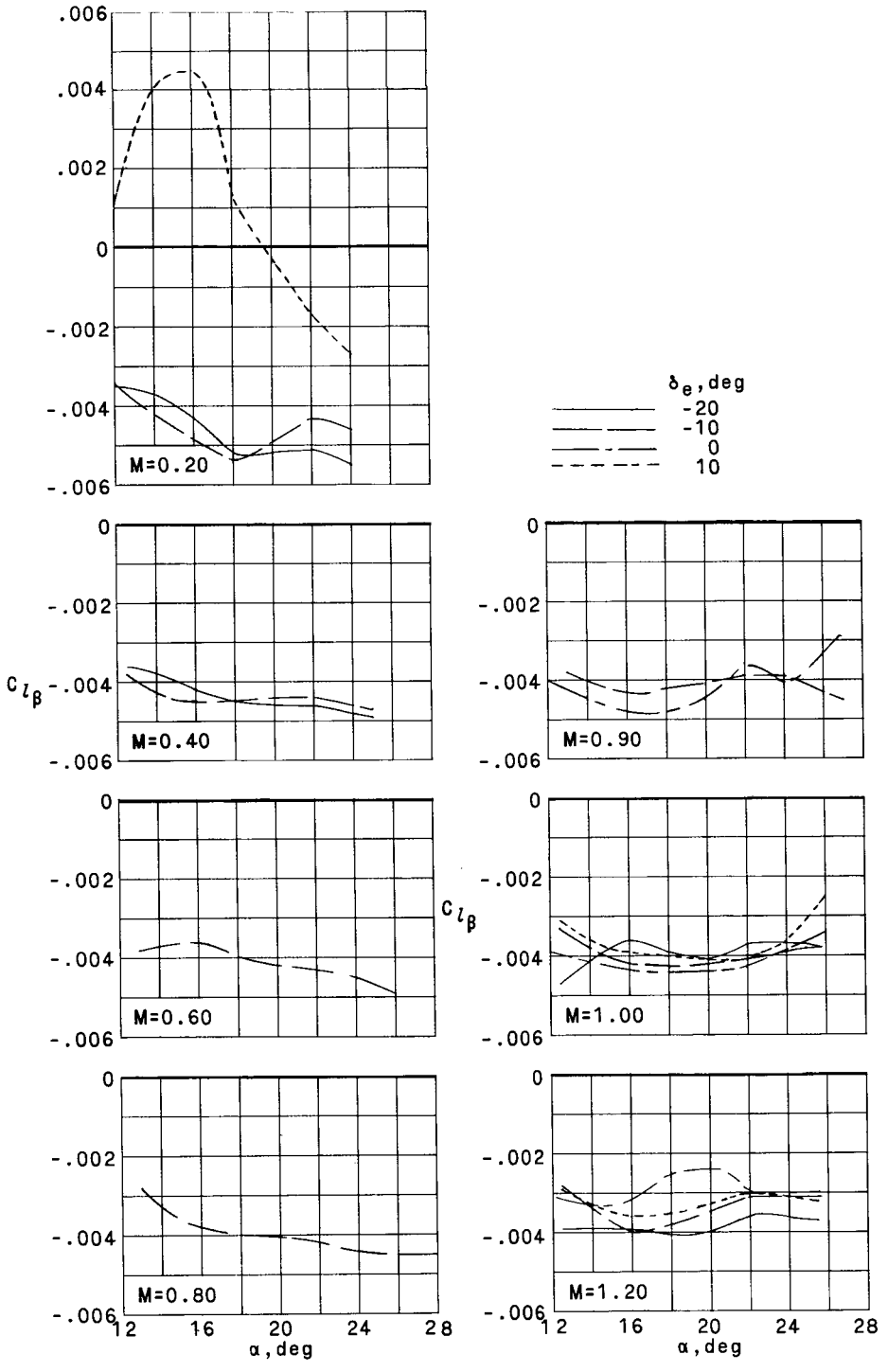

(b) C_{l_β} against α.

Figure 17.- Concluded.